STRUCTURAL CHEMISTRY OF FAST ION CONDUCTORS IN THE SYSTEM AgI-AgBr

1988

Akira YOSHIASA

The investigation described in this thesis and related studies have been published or will be published, with some minor modifications, in the following papers:

1. Local structure of the $AgBr_{1-x}I_x$ rock-salt type solid-solution.
   A. Yoshiasa, K. Koto, S. Emura and F. Kanamaru,
   Journal de Physique Colloque C8 (1986) **47**, 803-807

2. EXAFS and XANES studies of the $AgBr_{1-x}I_x$ rock-salt type solid-solution.
   A. Yoshiasa, K. Koto, S. Emura and F. Kanamaru,
   KEK Activity Report (1986) 208

3. Anharmonic thermal vibrations in wurtzite-type AgI.
   A. Yoshiasa, K. Koto, F. Kanamaru, S. Emura and H. Horiuchi,
   Acta Crystallographica (1987) **B43**, 434-440

4. Non-periodic Patterson function of β-AgI.
   M. Tokonami, N. Haga, K. Koto and A. Yoshiasa,
   Acta Crystallographica (1987) **A43**, C147

5. Local structure of the α-$AgI_{1-x}Br_x$ solid-solution.
   A. Yoshiasa, F. Kihara, S. Emura, F. Kanamaru and K. Koto,
   KEK Activity Report (1987) in press

6. Local structure of the superionic conducting α-AgI type $AgI_{1-x}Br_x$ solid-solution.
   A. Yoshiasa, F. Kanamaru and K. Koto,
   to be submitted to Solid State Ionics

7. Variations of Ag bonding distances in the $AgBr_{1-x}I_x$ rock-salt type solid-solution by X-ray and EXAFS analyses.
   A. Yoshiasa, F. Kanamaru, S. Emura and K. Koto,
   to be submitted to Solid State Ionics

Contents

	page
Chapter 1 General introduction	1-18
1) Historical background	2
2) Methods	12
3) Purpose of this study	14
4) References	17
Chapter 2 Anharmonic thermal vibrations in wurtzite-type AgI	19-51
1) Introduction	20
2) Experimental	
2-1 Specimen	21
2-2 Temperature dependence of cell dimensions	26
2-3 Intensity mesurements	26
2-4 Refinement of the structure	35
3) Results and discussion	
3-1 Anharmonic thermal vibrations and forbidden reflections	39
3-2 Structure changes and temperature dependence of anharmonic thermal vibrations	42
3-3 Relation of anharmonicity to the phase transition and to the ionic conduction	43
3-4 Structural variations in wurtzite-type compounds	45
4) References	50
Chapter 3 Variations of Ag bonding distances in the $AgBr_{1-x}I_x$ rock-salt type solid-solution by X-ray and EXAFS analyses	52-78
1) Introduction	53
2) Experimental	

2-1 Synthesis 54

2-2 X-ray single crystal structure analysis 54

2-3 X-ray absorption measurements 57

2-4 EXAFS data analysis 57

3) Results and discussion

3-1 Local structure of the solid-solution 65

3-2 Average distribution of atoms in the unit cell 69

3-3 Local structure and ionic conduction in the solid-solution 76

4) References 77

Chapter 4 Local structure of the superionic conducting α-AgI type $AgI_{1-x}Br_x$ solid-solution 79-112

1) Introduction 80

2) Experimental and results

2-1 Synthesis 83

2-2 Furnace 83

2-3 X-ray absorption measurements 86

2-4 Structure analysis 86

3) Discussion

3-1 The effective one-particle potentials in the high and low temperature phases of AgI 96

3-2 Local environment of the Ag ion in α-AgI 102

3-3 Local structure of the α-$AgI_{1-x}Br_x$ solid-solution 105

3-4 Superionic conduction of α-AgI 106

4) References 111

Chapter 5 General conclusion 113-118

Acknowledgement 119

Chapter 1.

General Introduction

Historical background

α-AgI is classical and typical superionic conductor of Ag ions which are mobile with large self-diffusion constant. α-AgI (high temperature form) transforms to β-AgI (low temp. form) at 420 K. α-AgI exhibits high conductivity with a low activation energy, while β-AgI exhibits low ionic conductivity with an appreciable activation energy; the high-conducting state of AgI is achieved through the first-order phase transition and the ionic conductivity increases by four orders of magnitude (Fig. 1). β-AgI exhibits a negative thermal expansion. A decrease in volume (ca. 7%) occurs at the transition from β- to α-AgI (Hoshino, 1957).

The crystal structure of α-AgI has been extensively discussed. The unique α-AgI type structure was found only in other systems of cuprous halides and argentous chalcogenides (Boyce & Huberman, 1979). Strock (1934 and 1936) proposed an "average structure" in which the Ag ions are distributed randomly over several kinds of available sites among interstices of the regular body-centered cubic lattice formed by iodine ions (Fig. 2). Superionic α-AgI crystal was thought of as consisting of two interpenetrating sublattices with an ordered framework and a "molten silver sublattice"; the silver ions were treated as a "liquid" confined to the channels of the b.c.c. lattice of I ions. Several different models were proposed for the statistically disordered distribution of the highly mobile Ag ions (e.g. Burley, 1967). Recently, such distribution has been reexamined in several high-accuracy structural studies, and it

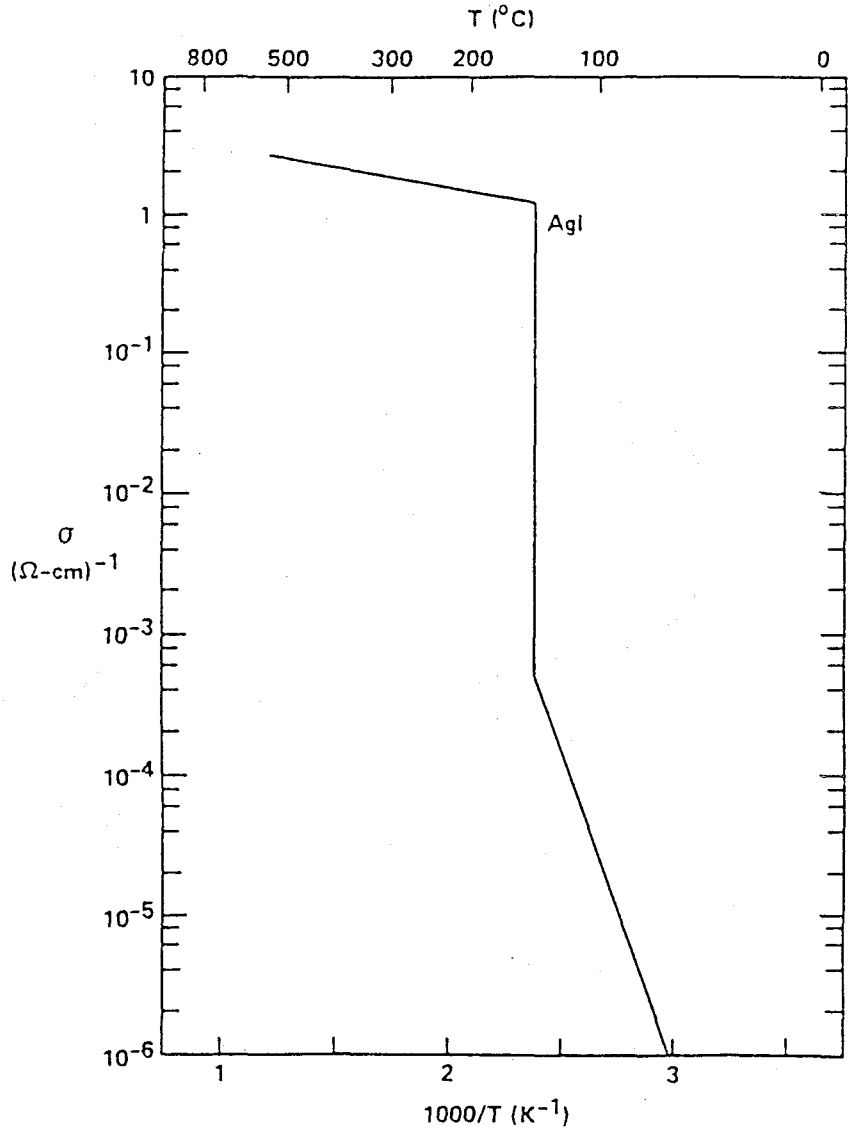

Fig. 1. Ionic conductivity of AgI showing the behavior observed on going from the low temperature β-phase to the high temperature superionic α-phase. After Boyce & Huberman (1979).

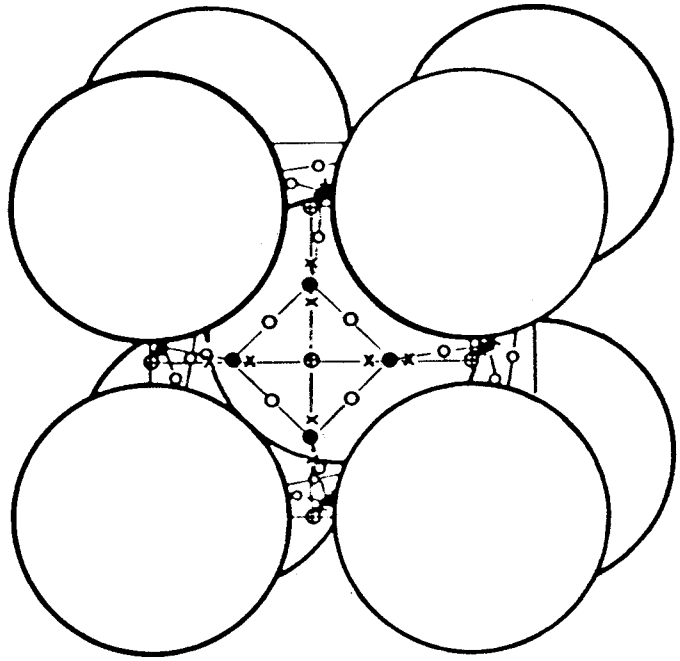

Fig. 2. Possible interstitial sites for the distribution of Ag ions in α-AgI. After Hoshino et al. (1977).

has been shown that the experimental data are very well explained by a structure model in which the Ag ions are distributed randomly over the 12(d) sites of the space group Im3m (only one sixth of the sites is occupied) with large anharmonic thermal vibrations (Hoshino et al., 1977 and Cava et al., 1977).

The dynamical behavior of atoms in α-AgI has been studied extensively through several techniques; far-infrared absorption (Bruesh et al., 1975), Raman spectroscopy (Hanson et al., 1975 and Delaney & Ushioda, 1976) and neutron scattering (Golin, 1968). From the crystallochemical considerations and interpretation of the observed spectra, it has been suggested that only tetrahedral 12(d) sites among interstices of the b.c.c. lattice formed by iodine are occupied at equilibrium. It was, however, only proposed from EXAFS study that the Ag ions in α-AgI occupy the sites displaced from the center of the tetrahedron (Boyce et al., 1977), and Boyce et al. (1977) concluded that all the previous conclusions about the distribution as well as about the dynamics of Ag ions were ruled out.

The low-temperature β-phase of AgI has the wurtzite type structure (Fig. 3, hexagonal closest packing of iodine atoms with tetrahedrally coordinated silver atoms whose coordination tetrahedra share only corners), and exhibits a peculiar thermal behavior. In spite of the simple basic structure of β-AgI, the details of the structure such as the anharmonic thermal vibrations are not well established yet. Helmholtz (1935) suggested that Ag ions were slightly displaced from the centers of their coordination tetrahedra at room temperature. Later diffraction studies (Burley, 1963 and Cava et al., 1977) failed

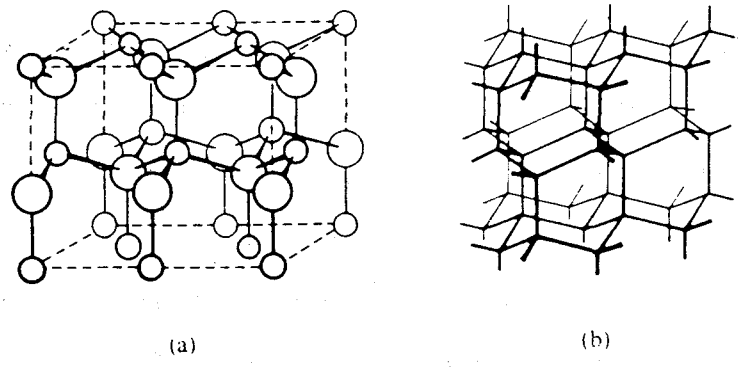

Fig. 3. Crystal structure of wurtzite (a) and hexagonal diamond (b).

to confirm this type of disorder and the detailed structure is not known yet. Several diffraction studies on the anharmonic thermal vibration of wurtzite type compounds have recently been reported (e.g. Stevenson & Barnea, 1984) and have shown that anharmonic effects are important even at room temperature. The importance of the anharmonicity of vibrating mobile ions near phase transitions of superionic conductors has also been pointed out (e.g. Matsubara, 1975). Anharmonic effects in the thermal vibration of atoms in β-AgI should, therefore, be taken into account in analysing diffraction data. It is clearly necessary to reexamine the structure of both α- and β-AgI, especially the distribution and the thermal behavior of Ag ions.

The phase diagram of the AgI-AgBr system (Fig. 4) has been reported by Stasiw & Teltow (1949). The dynamical and structural properties of the silver halides are governed by the competition of ionic bonding versus covalent bonding. Covalent character in the AgI-AgBr system is increasing from AgBr to AgI. The ionicities (f) of both AgI (f_{AgI}=0.77) and AgBr (f_{AgBr}=0.85) based on the Phillips scale are close to the critical value of 0.785 which separates tetrahedral covalent compounds from octahedral ionic ones (Phillips, 1970). In the rock-salt type structure of AgBr, each Ag ion is octahedrally surrounded by six Br ions and vice versa. On the other hand, AgI stably crystallizes in the tetrahedrally coordinated wurtzite type structure (β-phase) under ambient conditions. Because AgBr differs from AgI in the nature of chemical bonding and in the structure type, the solid-solution range for each structure type

AgBr–AgI

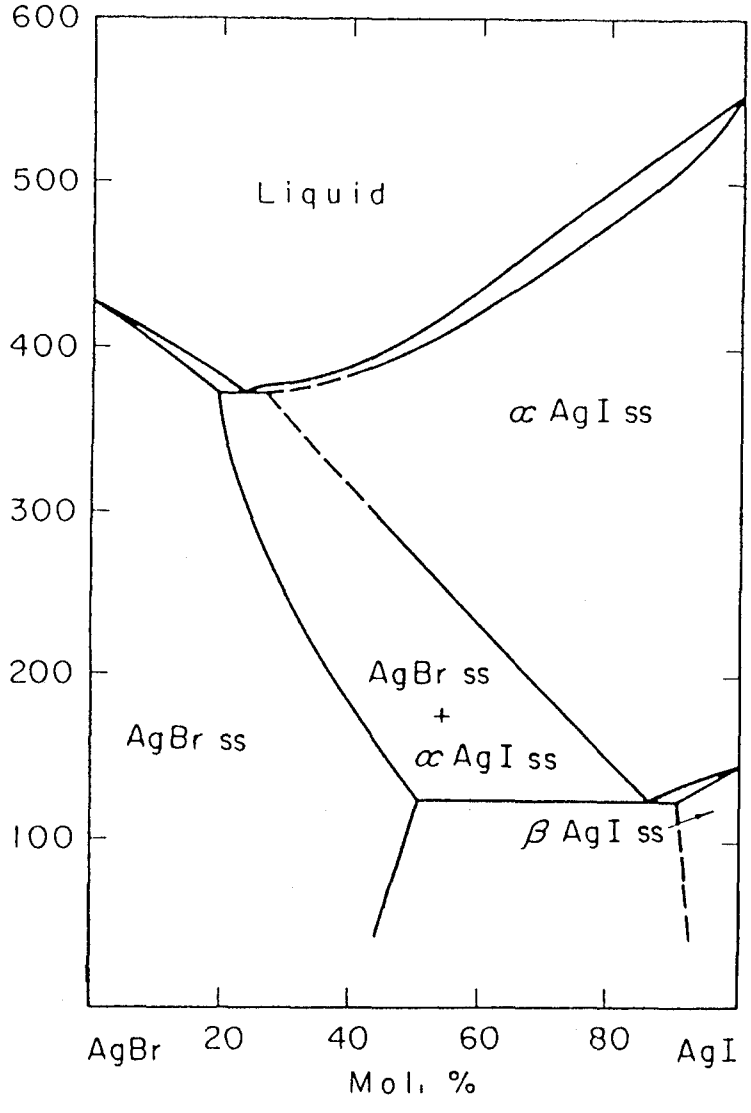

Fig. 4. The phase diagram of AgI-AgBr system by Stasiw & Teltow (1949).

is limited. The superionic conductor α-AgI is stable over a wide range of temperature to the melting point of 825 K and AgBr is stable only in the rock-salt type structure up to the melting point of 707 K. Both α-AgI type and rock-salt type solid-solutions with cubic symmetry are stable over a wide range of composition and temperature.

AgBr exhibits a considerable ionic conductivity even at room temperature by the diffusion of Ag ions through the lattice, though it does not exhibit superionic conduction. The migration of Ag ions in AgBr is applied in the photographic process (Hamilton, 1984). The movement of the Ag ions is believed to be the interstitialcy mechanism (Friauf, 1957). The introduction of AgI into AgBr leads to a large increase in the ionic conductivity (Fig. 5 and 6).

Ionic conduction mechanism in the solid-solutions has not been sufficiently explained from a structural point of view. One of the techniques employed to increase ionic conductivity is the addition of foreign ions having wrong charge. According to classical theories, an ionic crystal in which foreign ions with wrong charge are dissolved adjusts charge neutrality by the formation of compensating point defects, and the defects enhance the diffusion of ions. However, an introduction of foreign ions with correct charge such as the introduction of AgI into AgBr also leads to a substantial increase in the ionic conductivity and the charge compensation mechanism cannot be applied to explain the behavior. There must be induced the diversity of local structure in solid-solution. Local structures in solid-solution are not so simple that it is not still understood why

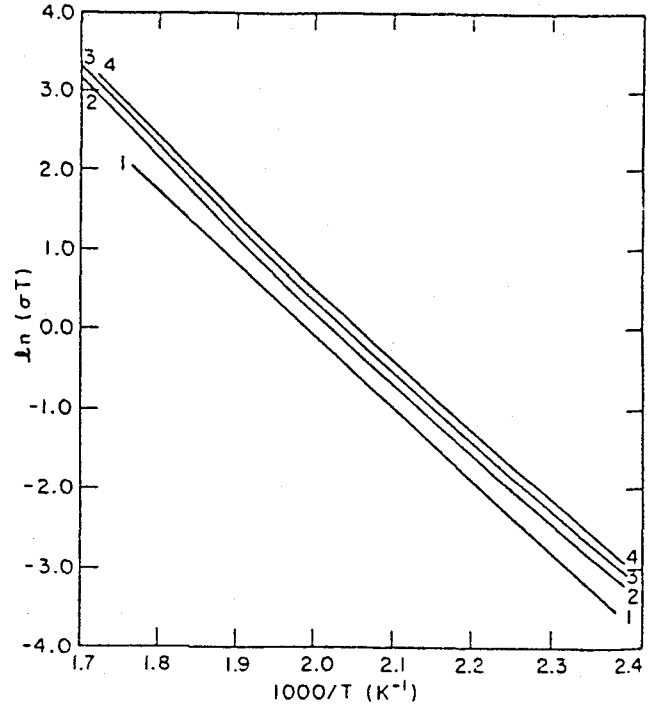

Fig. 5. Ionic conductivity of single crystal of $AgBr_{1-x}I_x$ solid-solution. Curve 1: AgBr; 2: AgBr-2.1 mol% AgI; 3: AgBr-3.7 % AgI; 4: AgBr-4.9 % AgI. After Cain & Slifkin (1980).

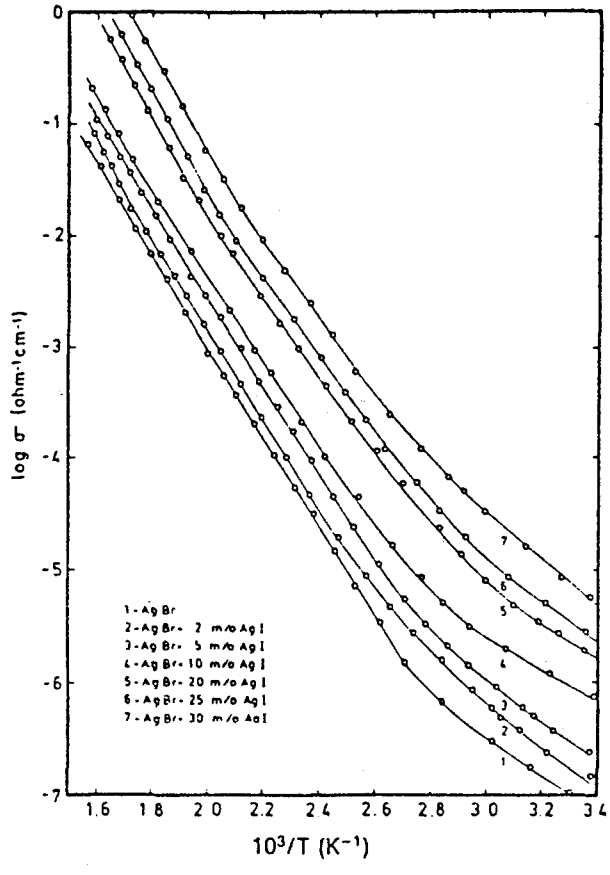

Fig. 6. Ionic conductivity of $AgBr_{1-x}I_x$ solid-solutions. After Shahi & Wagner (1982).

the introduction of homovalent foreign ions leads to the enhancement of ionic conductivity. The chemical composition and basic structure of the rock-salt type $AgBr_{1-x}I_x$ solid-solutions are simple. Nevertheless, it will be presumed that the local environments of the I ions differ from those of the Br ions. It is necessary to know what occurs around the substituted ions in the solid-solution, and the knowledge of the correlation between the substituted ions and the local structure should be of primary importance for understanding of the ionic conduction.

Methods

X-ray diffraction experiments allow the determination of the three-dimensional distribution of atoms in the unit cell. The Fourier transformation of the temperature factor determined by X-ray diffraction is the probability-density function (p.d.f.). The p.d.f. is defined as the probability of finding an atom in a volume element and provides information about the distribution of atoms around the equilibrium positions. Fig. 7 shows the ensemble of all atoms occupying the equivalent sites superimposed in their common potential. All of these atoms occupy different states of thermal excitation in the potential. The effective one-particle potentials (o.p.p.) has an absolute energy scale and is almost independent of temperature. The p.d.f. maps involve valuable information about diffusion paths and that the o.p.p. curves allow estimation of the potential barrier along the diffusion path of the mobile ions.

The local environment around a particular kind of X-ray absorbing atom is determined by analysing EXAFS. The XANES region

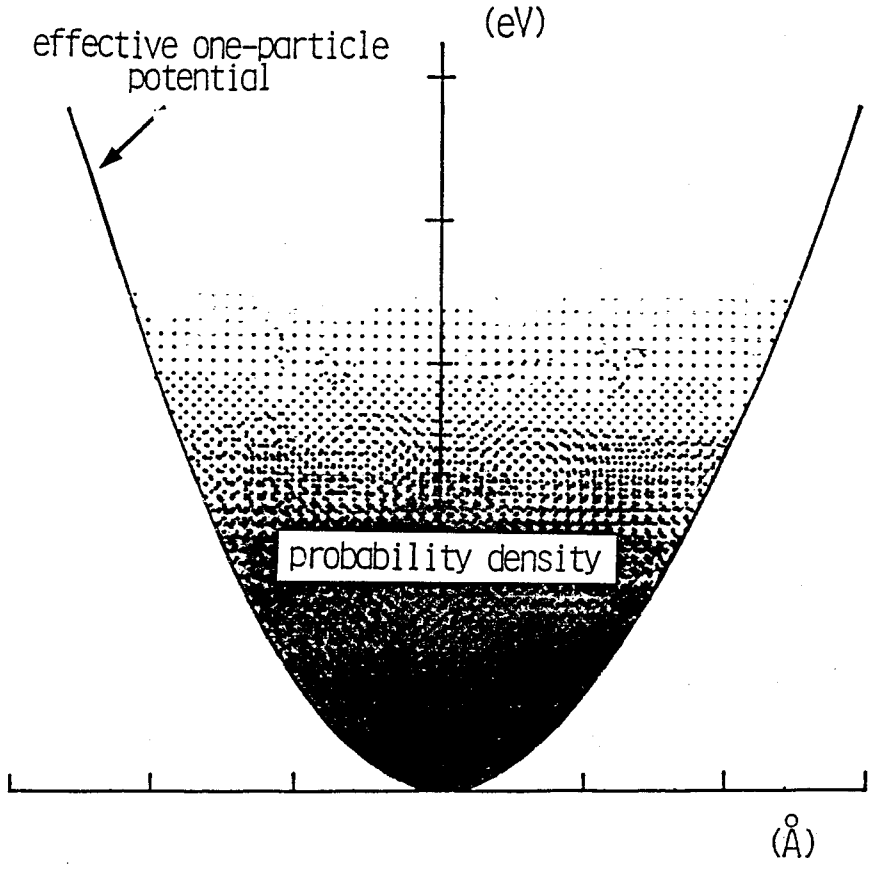

Fig. 7. Relations between the effective one-particle potentials and the probability-density function.

of the absorption spectrum contains the information on relative orientation and bond angles of atoms surrounding X-ray absorbing atoms. Diffraction technique is a powerful method to determine periodical arrangement, while EXAFS spectrum can be measured not only from crystalline materials but also from noncrystalline materials. Moreover, the local structure arround the specified atom is determined by EXAFS even if the material contains several kinds of atoms at a crystallographically equivalent position. In solid-solutions, positionally averaged information for different kinds of atoms occupying an equivalent position is obtained by the diffraction studies. Because α-AgI type structure has a statistical distribution of Ag ions over an equivalent position, the averaged informations of both one tetrahedral site occupied by the Ag ion and five unoccupied tetrahedral sites is only obtained by diffraction.

Purpose of this study

A number of superionic conductors has been extensively investigated in view of both fundamental and applied point. In the absence of detailed structural knowledge, the models which have been proposed to explain superionic conduction are based on either hypothetical structure or general considerations on residence and hopping times (e.g. Eckold et al., 1976). AgI has been of interest as a model compound for the study of fast-ion transport in solids.

The structures of superionic conductors such as α-AgI are related to the partially covalent bond (Phillips, 1976). The nature of chemical bonding in the superionic conductors is,

therefore, particularly interesting in relation to the origin of high ionic conductivity. It is necessary to investigate the effects of covalent and ionic characters on the superionic conduction.

The crystal structure analyses are fundamentally necessary for understanding of the chemical and physical properties of the materials. The detailed structure of β-AgI was not yet been well established because of difficulty. In this study the structure of β-AgI was refined in a temperature range from 123 K to the vicinity of the β-α phase transition point. Anharmonic thermal vibration of β-AgI, which was obtained by X-ray diffraction method, was analysed as a function of temperature. We applied the cumulant-expansion formalism proposed by Johnson (1969) in order to determine the accurate positional parameters and the p.d.f at individual temperatures. The o.p.p are derived from the p.d.f.. The contribution of the anharmonic thermal vibrations to X-ray diffraction intensities is also investigated. The crystal chemistry of the wurtzite-type compounds is discussed based on the effect of chemical-bond character on the thermal behavior of atoms.

EXAFS and XANES structural analyses were made for the α-AgI type and rock-salt type solid-solutions to elucidate the local structure and to determine the actual nearest neighbor distance in disordered structures and in solid-solution. We have also calculated the p.d.f. and o.p.p. of both Ag and I atoms in α-AgI. The crystal structure of β-AgI is reviewed in comparison with that of β-AgI and the mechanism of ionic conduction of α-AgI is

discussed from a view point of structural chemistry, especialy the thermal vibration.

References

J.B. Boyce, T.M. Hayes, W. Stutius and J.C. Mikkelsen, Jr. (1977) Physical Review Letters, 38, 1362-1365

J.B. Boyce, B.A. Huberman (1979) Physics Reports (Review Section of Physics Letters) 51, No.4, 189-265

P. Bruesch, S. Strassler and H.R. Zeller (1975) Phys. Stat. Sol., 31,217-226

G. Burley (1963) J. Chem. Phys., 38, 2807

G. Burley (1967) Acta Cryst., 23, 1

L.S. Cain and L.M. Slifkin (1980) J. Phys. Chem. Solids, 41, 173-178

R.J. Cava, F. Reidinger and B.J. Wuensch (1977) Solid State Commun., 24, 411-416

M.J. Delaney and S. Ushioda (1976) Solid State Commun., 19, 297-301

G. Eckold, K. Funke, J. Kalus and R.E. Lechner (1976) J. Phys. Chem. Solids, 37, 1097

R.J. Friauf (1957) Phys. Review, 105, 843-848

S. Golin (1968) Phys. Rev., 160, 643

J.F. Hamilton (1984) The Physics of Latent Image Formation in Silver Halides, ed. by A. Baldereschi, W. Czaja, E. Tosatti and M. Tosi, World Scientific, Singapore

R.C. Hanson, T.A. Fjeldly and H.D. Hockheimer (1975) Phys. Stat. Sol., 70, 567-576

L. Helmholtz (1935) J. Chem. Phys., 3, 740

S. Hoshino (1957) J. Phys. Soc. Japan, 12, 315-326

S. Hoshino, T. Sakuma and Y. Fujii (1977) Solid State Commun., 22, 763-765

Matsubara, T. (1975) J. Phys. Soc. Japan, 38, 1076-1079

J.C. Phillips (1970) Rev. Mod. Phys., 42, 317-356

J.C. Phillips (1976) J. Electrochem. Soc., 123, 934-940

C.K. Johonson (1969) Acta Cryst., A25, 187-194

K. Shahi and J.B. Wagner Jr. (1982) J. Phys. Chem. Solids, 43, 713-722

O. Stasiw and J. Teltow (1949) Z. Anorg. Allgen. Chem., 259, 143-153

A.W. Stevenson and Z. Barnea (1984) Acta Cryst., B40, 530-537

L.W. Strock (1934) Z. Phys. Chem., B25, 441

L.W. Strock (1936) Z. Phys. Chem., B31, 132

Chapter 2.

Anharmonic Thermal Vibrations in the Wurtzite-type AgI

1) Introduction

The wurtzite-type silver iodide (β-AgI) shows a considerable ionic conductivity due to diffusion of silver ions even at room temperature. It exhibits a negative thermal expansion, and undergoes a first order phase transition at 420 K to the superionic conducting phase, α-AgI, with higher density. The cleavage and gliding perpendicular to the c-axis occur because of the anisotropy of interatomic force.

Mair & Barnea (1975) presented a detailed theoretical study of anharmonic thermal vibrations in wurtzite-type structures. A number of X-ray studies on the anharmonic thermal vibration of wurtzite-type compounds have been reported (e.g. Whiteley, Moss & Barnea, 1978; Stevenson, Milanko & Barnea, 1984; Kihara & Donnay, 1985). Cava, Reidinger & Wuensch (1977) refined the structure of α-AgI using neutron diffraction method and showed that the complex silver distribution is completely accounted for by higher-order thermal tensors. Piltz & Barnea (1987) have studied anharmonicity of β-AgI using X-ray diffraction at room temperature and revealed the presence of considerable cubic anharmonic effects.

The dispersion relation of the normal modes of lattice vibration in β-AgI was determined based on the coherent neutron inelastic scattering experiments by Bührer & Brüesch (1975) and Buhrer, Nicklow & Brüesch (1978). They reported that the characteristics of phonon spectra showed some strong anharmonic effects, and analyzed a peculiar dispersion relation by a valence-shell model. Beyeler, Brüesch, Hibma & Bührer (1978)

calculated the diffuse scattering pattern of β-AgI with parameters of the valence-shell model. They concluded that β-AgI exhibits a low-frequency phonon-induced diffuse scattering but no additional diffuse scattering due to static disorder. The large temperature factors of both atoms, therefore, should not be attributed to the statistical distribution.

In this work we studied the behaviour of anharmonic thermal vibrations in β-AgI as a function of temperature by X-ray diffraction method, and the effect of chemical-bond character on the anharmonicity. We applied the cumulant-expansion formalism proposed by Johnson (1969, 1970) in order to determine the accurate positional parameters and the probability-density function (P.D.F.) at 123, 297, 363 and 413 K. The mechanism of ionic conduction of β-AgI is discussed based on the thermal vibration of atoms. The crystal chemistry of the wurtzite-type compounds is also discussed based on the results of the structure of β-AgI.

2) Experimental

2-1 Specimen

β-AgI single crystals were grown by a method reported by Cochrane (1967) and also grown in silica gel (Photo. 1 and 2). As the crystals are easily cleaved and glided normal to the c-axis (Photo. 3), a single crystal used for X-ray work was carefully ground to a sphere by hand using emery paper under microscope. The spherical crystal with a diameter of 0.20 mm was examined by means of precession photography before intensity measurements.

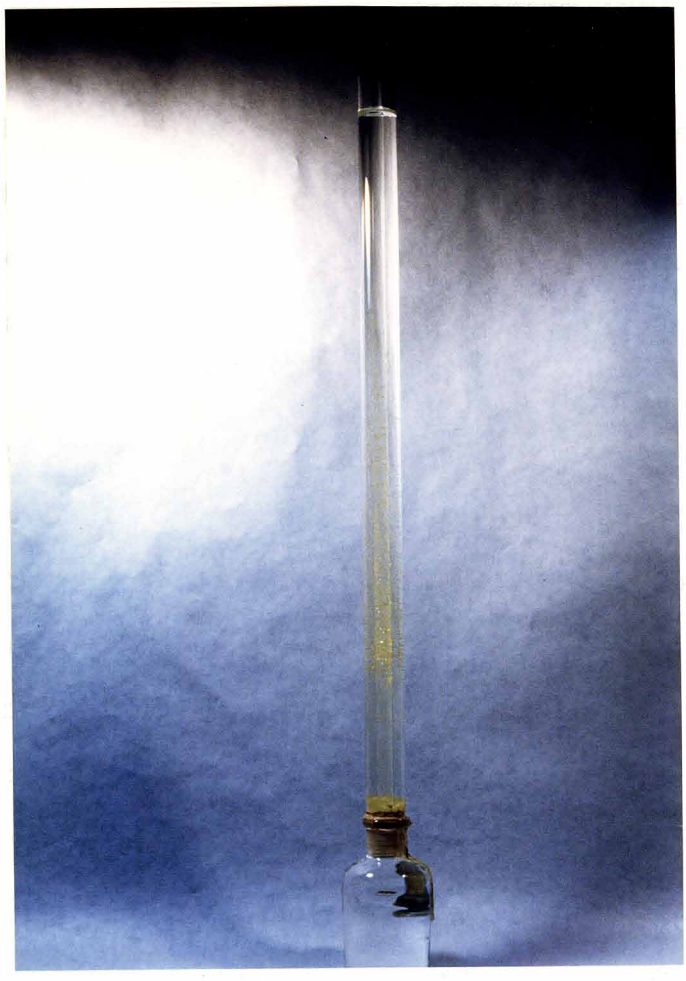

(a)

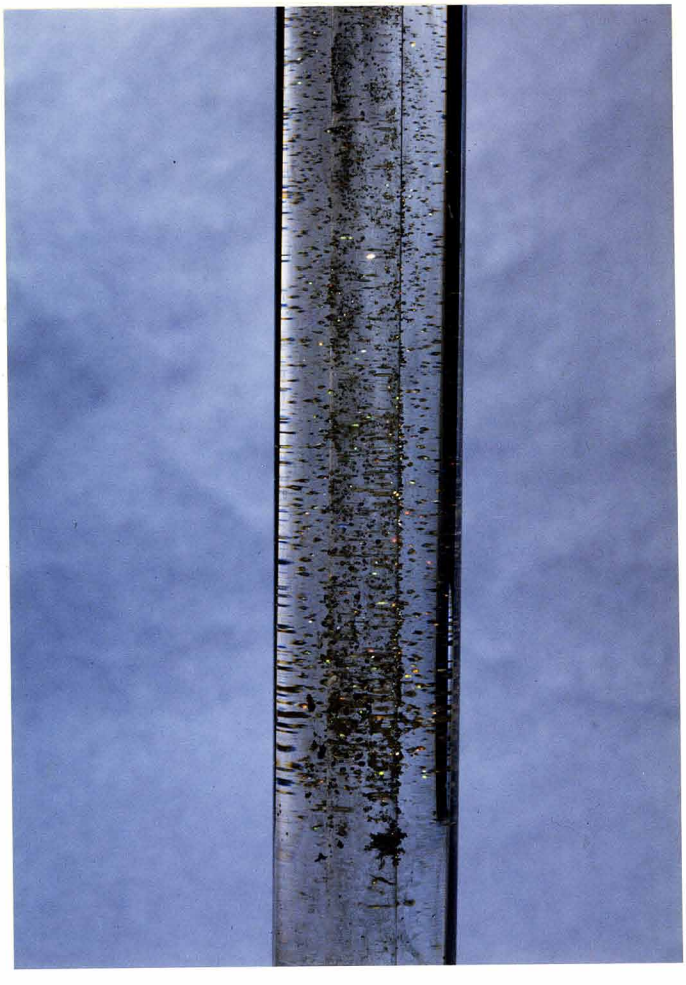

(b)

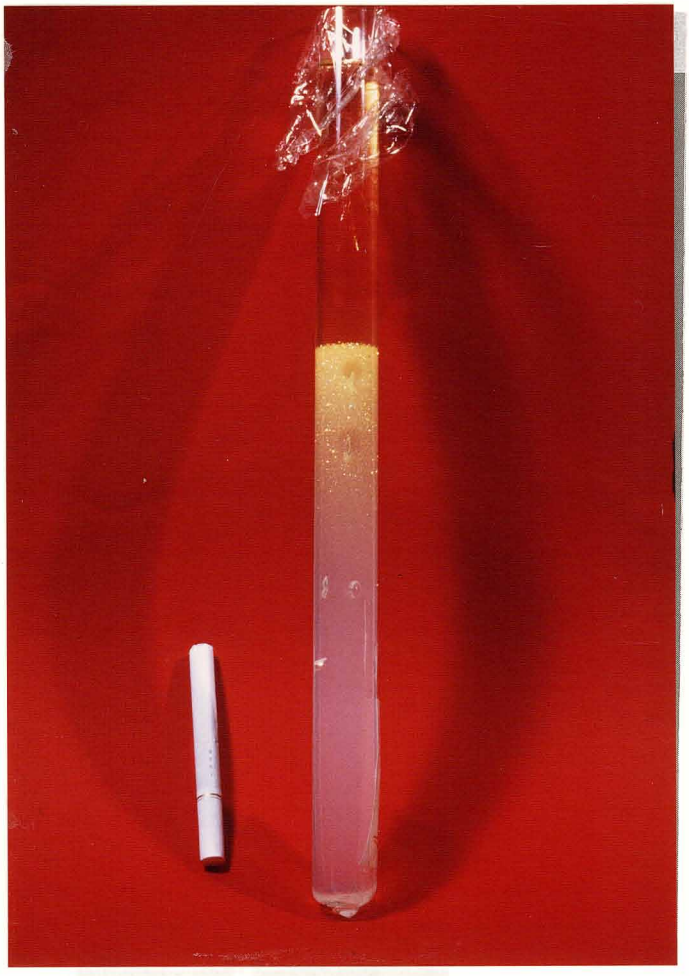

Photo. 1. (a) Single crystals of β-AgI are grown by slow diffusive dilution of a solution of AgI in concentrated aquous KI solution. The lower half of the long-necked glass bottle was filled with the saturated KI and AgI solution, and the upper part of bottle with distilled water. (b) Growth of single crystals in silica gel.

(a)

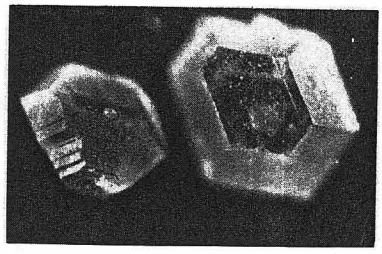

(b)

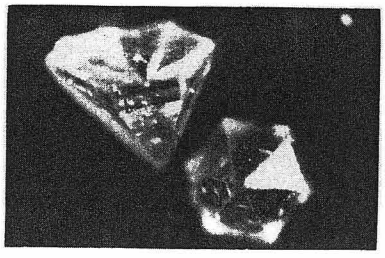

Photo. 2. Typical habit of β-AgI single crystals (a) grown by the Cochrane's method; characterized by well developed $\{10\bar{1}1\}$, $\{10\bar{1}\bar{1}\}$, $\{000\bar{1}\}$ and $\{0001\}$ faces, (b) grown in silica gel, characterized by $\{10\bar{1}1\}$, $\{10\bar{1}2\}$ and $\{000\bar{1}\}$ faces.

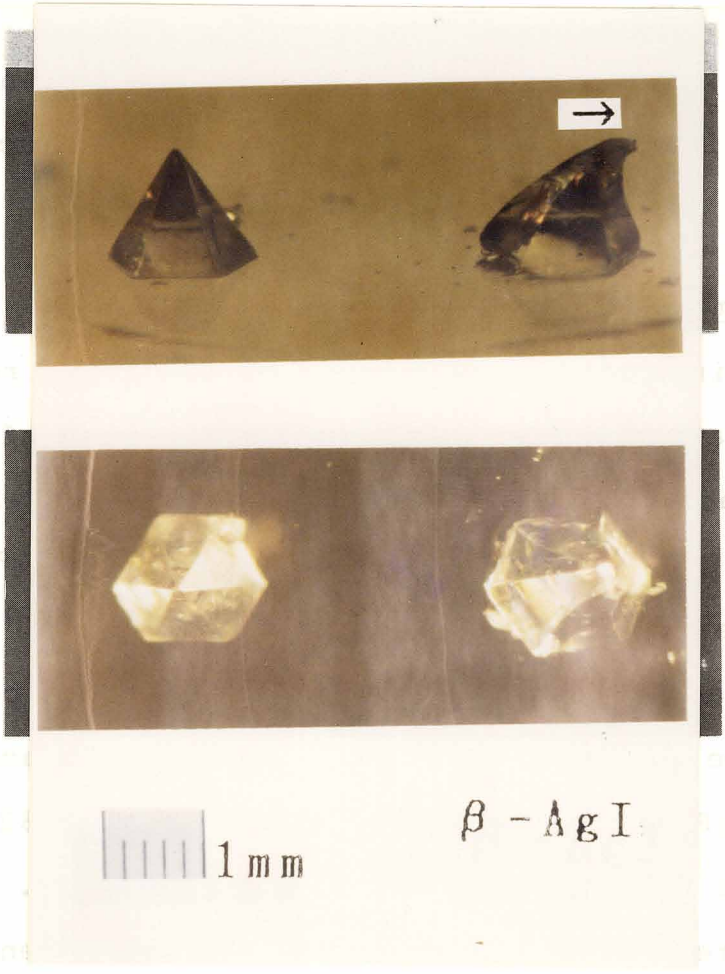

Photo. 3. β-AgI crystal shape before (left) and after (right) application of stress.

2-2 Temperature dependence of cell dimensions

Cell dimensions at various temperatures between 115 and 413 K were determined by the least-squares method using the 2θ values of fifteen reflections within the range of $20° < 2\theta < 50°$ measured on a Rigaku AFC5FOS four-circle diffractometer (Table 1, Fig. 1). Mo$K\alpha$ radiation (λ=0.71069 Å) monochromatized by pyrolytic graphite was obtained from a rotating-anode X-ray generator (60 kV, 200 mA). The same set of fifteen reflections was used in all the measurements. Temperature fluctuations were within $\pm$2 K.

2-3 Intensity measurements

Accurate intensity measurements of the Bragg reflections at 123, 297, 363 and 413 K were made. Intensities of reflections within one quadrant were measured adopting the θ-2θ scan mode, scan width of $1.8° + 0.8° \tan\theta$ and scanning speed of 5° min^{-1} in 2θ. Reflections were measured within $(\sin\theta)/\lambda < 1.15$ Å^{-1}. Lorentz and polarization factors were applied and absorption correction for spherical shape was made; μr=1.81. The significant intensities with $|F_o| > 3\sigma(|F_o|)$ were observed within 1.04, 0.82 and 0.78 Å^{-1} of $(\sin\theta)/\lambda$ at 297, 363 and 413 K, respectively. Independent reflections were obtained by averaging the equivalent reflections and are 323 at 123 K, 170 at 297 K, 108 at 363 K and 90 at 413 K. The amplitude variations of standard reflections throughout the measurements were within $\pm$1.7 % at 413 K. The deviations from the averaged values of $|F_o|$ of equivalent reflections were within about 2.5 %. The corrections for thermal diffuse scattering (TDS) were made by adopting a model of first-order scattering due

Table 1. Cell dimensions and atomic parameters in the harmonic and anharmonic models. Bond distances and angles were calculated based on the results of the anharmonic model. Ag* indicates the apical atom of trigonal pyramid.

temperature	123K		297K		363K		413K	
Cell dimensions(Å)	a 4.591(1)	c 7.511(4)	a 4.592(1)	c 7.510(2)	a 4.591(1)	c 7.508(2)	a 4.590(1)	c 7.506(2)
Harmonic model	R=0.025	wR=0.031	0.046	0.051	0.038	0.045	0.044	0.049
	I	Ag	I	Ag	I	Ag	I	Ag
z	0.0	0.6257(1)	0.0	0.6274(5)	0.0	0.6278(8)	0.0	0.6289(10)
$\beta 11 \times 10^4$	235(2)	356(3)	629(7)	975(14)	793(12)	1253(23)	936(17)	1487(35)
$\beta 33 \times 10^4$	71(1)	108(1)	163(2)	271(5)	214(4)	346(8)	251(5)	413(10)
Anharmonic model	R=0.023	wR=0.028	0.029	0.030	0.020	0.020	0.017	0.018
	I	Ag	I	Ag	I	Ag	I	Ag
z	0.0	0.6247(3)	0.0	0.6274(8)	0.0	0.6267(10)	0.0	0.6273(10)
$\beta 11 \times 10^4$	243(5)	365(8)	668(17)	1059(26)	851(21)	1372(32)	981(25)	1638(38)
$\beta 33 \times 10^4$	76(2)	110(3)	161(5)	279(6)	221(6)	367(8)	250(7)	442(9)
$\gamma 111 \times 10^6$	-30(27)	351(65)	62(68)	2199(203)	207(94)	3293(293)	209(127)	4717(391)
$\gamma 333 \times 10^6$	52(10)	-52	134(38)	-134	310(60)	-310	429(74)	-429
$\gamma 113 \times 10^6$	-23(15)	23	-380(73)	380	-540(116)	540	-813(144)	813
$\delta 1111 \times 10^6$	8(7)	11(17)	137(38)	394(94)	218(57)	668(150)	260(83)	1119(216)
$\delta 3333 \times 10^6$	2(1)	2(2)	-4(4)	31(10)	0(6)	53(16)	-8(8)	94(20)
$\delta 1113 \times 10^6$	-11(14)	-14(15)	-3(32)	-15(36)	-98(80)	-24(78)	-94(43)	-4(64)
$\delta 1133 \times 10^6$	2(1)	1(2)	1(4)	14(12)	12(6)	22(17)	15(9)	40(24)
Bond distances(Å)								
Ag - I	2.811(1)		2.819(2)		2.816(3)		2.817(3)	
Ag*- I	2.819(3)		2.798(6)		2.803(8)		2.797(8)	
Ag - Ag	4.591(1)		4.592(1)		4.591(1)		4.590(1)	
Ag*- Ag	4.597(2)		4.597(1)		4.595(1)		4.594(1)	
Bond angles (°)								
Ag-I-Ag	109.48(4)		109.1(1)		109.2(2)		109.1(2)	
Ag-I-Ag*	109.47(5)		109.8(1)		109.7(1)		109.8(2)	

Table 1. (continued)

Name	silver iodide			
Chemical formula	AgI			
Formula weight	234.772			
Space group	$P6_3mc$			
Z	2			
F(000)	200			
Method used to culculate w	$\sigma\|F_0\|$ based on counting statistics			
Temperature of measurement	123K	297K	363K	413K
Volume of unit cell($\AA^3$)	137.1(1)	137.1(1)	137.0(1)	137.0(1)
Calculated densites, Dx	5.708	5.706	5.710	5.714
Number of reflections measured	1359	1338	1125	491
Number of unobserved reflections	84	133	155	64
G(ext)	$0.67(7)\times10^{-8}$	$0.77(25)\times10^{-8}$	$0.34(4)\times10^{-7}$	$0.31(3)\times10^{-7}$

Table 1. (continued)

$|F_o|$ - $|F_c|$ tables for β-AgI at 413 K.

h	k	$\lvert F_o \rvert$	$\lvert F_c \rvert$
		l = 0	
2	0	36.91(25)	38.23
3	0	36.39(24)	36.81
4	0	6.76(13)	6.90
5	0	3.51(13)	3.66
6	0	1.78(20)	1.88
2	1	25.10(15)	25.10
3	1	13.07(10)	12.97
4	1	8.97(11)	9.12
2	2	27.14(23)	26.15
3	2	5.66(13)	5.44
4	2	2.51(12)	2.54
3	3	4.77(22)	4.93
		l = 1	
2	0	27.25(19)	27.73
3	0	2.31(18)	1.76
4	0	7.76(12)	7.65
5	0	3.27(11)	3.48
2	1	19.97(12)	19.91
3	1	10.80(10)	10.78
5	1	1.77(16)	1.81
3	2	5.80(13)	5.67
4	2	2.34(13)	2.50
		l = 2	
1	0	36.02(25)	35.88
2	0	25.46(18)	25.58
3	0	25.96(18)	25.87
4	0	5.93(15)	5.53
5	0	2.52(13)	2.54
2	1	16.80(12)	16.97
3	1	8.82(11)	8.68
4	1	6.88(11)	6.89
2	2	18.62(17)	18.45
3	2	4.24(13)	4.17
3	3	3.73(16)	3.81
		l = 3	
1	0	56.07(36)	55.21
2	0	40.82(27)	40.79
3	0	1.75(22)	1.71
4	0	9.88(12)	10.13
5	0	3.41(13)	3.38
2	1	29.51(17)	29.20
3	1	13.46(10)	13.47
5	1	2.29(12)	2.14
3	2	7.09(12)	7.05
4	2	3.03(11)	2.57
		l = 4	
0	0	17.32(23)	16.90
1	0	8.40(13)	8.54
2	0	6.89(15)	6.92
3	0	10.03(12)	10.19
4	0	3.26(12)	3.35
1	1	15.44(16)	15.31
2	1	6.36(14)	6.31
3	1	3.42(12)	3.21
4	1	3.50(11)	3.61
2	2	7.84(16)	7.85
3	2	2.30(13)	2.25
		l = 5	
1	0	35.29(23)	34.96
2	0	24.55(17)	24.57
4	0	6.22(14)	6.47
5	0	2.09(15)	2.36
2	1	17.46(11)	17.41
3	1	8.41(11)	8.53
3	2	4.57(13)	4.64
4	2	1.75(16)	1.82
		l = 6	
0	0	29.42(35)	28.89
1	0	12.93(12)	13.12
2	0	8.79(12)	8.98
3	0	9.22(12)	9.35
4	0	1.79(19)	2.12
1	1	19.72(17)	19.66
2	1	5.93(13)	5.86
3	1	3.23(11)	3.16
4	1	2.67(12)	2.55
2	2	6.64(16)	6.58
		l = 7	
1	0	8.23(13)	8.44
2	0	6.81(13)	6.73
2	1	5.28(14)	5.12
3	1	2.99(11)	3.12
3	2	2.02(16)	1.79
		l = 8	
0	0	13.32(21)	13.62
1	0	6.14(15)	6.08
2	0	4.29(13)	4.35
3	0	5.13(16)	4.91
1	1	9.64(15)	9.58
2	1	3.07(12)	3.00
3	1	1.91(15)	1.72
4	1	1.76(17)	1.48
2	2	3.48(16)	3.57
		l = 9	
1	0	4.75(18)	4.85
2	0	3.30(12)	3.36
2	1	2.60(11)	2.42
		l = 10	
0	0	2.76(22)	2.51
		l = 11	
1	0	1.98(16)	1.90

Table 1. (continued)

$|F_o|$ - $|F_c|$ tables for β-AgI at 363 K.

h	k	$\lvert F_o \rvert$	$\lvert F_c \rvert$
		l = 0	
2	0	38.49(26)	39.66
3	0	40.33(26)	41.05
4	0	8.86(9)	9.06
5	0	4.78(13)	4.90
6	0	2.91(9)	2.98
2	1	28.02(17)	27.91
3	1	15.40(8)	15.40
4	1	12.16(8)	12.12
5	1	1.98(12)	1.81
6	1	1.13(29)	1.11
2	2	31.68(21)	30.66
3	2	7.35(9)	7.17
4	2	3.59(8)	3.50
5	2	2.33(10)	2.38
3	3	6.88(10)	6.88
		l = 1	
2	0	28.31(19)	28.82
3	0	2.25(18)	1.56
4	0	9.38(9)	9.22
5	0	4.29(11)	4.49
2	1	21.57(14)	21.50
3	1	12.26(8)	12.32
5	1	2.52(9)	2.61
3	2	7.26(9)	7.07
4	2	3.35(8)	3.41
		l = 2	
1	0	36.84(25)	36.49
2	0	26.74(18)	27.20
3	0	29.06(20)	29.18
4	0	7.32(10)	6.94
5	0	3.33(10)	3.38
6	0	2.19(12)	2.45
2	1	18.56(12)	18.97
3	1	10.33(8)	10.31
4	1	8.86(8)	8.99
2	2	21.90(15)	21.65
3	2	5.46(11)	5.35
4	2	2.69(9)	2.53
5	2	1.86(12)	1.95
3	3	5.37(16)	5.25
		l = 3	
2	0	44.31(30)	43.83
4	0	12.83(9)	13.06
5	0	4.81(13)	4.90
2	1	33.27(19)	33.02
3	1	16.74(9)	16.88
5	1	3.18(8)	3.25
3	2	9.49(9)	9.41
4	2	4.01(9)	3.81
		l = 4	
0	0	15.82(22)	15.47
1	0	7.93(13)	7.93
2	0	6.72(15)	6.85
3	0	10.52(11)	10.81
4	0	3.76(10)	3.88
5	0	1.62(17)	1.53
1	1	14.97(15)	14.76
2	1	6.41(13)	6.45
3	1	3.89(9)	3.71
4	1	4.44(10)	4.55
2	2	8.70(12)	8.74
3	2	2.98(9)	2.76
3	3	2.68(13)	2.82
		l = 5	
1	0	39.43(25)	38.53
2	0	28.72(20)	28.45
4	0	8.45(9)	8.62
5	0	3.28(9)	3.56
2	1	21.05(13)	20.98
3	1	11.09(8)	11.12
5	1	2.15(9)	2.38
3	2	6.46(10)	6.38
4	2	2.65(8)	2.77
		l = 6	
0	0	32.81(38)	31.75
1	0	14.61(12)	14.88
2	0	10.32(12)	10.64
3	0	11.78(11)	11.88
4	0	2.76(10)	2.90
1	1	23.09(19)	22.81
2	1	7.39(11)	7.28
3	1	4.16(9)	4.24
4	1	3.71(8)	3.76
2	2	8.71(12)	8.69
3	2	2.19(11)	2.17
3	3	2.91(12)	2.19
		l = 7	
1	0	9.79(11)	9.96
2	0	7.65(16)	8.10
4	0	3.12(8)	3.19
5	0	1.36(20)	1.78
2	1	6.72(11)	6.36
3	1	3.99(9)	4.13
3	2	2.52(9)	2.53
		l = 8	
0	0	17.06(22)	17.45
1	0	7.74(13)	7.93
2	0	5.83(15)	5.84
3	0	7.14(13)	6.97
1	1	12.69(14)	12.73
2	1	4.29(13)	4.19
3	1	2.58(9)	2.53
4	1	2.22(9)	2.38
2	2	5.52(15)	5.22
		l = 9	
1	0	6.18(14)	6.12
2	0	4.34(15)	4.47
4	0	1.84(14)	1.60
2	1	3.37(11)	3.37
3	1	1.89(13)	1.96
		l = 10	
0	0	4.40(31)	4.05
1	0	1.85(18)	1.89
3	0	2.07(15)	2.10
1	1	3.42(14)	3.26
2	2	1.73(15)	1.68
		l = 11	
1	0	3.02(12)	2.99
2	0	2.25(12)	2.25

Table 1. (continued)

$|F_o|$ - $|F_c|$ tables for β-AgI at 297 K.

h	k	$\|F_o\|$	$\|F_c\|$
		l = 0	
3	0	54.86(26)	54.49
4	0	13.27(7)	13.11
5	0	7.35(6)	7.43
6	0	5.72(6)	5.55
2	1	34.44(13)	34.58
3	1	20.72(8)	19.96
4	1	18.68(7)	18.25
5	1	3.57(6)	3.42
6	1	2.08(7)	2.07
2	2	42.62(22)	41.14
3	2	10.88(5)	10.56
4	2	5.71(5)	5.60
5	2	4.40(6)	4.55
3	3	11.56(9)	11.21
4	3	2.57(5)	2.51
4	4	2.24(9)	2.53
		l = 1	
3	0	1.69(9)	1.25
4	0	11.58(6)	11.79
5	0	6.69(6)	6.46
7	0	1.28(12)	1.34
2	1	24.63(9)	25.21
3	1	15.37(6)	15.26
4	1	1.37(9)	0.92
5	1	4.10(6)	4.02
6	1	1.80(8)	2.11
3	2	9.70(5)	9.45
4	2	5.29(5)	5.15
6	2	1.38(11)	1.12
4	3	2.79(6)	2.76
		l = 2	
1	0	44.83(21)	44.40
2	0	30.58(14)	32.05
3	0	35.48(16)	37.17
4	0	9.35(6)	9.51
5	0	5.25(6)	5.22
6	0	4.11(7)	4.35
2	1	22.18(8)	22.85
3	1	13.32(6)	13.46
4	1	13.17(6)	13.19
5	1	2.85(6)	2.86
6	1	1.45(9)	1.53
2	2	28.74(15)	28.29
3	2	7.82(4)	7.63
4	2	4.15(5)	4.06
5	2	3.45(6)	3.58
3	3	8.50(7)	8.35
4	3	2.23(6)	2.00
4	4	1.69(12)	2.04
		l = 3	
3	0	1.19(11)	1.07
4	0	17.68(9)	18.72
5	0	7.91(6)	8.21
7	0	1.49(11)	1.63
2	1	42.31(16)	43.13
3	1	22.39(9)	23.76
5	1	5.28(5)	5.57
6	1	2.05(7)	2.18
3	2	14.29(6)	14.22
4	2	6.66(5)	6.62
6	2	1.14(15)	1.35
4	3	3.46(7)	3.55
5	3	1.58(9)	1.53
		l = 4	
0	0	15.69(15)	15.64
1	0	7.94(5)	7.93
2	0	7.25(5)	7.11
3	0	11.71(6)	12.10
4	0	4.42(6)	4.73
5	0	2.10(8)	1.93
6	0	2.58(7)	2.54
1	1	15.32(8)	15.26
2	1	7.02(4)	6.95
3	1	4.51(5)	4.38
4	1	5.72(5)	6.08
5	1	1.68(8)	2.00
2	2	10.47(7)	10.28
3	2	3.94(6)	3.61
4	2	1.99(7)	1.76
5	2	1.89(7)	2.10
3	3	4.31(7)	4.19
4	3	1.18(12)	1.22
4	4	1.14(17)	1.23
		l = 5	
1	0	53.11(25)	50.69
2	0	38.67(18)	37.86
4	0	12.91(7)	13.26
5	0	6.21(6)	6.10
2	1	29.62(11)	28.76
3	1	16.56(7)	16.53
5	1	3.87(6)	4.25
6	1	1.51(9)	1.68
3	2	10.68(5)	10.27
4	2	4.97(5)	4.98
4	3	2.69(5)	2.76
		l = 6	
0	0	42.23(39)	41.31
1	0	18.80(9)	18.99
2	0	13.89(7)	14.07
3	0	17.17(8)	17.24
4	0	4.29(6)	4.60
5	0	2.28(7)	2.40
6	0	1.93(9)	2.15
7	0	1.12(23)	0.54
1	1	31.05(17)	30.55
2	1	10.93(5)	10.35
3	1	6.19(4)	6.16
4	1	6.18(5)	6.27
5	1	1.37(10)	1.53
2	2	13.37(8)	13.18
3	2	3.63(6)	3.64
4	2	2.56(6)	1.88
5	2	1.81(7)	1.75
3	3	4.13(8)	3.98
4	4	1.33(24)	0.98
		l = 7	
1	0	13.45(8)	13.52
2	0	11.14(6)	11.15
4	0	4.99(6)	5.00
5	0	2.71(6)	2.86
2	1	9.16(5)	9.10
3	1	6.12(5)	6.18
5	1	1.96(7)	1.95
3	2	4.23(5)	4.14
4	2	2.32(6)	2.36
4	3	1.31(10)	1.36
		l = 8	
0	0	26.08(25)	26.42
1	0	11.80(8)	12.10
2	0	9.13(6)	9.29
3	0	11.72(7)	11.89
4	0	3.29(7)	3.16
5	0	1.86(9)	1.87
1	1	20.01(11)	20.08
2	1	7.01(5)	6.99
3	1	4.52(5)	4.42
4	1	4.62(5)	4.57
2	2	9.46(7)	9.27
3	2	2.78(6)	2.60
4	2	1.47(9)	1.45
3	3	2.91(8)	2.95
		l = 9	
1	0	8.77(6)	8.96
2	0	6.85(6)	6.90
4	0	2.70(7)	2.66
5	0	1.47(11)	1.49
2	1	5.41(5)	5.36
3	1	3.47(6)	3.38
6	1	0.86(41)	0.51
3	2	2.16(7)	2.16
4	2	1.35(10)	1.21
4	3	1.32(17)	0.66
		l = 10	
0	0	7.57(12)	7.90
1	0	3.71(8)	3.68
2	0	2.97(7)	3.00
3	0	4.22(7)	4.25
4	0	1.29(14)	1.30
5	0	1.10(16)	0.77
1	1	6.50(7)	6.41
2	1	2.48(6)	2.43
3	1	1.77(8)	1.64
4	1	1.79(8)	1.92
2	2	3.47(7)	3.47
3	2	1.29(10)	1.08
		l = 11	
1	0	6.14(6)	5.93
2	0	4.26(7)	4.60
4	0	1.74(10)	1.82
5	0	1.23(22)	0.91
2	1	3.50(6)	3.62
3	1	2.38(6)	2.23
5	1	1.39(22)	0.63
3	2	1.57(9)	1.44
		l = 12	
0	0	3.08(17)	2.66
1	0	1.18(14)	1.23
3	0	1.29(13)	1.40
1	1	2.16(9)	2.13
2	2	1.08(18)	1.14
		l = 13	
1	0	2.01(9)	1.85
2	0	1.33(13)	1.51

Table 1. (continued)

$|F_o|$ - $|F_c|$ tables for β-AgI at 123 K.

h	k	$\|F_o\|$	$\|F_c\|$
		l = 0	
2	0	57.51(37)	59.49
3	0	80.77(50)	82.59
4	0	29.66(19)	30.64
5	0	20.61(15)	21.24
6	0	25.64(17)	26.61
7	0	7.61(15)	7.88
8	0	5.10(16)	5.36
9	0	5.46(15)	5.81
2	1	49.50(27)	49.67
3	1	36.25(21)	36.31
4	1	48.24(26)	48.39
5	1	16.51(12)	15.74
6	1	10.82(11)	10.79
7	1	12.41(11)	12.67
8	1	3.52(15)	3.48
2	2	72.76(56)	72.07
3	2	26.74(15)	26.82
4	2	18.63(12)	18.59
5	2	23.92(14)	23.83
6	2	7.35(14)	7.20
7	2	5.08(15)	4.81
8	2	4.93(16)	5.30
3	3	38.50(29)	37.75
4	3	12.96(12)	12.76
5	3	8.47(13)	8.55
6	3	10.46(12)	10.40
7	3	3.07(17)	2.96
4	4	17.23(17)	17.29
5	4	5.41(15)	5.49
6	4	3.45(17)	3.51
5	5	7.01(19)	7.07
		l = 1	
1	0	49.09(32)	49.52
2	0	39.38(25)	40.36
3	0	3.56(22)	0.44
4	0	20.99(15)	21.79
5	0	14.62(13)	15.26
6	0	2.97(25)	0.91
7	0	6.75(15)	6.89
8	0	4.42(15)	4.92
2	1	33.68(19)	33.80
3	1	24.88(14)	25.03
4	1	2.64(25)	0.68
5	1	12.15(11)	12.12
6	1	8.00(13)	8.53
8	1	3.60(14)	3.62
3	2	19.22(12)	19.19
4	2	13.79(11)	13.63
6	2	6.45(15)	6.35
7	2	4.54(13)	4.52
4	3	10.11(12)	9.99
5	3	6.82(15)	7.11
7	3	3.15(17)	3.13
5	4	5.02(13)	5.05
6	4	3.67(15)	3.52
		l = 2	
1	0	49.20(32)	49.97
2	0	39.99(25)	40.93
3	0	58.83(38)	58.77
4	0	20.76(15)	21.24
5	0	14.66(13)	14.82
6	0	18.63(14)	19.09
7	0	5.95(16)	5.93
8	0	3.98(16)	3.90
9	0	4.29(14)	4.55
1	1	80.93(62)	79.17
2	1	33.81(19)	34.02
3	1	24.59(14)	24.97
4	1	34.10(19)	34.06
5	1	11.26(11)	11.26
6	1	7.84(13)	7.69
7	1	9.43(11)	9.44
8	1	2.75(19)	2.82
2	2	52.06(40)	50.86
3	2	18.90(12)	18.66
4	2	13.05(11)	13.06
5	2	17.42(12)	17.17
6	2	5.58(15)	5.42
7	2	3.68(16)	3.54
3	3	27.13(22)	26.73
4	3	9.61(12)	9.18
5	3	6.26(16)	6.21
6	3	7.94(13)	7.85
7	3	2.45(22)	2.40
4	4	12.82(16)	12.67
5	4	4.29(15)	4.16
6	4	3.05(21)	2.67
5	5	5.80(21)	5.47
		l = 3	
1	0	89.24(58)	88.12
2	0	77.37(48)	76.49
4	0	43.08(27)	43.39
5	0	28.91(18)	29.29
7	0	12.67(12)	12.41
8	0	7.09(14)	7.36
2	1	66.90(37)	66.08
3	1	49.87(27)	49.45
5	1	23.58(14)	23.50
6	1	14.70(11)	14.87
8	1	5.38(15)	5.72
3	2	38.70(22)	37.95
4	2	26.59(15)	26.06
6	2	11.32(11)	11.18
7	2	6.50(14)	6.70
4	3	18.91(12)	18.69
5	3	12.18(12)	12.15
7	3	4.65(14)	4.72
5	4	8.43(13)	8.24
6	4	5.15(13)	5.08
		l = 4	
0	0	11.19(18)	11.26
1	0	6.03(13)	5.83
2	0	6.16(16)	5.98
3	0	11.38(12)	11.81
4	0	5.29(18)	5.62
5	0	4.03(18)	3.73
6	0	6.57(16)	6.90
7	0	3.01(23)	3.24
8	0	2.17(29)	1.59
1	1	12.24(14)	12.05
2	1	6.32(14)	6.16
3	1	5.70(15)	5.24
4	1	9.20(12)	9.32
5	1	4.28(14)	4.31
6	1	3.22(19)	2.50
7	1	4.43(14)	4.62
2	2	11.49(15)	11.24
3	2	5.23(15)	5.02
4	2	4.30(18)	3.72
5	2	6.97(14)	6.50
6	2	3.02(21)	2.93
3	3	8.25(17)	8.21
4	3	3.71(18)	3.52
6	3	4.13(14)	4.08
4	4	6.34(21)	5.47
5	4	2.48(29)	2.21
5	5	3.17(24)	3.16
		l = 5	
1	0	72.23(45)	70.84
2	0	61.19(38)	61.16
4	0	35.09(21)	35.75
5	0	24.07(16)	24.62
7	0	10.44(15)	10.82
8	0	5.97(16)	6.44
2	1	52.93(28)	53.10
3	1	40.95(23)	40.36
5	1	19.98(12)	20.03
6	1	12.82(11)	12.83
8	1	5.14(15)	5.07
3	2	32.08(17)	31.51
4	2	22.36(13)	22.05
6	2	10.16(12)	9.76
7	2	5.81(15)	5.88
4	3	16.38(12)	16.06
5	3	10.61(12)	10.56
5	4	7.77(13)	7.24
6	4	4.57(12)	4.49
		l = 6	
0	0	57.77(61)	57.02
1	0	28.55(19)	27.97
2	0	23.61(16)	23.97
3	0	37.03(23)	37.29
4	0	13.64(13)	13.89
5	0	9.96(14)	9.94
6	0	13.44(13)	13.35
7	0	4.01(17)	4.55
8	0	2.77(22)	2.94
1	1	49.92(38)	49.22
2	1	20.31(12)	20.68
3	1	15.62(11)	15.86
4	1	22.43(13)	22.77
5	1	8.11(13)	7.94
6	1	5.59(17)	5.42
7	1	6.66(14)	6.91
8	1	2.00(29)	2.40
2	2	32.76(25)	32.73
3	2	14.33(12)	12.33
4	2	9.03(12)	8.85
5	2	12.15(11)	12.06
6	2	4.28(15)	4.10
7	2	2.87(19)	2.64
3	3	18.46(17)	18.21
4	3	6.50(16)	6.44
5	3	4.39(15)	4.39
6	3	5.56(16)	5.73
4	4	9.09(18)	9.01
5	4	3.32(21)	3.04
		l = 7	
1	0	23.85(16)	23.02
2	0	20.10(14)	20.29
4	0	12.67(13)	13.02
5	0	9.80(15)	9.80
7	0	4.90(14)	4.98
8	0	3.02(22)	3.51
2	1	17.75(12)	18.02
3	1	14.56(11)	14.44
5	1	8.66(12)	8.17
6	1	5.80(17)	5.95
3	2	11.92(11)	11.80
4	2	9.17(12)	8.96
6	2	4.91(13)	4.62
7	2	3.10(19)	3.25
4	3	7.17(14)	6.93
5	3	5.34(16)	5.07
5	4	3.48(17)	3.70
		l = 8	
0	0	53.43(57)	53.01
1	0	25.72(17)	25.92
2	0	22.81(16)	22.71
3	0	37.24(23)	36.37
4	0	13.92(13)	13.78
5	0	10.31(13)	10.26
6	0	13.24(13)	13.70
7	0	4.48(16)	4.43
8	0	2.88(23)	3.12
1	1	48.31(37)	46.58
2	1	19.93(13)	19.91
3	1	15.46(10)	15.75
4	1	23.10(13)	23.05
5	1	7.94(14)	7.97
6	1	5.51(17)	5.71
7	1	6.75(16)	6.99
2	2	32.15(25)	32.31
3	2	12.05(10)	12.38

$|F_o|$ - $|F_c|$ tables for β-AgI at 123 K (continued).

h	k	$\|F_o\|$	$\|F_c\|$
4	2	9.10(12)	9.13
5	2	12.51(12)	12.38
6	2	4.04(16)	4.01
3	3	18.34(14)	18.60
4	3	6.84(13)	6.56
5	3	4.93(14)	4.57
6	3	5.77(14)	5.77
4	4	9.70(18)	9.21
5	4	3.28(21)	3.03
		l = 9	
1	0	15.82(13)	16.20
2	0	14.24(13)	14.44
4	0	9.28(13)	9.49
5	0	6.92(15)	7.38
7	0	3.45(18)	3.81
2	1	12.87(11)	12.91
3	1	10.33(11)	10.55
5	1	5.57(15)	6.08
6	1	4.08(15)	4.63
3	2	8.85(12)	8.66
4	2	6.83(14)	6.73
6	2	3.47(16)	3.52
4	3	5.05(14)	5.20
5	3	3.80(16)	3.89
5	4	2.79(20)	2.81
		l = 10	
0	0	23.65(28)	24.19
1	0	11.27(13)	11.69
2	0	10.10(13)	10.48
3	0	17.33(13)	17.48
4	0	6.93(16)	6.85
5	0	4.86(18)	5.29
6	0	7.42(15)	7.44
7	0	2.62(24)	2.56
1	1	20.45(18)	21.64
2	1	9.32(12)	9.37
3	1	7.73(13)	7.68
4	1	10.41(12)	11.76
5	1	3.93(16)	4.26
2	2	15.09(16)	15.78
3	2	6.33(15)	6.25
4	2	4.77(14)	4.78
5	2	6.37(14)	6.81
3	3	9.48(17)	9.75
4	3	3.39(18)	3.59
4	4	5.41(19)	5.25
		l = 11	
1	0	20.90(15)	21.18
2	0	18.77(14)	18.95
4	0	12.57(13)	12.47
5	0	8.76(14)	9.22
7	0	4.34(14)	4.49
2	1	17.57(12)	17.01
3	1	13.97(11)	13.76
5	1	7.60(13)	7.67
6	1	5.01(13)	5.28
3	2	11.55(11)	11.25
4	2	8.66(13)	8.36
4	3	6.47(15)	6.31
5	3	4.30(14)	4.37
		l = 12	
0	0	6.48(29)	6.56
1	0	3.15(22)	3.22
2	0	3.20(21)	3.02
3	0	6.05(16)	5.53
4	0	2.97(20)	2.52
6	0	3.23(20)	3.29
1	1	6.40(21)	6.19
2	1	3.51(17)	2.89
4	1	4.84(13)	4.41
2	2	5.38(19)	5.23
5	2	3.00(17)	3.09
3	3	4.18(20)	3.92
		l = 13	
1	0	12.77(13)	12.17
2	0	11.46(13)	11.02
4	0	7.75(15)	7.57
5	0	5.86(17)	5.72
2	1	10.59(12)	10.02
3	1	8.80(12)	8.27
5	1	4.82(13)	4.85
3	2	7.35(13)	6.89
4	2	5.42(14)	5.23
		l = 14	
0	0	9.55(24)	10.11
1	0	4.65(16)	4.90
2	0	4.47(16)	4.45
3	0	7.58(15)	7.62
4	0	2.85(23)	3.10
5	0	2.10(29)	2.39
1	1	9.05(17)	9.19
2	1	4.11(15)	4.05
3	1	3.34(18)	3.37
4	1	5.13(14)	5.32
2	2	6.85(20)	6.95
3	2	2.62(22)	2.82
4	2	2.15(24)	2.17
3	3	4.24(19)	4.46
		l = 15	
1	0	3.73(18)	3.84
2	0	3.59(18)	3.61
4	0	2.78(23)	2.79
2	1	3.30(18)	3.38
3	1	2.84(19)	2.99
3	2	2.14(25)	2.62
		l = 16	
0	0	5.79(32)	6.93
1	0	3.07(22)	3.36
2	0	2.86(23)	3.07
3	0	4.92(16)	5.29
1	1	6.20(20)	6.33
2	1	2.69(20)	2.80
2	2	4.89(23)	4.84
		l = 17	
1	0	2.84(21)	3.18

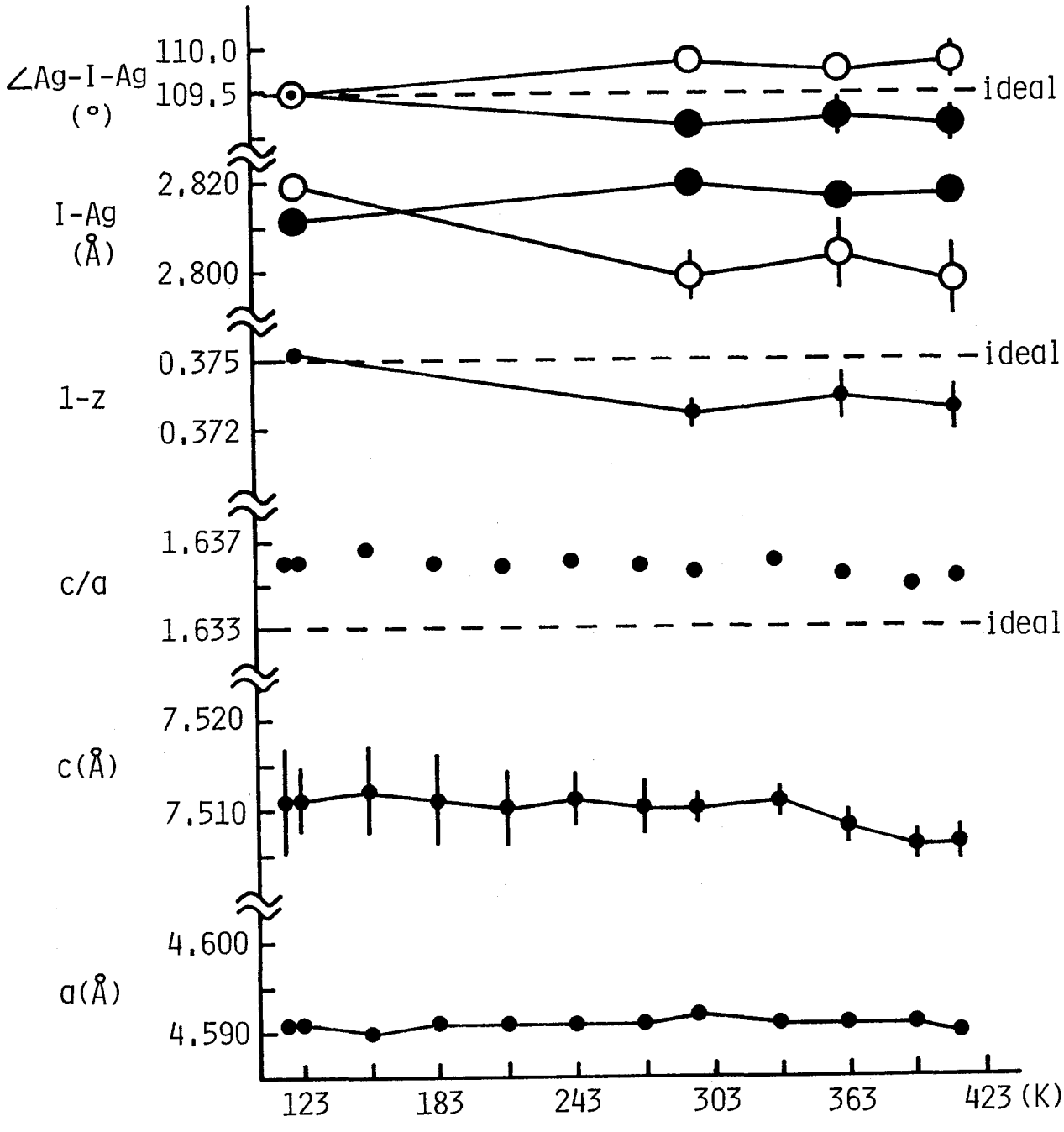

Fig. 1. The temperature variations of cell dimensions (a,c), axial ratio (c/a), coordinate of Ag atom (1-z), bond distances (Ag-I) and angles(∠Ag-I-Ag) in β-AgI. Open circles (○) : apical ones (i.e. including the apex of trigonal pyramid), solid circles (●) : basal ones.

to one-phonon process of acoustic mode (Sakata & Harada, 1976). The program TDS2 (Stevens, 1974) was used for the evaluation of the TDS correction factor. The elastic constants for each temperature were taken from Fjeldly & Hanson (1974).

2-4 Refinement of the structure

Refinements were carried out using the program RFINE4 (Finger & Prince, 1975). Cumulant expansion up to the fourth-order terms was applied to the temperature factors. The temperature factor T(h) is expressed as $T(h) = \exp[(i^2/2!)\Sigma\Sigma\beta_{jk}h_jh_k + (i^3/3!)\Sigma\Sigma\Sigma\gamma_{jkl}h_jh_kh_l + (i^4/4!)\Sigma\Sigma\Sigma\Sigma\delta_{jklm}h_jh_kh_lh_m]$ (Johnson, 1969 and 1970), where β_{jk}, γ_{jkl} and δ_{jklm} are the coefficients in the second-, third- and fourth-order cumulant terms, respectively. In order to calculate T(h) with harmonic model for β-AgI, four independent coefficients β_{jk} and the positional parameter z for Ag are necessary. The anharmonic model requires additional fourteen independent coefficients γ_{jkl} and δ_{jklm} (seven for each atom); $\gamma_{111}(=-\gamma_{222}=2\gamma_{112}=-2\gamma_{122})$, γ_{333}, $\gamma_{113}(=\gamma_{223}=2\gamma_{123})$, $\delta_{1111}(=\delta_{2222}=2\delta_{1112}=2\delta_{1222}=2\delta_{1122})$, δ_{3333}, $\delta_{1113}(=-\delta_{2223}=2\delta_{1123}=-2\delta_{1223})$ and $\delta_{1133}(=\delta_{2233}=2\delta_{1233})$ [referred to International Tables for X-ray Crystallography, Vol.IV]. In addition, a scale factor and an isotropic extinction factor are included in the least-squares refinements. Simultaneous refinement of the four independent terms, $\gamma_{333}(I)$, $\gamma_{333}(Ag)$, $\gamma_{113}(I)$, $\gamma_{113}(Ag)$ was unsuccessful because of the strong correlations between $\gamma_{333}(I)$ and $\gamma_{333}(Ag)$, and between $\gamma_{113}(I)$ and $\gamma_{113}(Ag)$. Then constraints of $\gamma_{333}(I)=-\gamma_{333}(Ag)$ and $\gamma_{113}(I)=-\gamma_{113}(Ag)$ were adopted, which are the same as used by

Kihara & Donnay (1985). Atomic scattering factors for neutral atoms and correction terms for anomalous dispersion were taken from International Tables for X-ray Crystallography, Vol.IV (1974).

The alternatives of indexing hkl and $\bar{h}\bar{k}\bar{l}$ are possible because of the non-centrosymmetric structure. The correct choice was decided based on the comparison of the final R-factors ($=\Sigma(||F_o| - |F_c||)/\Sigma|F_o|$) of both cases. The difference in the R-factors between the alternatives was 0.2 % for the 297 K data. The results of the refinements and the experimental conditions are given in Table 1. The refinements based on the anharmonic model remarkably reduced the R-factor compared with those based on the harmonic model. Consequently it is concluded that the anharmonic model is essential to the β-AgI structure. Maxima in positive and negative electron densities in the difference-Fourier maps for the data at 413 K were 0.28 and -0.43 $e\mathring{A}^{-3}$, respectively after the refinements with the anharmonic model. Bond distances and angles are plotted versus temperatures in Fig. 1. The P.D.F. maps computed using PDFED program (Kihara, Matsumoto & Imamura, 1986) are presented in Fig. 2.

The effective one-particle potential (O.P.P.) of an isolated atom, V(r), is derived from the P.D.F. by the following equation (Willis, 1969; Bachmann & Schulz, 1984),

$$V(r)=V_0-kT\ln[pdf(r)]$$

where k is the Boltzmann constant, T is absolute temperature, and V_0 is an arbitrary numerical factor. The O.P.P. curves of both atoms along the basal Ag-I bond at individual temperature are

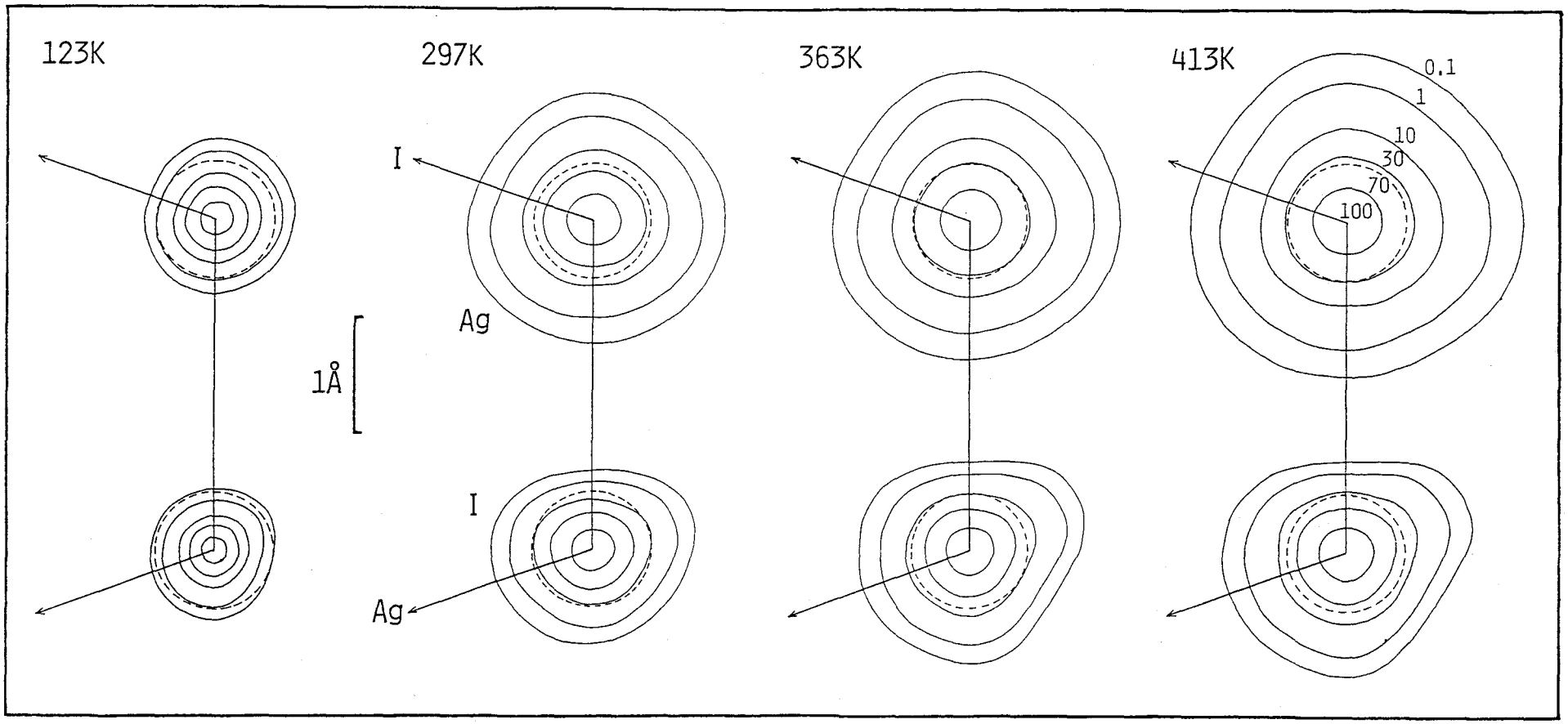

Fig. 2. The probability density function in $(11\bar{2}0)$. The contours are scaled to 100 units at the centeres. The broken lines are 0.5 Å from the centers.

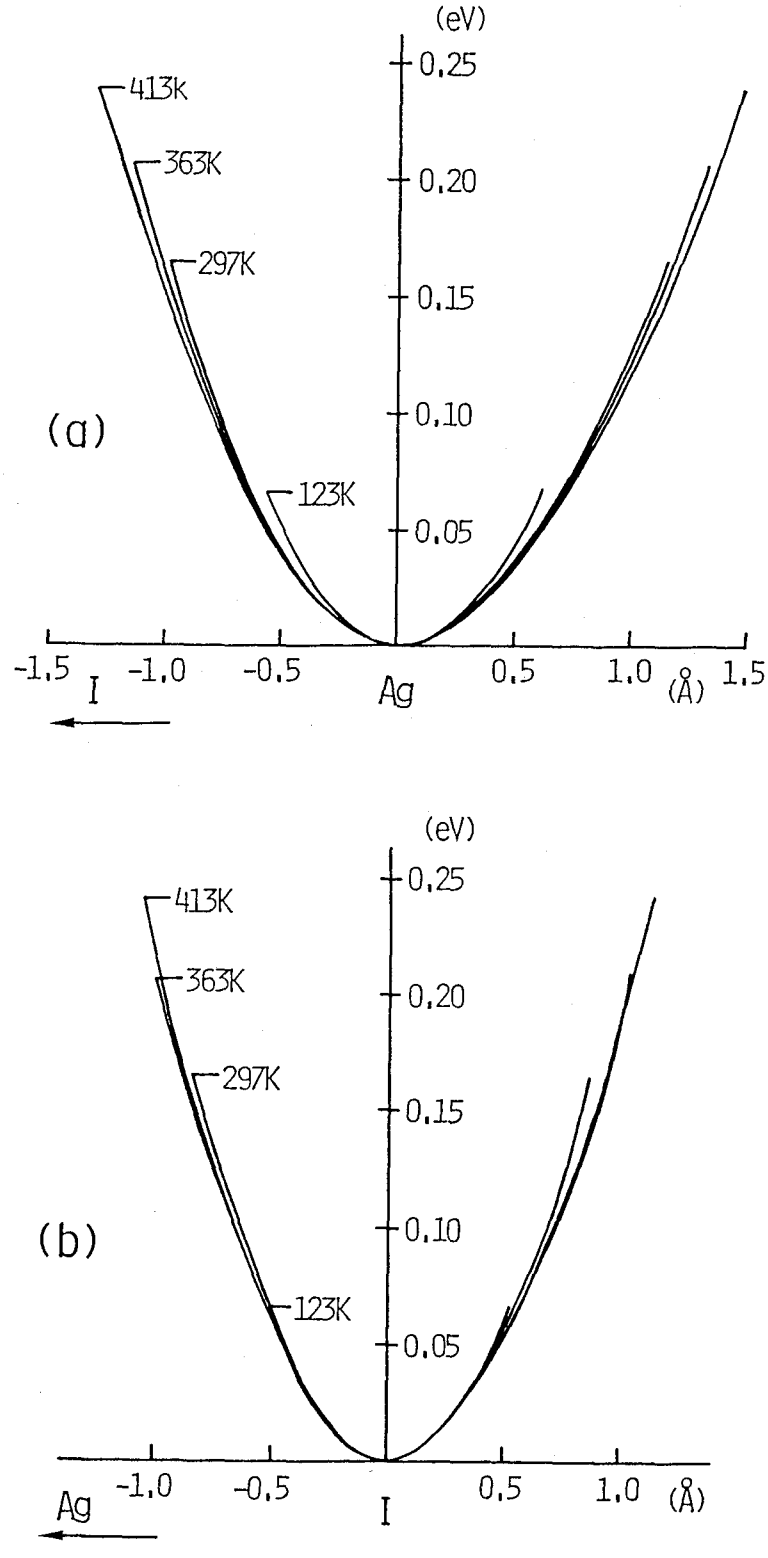

Fig. 3. Effective one-particle potentials of Ag (a) and I (b) atoms in β-AgI along the basal Ag-I bond, showing the potential curves at 123, 297, 363 and 413 K.

plotted in Fig. 3.

3) Results and Discussion

3-1 Anharmonic thermal vibrations and forbidden reflections

The wurtzite-type structure belongs to space group $P6_3mc$. Because both Ag and I atoms are located in 2b positions of Wyckoff letter, site symmetry of which is 3m, the systematic absence of reflections has the extra conditions provided that atomic thermal vibrations are harmonic. That is, reflections of hkl with h-k=3n are absent if l is odd in addition to the normal systematic absence. However, these reflections were observed to have intensities owing to the strong anharmonicity of thermal vibrations in β-AgI (Fig. 4). Agreement of the observed structure amplitudes among the equivalent reflections was sufficiently good. Agreement of the observed and calculated structure amplitudes for these reflections is well in the anharmonic model mentioned above (Table 2).

Whiteley, Moss & Barnea (1978) reported that the paired reflections, 701 and 531, with the same l value (non-symmetry-related reflections with the same Bragg angle) of the wurtzite-type structure can have different amplitudes in the anharmonic model, whereas they must have the same amplitudes in the harmonic one. In β-AgI, the significant differences of amplitudes between 701 and 531 were observed (Table 3). This characteristic is the same as in other wurtzite-type structures (Stevenson & Barnea, 1984; Kihara & Donnay, 1985).

The P.D.F. maps (Fig. 2) revealed that the motions of both

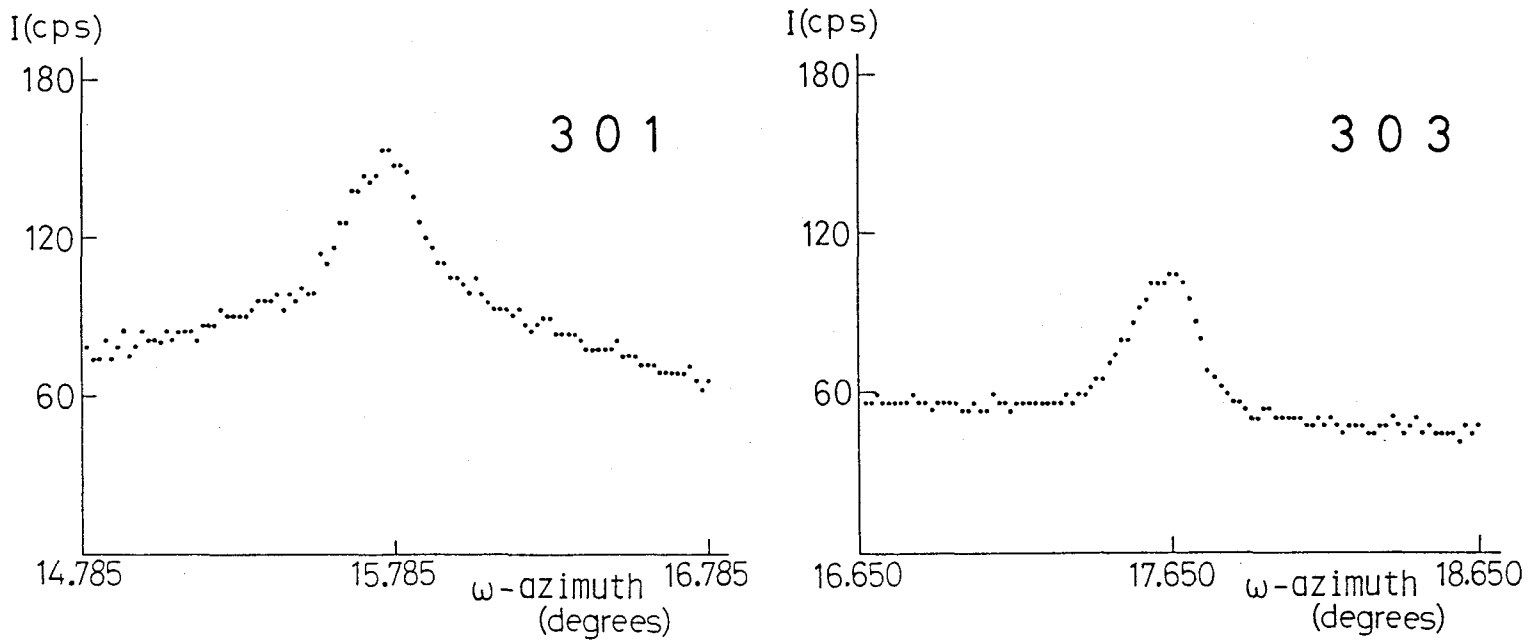

Fig. 4. Examples of the observed reflections violating the extra conditions of the systematic absences owing to the anharmonic thermal vibrations. The intensity distributions (count/sec) were obtained by θ-2θ scan mode.

Table 2. Observed amplitudes of the reflections violating the extra conditions of the systematic absences at room temperature. These structure amplitudes can be explained by the anharmonic model.

h	k	l	$\|F_o\|$	$\|F_c\|$harmonic	$\|F_c\|$anharmonic
3	0	1	1.69(9)	0.0	1.25
3	0	3	1.19(11)	0.0	1.08
4	1	1	1.37(9)	0.0	0.92

Table 3. Structure amplitudes of reflections 701 and 531 at 123K. $|F_c|$s were calculated with anharmonic model.

h	k	l	$\|F_o\|$	$\|F_c\|$	$\sigma\|F_o\|$	h	k	l	$\|F_o\|$	$\|F_c\|$	$\sigma\|F_o\|$
7	0	0	7.61	7.88	0.15	5	3	0	8.47	8.55	0.13
7	0	1	6.75	6.89	0.15	5	3	1	6.82	7.11	0.15
7	0	2	5.95	5.93	0.16	5	3	2	6.26	6.21	0.16
7	0	3	12.67	12.41	0.12	5	3	3	12.18	12.15	0.12
7	0	5	10.44	10.82	0.13	5	3	5	10.61	10.56	0.12
7	0	6	4.01	4.55	0.17	5	3	6	4.39	4.39	0.15
7	0	7	4.90	4.98	0.14	5	3	7	5.34	5.07	0.16
7	0	8	4.48	4.43	0.16	5	3	8	4.93	4.57	0.14
7	0	11	4.34	4.49	0.14	5	3	11	4.30	4.37	0.14

atoms are strongly anharmonic even at lower temperature. The O.P.P. is given with the assumption that an atom independently vibrates within the range of the average potential caused by the interaction with all the other atoms in the crystal. The O.P.P. curves of both atoms (Fig. 3) revealed the softening of the potentials with increasing temperature, and should also justify the validity of the thermal tensor coefficients (Table 1) obtained independently from each data set.

3-2 Structure changes and temperature dependence of anharmonic thermal vibrations

Fig. 1 shows structure changes of β-AgI as a function of temperature up to the vicinity of phase transition point. In the ideal wurtzite-type structure based on the hexagonal closest packing, the axial ratio (c/a), a variable coordinate 1-z and the bond angle are $\sqrt{8/3}$, 0.375 and 109.47°, respectively. With increasing temperature, the 1-z and the bond angles of β-AgI deviate from the ideal values, whereas the axial ratio which is slightly larger than the ideal value at lower temperature approaches to the ideal one. The manner of the decrease in axial ratio with temperature is similar to other wurtzite-type compounds (e.g. Mair & Barnea, 1975; Kihara & Donnay, 1985). The axial ratio is closely related to the elongation or compression of AgI_4 or Ag_4I tetrahedra along the c-axis. The c-axis becomes short when the temperature is raised. With increasing temperature, the apical Ag-I distance (parallel to the c-axis) becomes short whilst the other three basal Ag-I distances become slightly larger. The three apical bond angles become larger

whilst the other three basal bond angles become smaller. The shortening of the apical bond distance makes the three apical bond angles larger as illustrated in Fig. 5.

These structural changes versus temperature can be explained from the anharmonic thermal vibration, especially of the iodine atom. The anharmonic thermal vibrations of both atoms in β-AgI are demonstrated in the P.D.F. maps (Fig. 2). The anisotropy of thermal motion of the I atom is getting predominant compared with that of the Ag atom at higher temperature. If we compare the magnitudes of vibrations of I atoms along four antibonding directions, the magnitude along the c-axis is smaller than the other three equivalent magnitudes. This causes a centroid of thermal vibration of the I atom to be relatively deviated toward the apical Ag with increasing temperature, which is shown schematically in Fig. 5.

3-3 Relation of anharmonicity to the phase transition and to the ionic conduction

The transition from β- to α-AgI of body-centered lattice was discussed based on the displacement of iodine atom by Burley (1967) and Buhrer & Bruesch (1975). In Fig. 2, it is noted that, at higher temperature, the magnitudes of anharmonic thermal motion of the I atom are larger along the three antibonding directions. This makes the structure closer into a body-centered cubic arrangement of α-AgI. In β-AgI, Bührer & Brüesch (1975) observed a low-lying optical mode which makes the large contribution to the thermal motion. So they also demonstrated that this mode plays an important role in the displacement of the

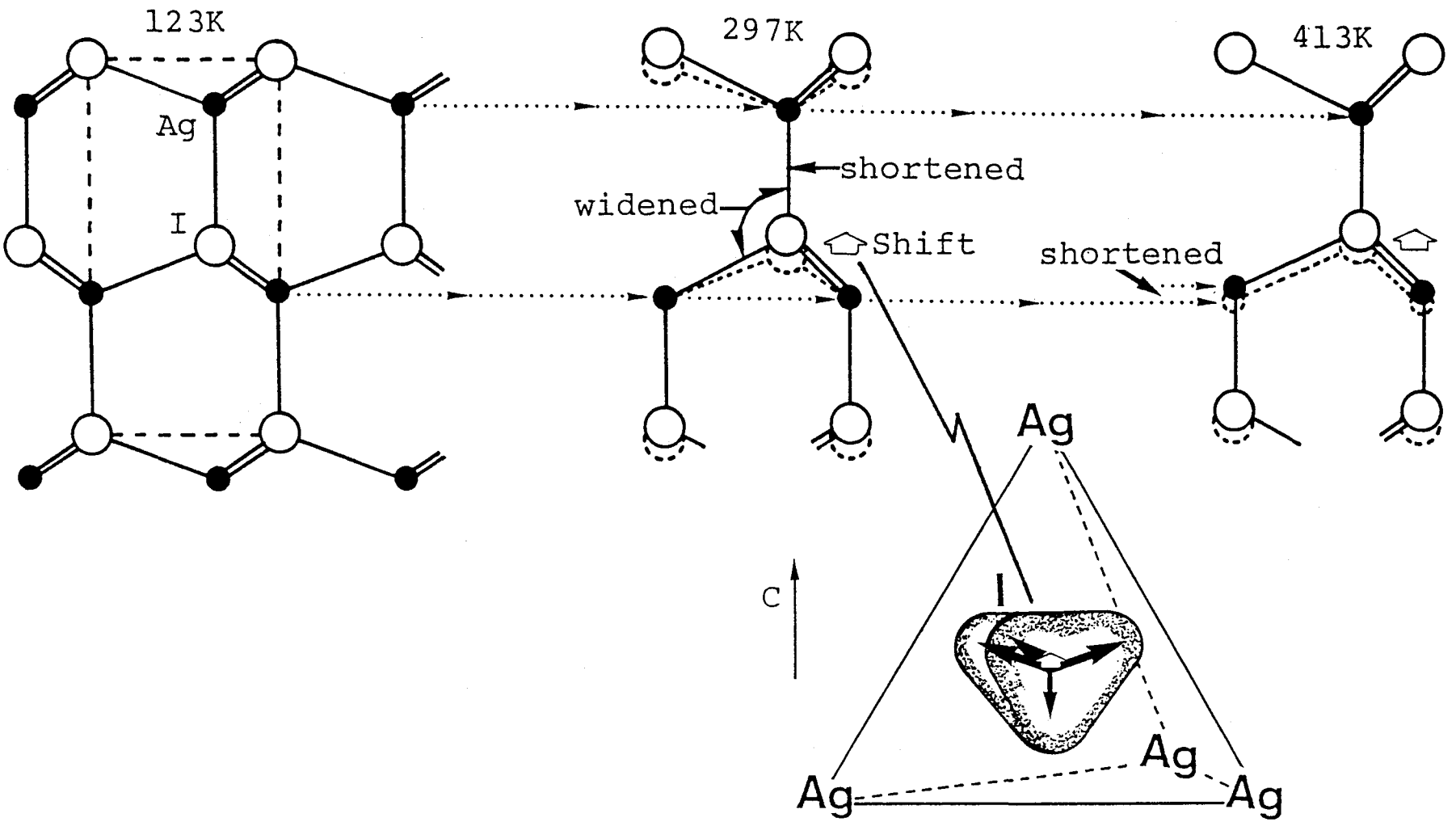

Fig. 5. Schematic representations of the structural changes in β-AgI with temperature. The position of the I atom shifts (white arrow) along the c-axis owing to the anharmonic thermal vibrations. Thus the c-axis becomes short with increasing temperature.

iodine arrangement at the phase transition. The displacements of the atoms in this mode mainly change the tetrahedral angles and slightly vary the Ag-I distances. The P.D.F. for the I atom along the antibonding direction of basal Ag atoms will evidently satisfy the matter. Therefore, their interpretation of thermal motion applying a lattice-dynamical treatment agrees with our results obtained by the analysis based upon the intensities of the Bragg reflections.

The temperature factors of the mobile Ag atoms are larger than those of the I atoms (Table 1, Fig. 2). This accords well with the results of lattice-dynamical studies (Bührer & Brüesch, 1975; Bührer, Nicklow & Brüesch, 1978); e.g. their theoretical r.m.s. radial displacements of the Ag atoms at room temperature (0.292 Å) are comparable well with our experimental ones (0.28(1) Å: obtained from the equivalent isotropic temperature factor of the Ag atom at 297 K). The ionic conductivity of β-AgI is due to Frenkel defects. The formation of Frenkel defects is closely related to the thermal motion of ions (Frenkel, 1926). Hence, the knowledge of the thermal motion should be of primary importance for understanding of the ionic conduction. On the measurements of ionic conductivity on single crystals of β-AgI, it was found that the silver-ion conductivity is essentially isotropic (Cava & Rietman, 1984). So it can be said that the appreciable anisotropy of the thermal motion in the hexagonal close-packed structure is not directly related to the macroscopic characteristics of ionic conduction in β-AgI.

3-4 Structural variations in wurtzite-type compounds

The wurtzite-type structure is closely related to the sphalerite-type structure. Both structures are classified into covalently bonded compounds. The notable difference in the environment around atoms in both structures is shown in Fig. 6. It is well known that wurtzite has a larger Madelung constant and it is more ionic than sphalerite. Table 4 presents the bond distances, bond angles and ratios of the apical distance to the basal one for wurtzite-type compounds. As shown by the dotted lines in Fig. 6, the electrostatic interaction between an atom and its third neighbors in the wurtzite-type structure is greater than that in the sphalerite-type structure. Thus the apical distances for most of the compounds are longer than the basal ones except for β-AgI at room temperature. This will be due to the electrostatic attraction and/or the difference in the contribution to hybridization between three directions and another symmetrically non-equivalent direction. In β-AgI (Fig. 1), the apical distance is longer than the basal ones at 123 K. However, it becomes shorter at higher temperature. Such a variation, as described above, results from the shortening of the apical bond distance owing to the anharmonic thermal vibrations.

With an increase in ionicity defined by Phillips (1970), the ratios (M-N*)/(M-N) decrease and accordingly the apical bond angles increase (Table 4). Since the electrostatic interaction should increase with the ionicity (f_i), the decrease in the ratios (M-N*)/(M-N) with the increase in ionicity is inconsistent. The thermal vibrations are generally dependent on the bonding force and thus the anharmonicity will cause the

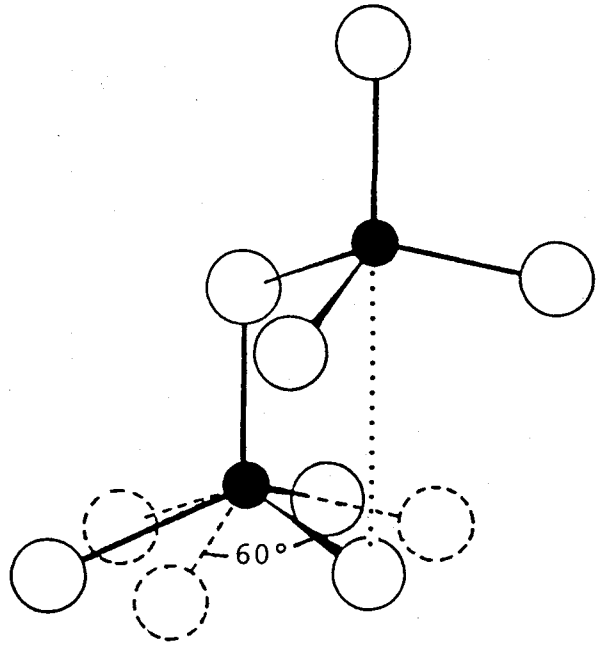

Fig. 6. Difference in the configurations of third-neighbor between wurtzite-type (solid line) and shalerite-type (broken line) structure.

Table 4. Observed bond distances and angles of various wurtzite-type compounds in order of decreasing the Phillips' ionicity f_i.

	f_i	M - N^* (Å) apical	M - N(Å) basal	$\frac{M - N^*}{M - N}$	$\angle N^*$-M-N(°) apical	$\angle$N-M-N(°) basal	References	R-factor
AgI(297K)	0.77	2.798(6)	2.819(2)	0.993	109.8(1)	109.1(1)	This study	0.029
AgI(123K)	0.77	2.819(3)	2.811(1)	1.003	109.5(1)	109.5(1)	This study	0.023
CdSe	0.70	2.6355(5**)	2.6299(6)	1.002	109.31(1)	109.63(2)	Stevenson, Milanko & Barnea,1984	0.007
CdS	0.69	2.5318(7**)	2.5263(6)	1.002	109.05(1)	109.89(2)	Srevenson & Barnea,1984	0.009
ZnO(473K)	0.62	1.9892(9)	1.9762(6)	1.007	108.12(3)	110.79(3)	Kihara & Donnay,1985	0.010
ZnO(293K)	0.62	1.9884(8)	1.9738(4)	1.007	108.12(2)	110.79(2)	Kihara & Donnay,1985	0.019
BeO	0.60	1.657(7)	1.646(2)	1.007	108.8(2)	110.1(2)	Sabine & Hogg,1969	0.036
GaN	0.50	1.956(4)	1.949(1)	1.004	109.1(1)	109.8(1)	Schulz & Thiemann,1977	0.041
AlN	0.45	1.903(2)	1.889(1)	1.007	108.11(4)	110.80(3)	Schulz & Thiemann,1977	0.015

N^* indicates the apical atom of trigonal pyramid.

** Calculated by assuming that the errors of cell dimensions were 0.001 Å.

structural variations in the wurtzite-type compounds. Martin (1970) and Fjeldly & Hanson (1974) observed that the elastic properties of the covalently bonded sphalerite-type and wurtzite-type compounds show a systematic tendency toward a lattice instability as the ionicity increases. Koto & Schulz (1979) have reported that the diffuse scattering increases in intensity with increasing the ionicity. The tendency toward the lattice instability should result in the increase in anharmonicity.

4) References

BEYELER,H.U., BRÜESCH,P., HIBMA,T. & BÜHRER,W. (1978). Phys. Rev. B18, 4570-4575

BACHMANN,R. & SCHULZ,H. (1984). Acta Cryst. A40, 668-675

BÜHRER,W. & BRÜESCH,P. (1975). Solid State Comm. 16, 155-158

BÜHRER,W., NICKLOW,R.M. & BRÜESCH,P. (1978). Phys. Rev. B17, 3362-3370

BURLEY,G. (1967). Acta Cryst. 23, 1-5

CAVA,R.J., REIDINGER,F. & WUENSCH,B.J. (1977). Solid State Comm. 24, 411-416

CAVA,R.J. & RIETMAN,E.A. (1984). Phys. Rev. B30, 6896-6902

COCHRANE,G. (1967). Brit. J. Appl. Phys. 18, 687-688

FINGER,L.W. & PRINCE,E. (1975). Natl Bur. Stand (US) Tech. Note No. 854

FJELDLY,T.A. & HANSON,R.C. (1974). Phys. Rev. B10, 3569-3577

FRENKEL,J. (1926). Z. Phys. 35, 652-669

International Tables for X-ray Crystallography (1974). Vol. IV. Birmingham;Kynoch Press.

JOHNSON,C.K. (1969). Acta Cryst. A25, 187-194

JOHNSON,C.K. (1970). Thermal Neutron Diffraction, edited by B.T.M. Willis, Chap. 9. Oxford; Clarendon Press

KIHARA,K. & DONNAY,G. (1985). Canad. Miner. 23, 647-654

KIHARA,K., MATSUMOTO,T. & IMAMURA,M. (1986). Z. Krist. In press.

KOTO,K. & SCHULZ,H. (1979). Acta Cryst. A35 971-974

MAIR,S.L. & BARNEA,Z. (1975). Acta Cryst. A31, 201-207

MARTIN,R.M. (1970). Phys. Rev. B1, 4005-4011

PHILLIPS,J.C. (1970). Rev. Mod. Phys. 42, 317-356

PILTZ,R.O. & BARNEA,Z. (1987). J. Appl. Cryst. 20, 3-7

SABINE,T.M. & HOGG,S. (1969). Acta Cryst. B25, 2254-2256

SAKATA,M. & HARADA,J. (1976). Acta Cryst. A32, 426-433

SCHULZ,H. & THIEMANN,K.H. (1977). Solid State Comm. 23, 815-819

STEVENS,E.D. (1974). Acta Cryst. A30, 184-189

STEVENSON,A.W., MILANKO,M. & BARNEA,Z. (1984). Acta Cryst. B40, 521-530

STEVENSON,A.W. & BARNEA,Z. (1984). Acta Cryst. B40, 530-537

WHITELEY,B., MOSS,G. & BARNEA,Z. (1978). Acta Cryst. A34, 130-136

WILLIS,B.T.M. (1969). Acta Cryst. A25, 277-300

Chapter 3.

Variations of Ag bonding distances in the $AgBr_{1-x}I_x$ rock-salt type solid-solution by X-ray and EXAFS analyses

1) Introduction

Silver bromide exhibits a considerable ionic conductivity even at room temperature by the diffusion of silver ions through the lattice. The migration of silver ions is applied in the photographic process.

The dynamical and structural properties of the silver halides are governed by the competition of ionic bonding versus covalent bonding (Bührer et al., 1978). Covalent character in the AgBr-AgI system is increasing from AgBr to AgI. In the rock-salt type structure of AgBr, each Ag ion is octahedrally surrounded by six Br ions and vice versa. On the other hand AgI adopts the tetrahedrally coordinated wurzite or zincblende type structure. Because AgBr differs from AgI in the nature of chemical bonding and in the structure type, the solid-solution range for each structure type is limited (Stasiw & Teltow, 1949).

In the $AgBr_{1-x}I_x$ rock-salt type solid-solution($0 \leq x \leq 0.4$ at 293 K), it is expected that the local environments of the I ions (e.g. the bond distances to the Ag ions) differ from those of the Br ions. Nevertheless, positionally averaged information for both ions has been obtained by the diffraction studies because the Br and I ions occupy the crystallographically equivalent positions. EXAFS spectroscopy is a useful probe of the local environment around a particular kind of absorbing atom in the random solid-solution. We have already reported on an important feature of the local structure of the solid-solution at 123 K in a brief publication (Yoshiasa et al., 1986).

This work presents an EXAFS structural analysis of the $AgBr_{1-x}I_x$ rock-salt type solid-solution at room temperature in

order to study the correlation between the substituted I ions and the structure. The crystal structure analyses using the single crystal X-ray diffraction methods have also been carried out, and then the local structure and chemical bond of the solid-solution are discussed.

2) Experimental

2-1 Synthesis

AgBr and AgI (99.99%, Koso Chem. Co., Ltd.) in powder form were used as starting materials without further purification. Appropriate amount of a well-blended mixture of AgBr and AgI (0-40 m/o) was first heated under the iodine atmosphere (about 100 mmHg) at 973 K for 40 hours in quartz tube and then quenched into cold water. The quenched samples were annealed at 443 K for 20 days and cooled down to room temperature. Special precaution was paid to prevent from exposure to light. Transparent yellow crystals were confirmed the rock-salt type by X-rays. We have measured the Raman spectra of the solid-solutionand the formation of the rock-salt type structure are supported because the first-order Raman scattering is forbidden. The rock-salt type solid-solution was synthesized with the compositions of 0-40 m/o AgI content. The lattice constants are given in Table 1 and Fig. 1.

2-2 X-ray single crystal structure analysis

All the single crystals for X-ray study were made to spherical shape. The lattice constant determination and intensity data collection of the Bragg reflections were made on a Rigaku AFC5FOS four circle diffractometer at room temperature. MoKα

Table 1. Cell parameters(a) and bond distances(d) in Å for the $AgBr_{1-x}I_x$ solid-solution. d[Ag-(Br,I)]=a/2.

	a	d [Ag-(Br,I)]
AgBr	5.776(1)	2.888
$AgBr_{0.90}I_{0.10}$	5.815(2)	2.908
$AgBr_{0.80}I_{0.20}$	5.851(2)	2.926
$AgBr_{0.75}I_{0.25}$	5.868(2)	2.934
$AgBr_{0.70}I_{0.30}$	5.889(2)	2.945
$AgBr_{0.65}I_{0.35}$	5.906(2)	2.953
$AgBr_{0.60}I_{0.40}$	5.924(1)	2.962

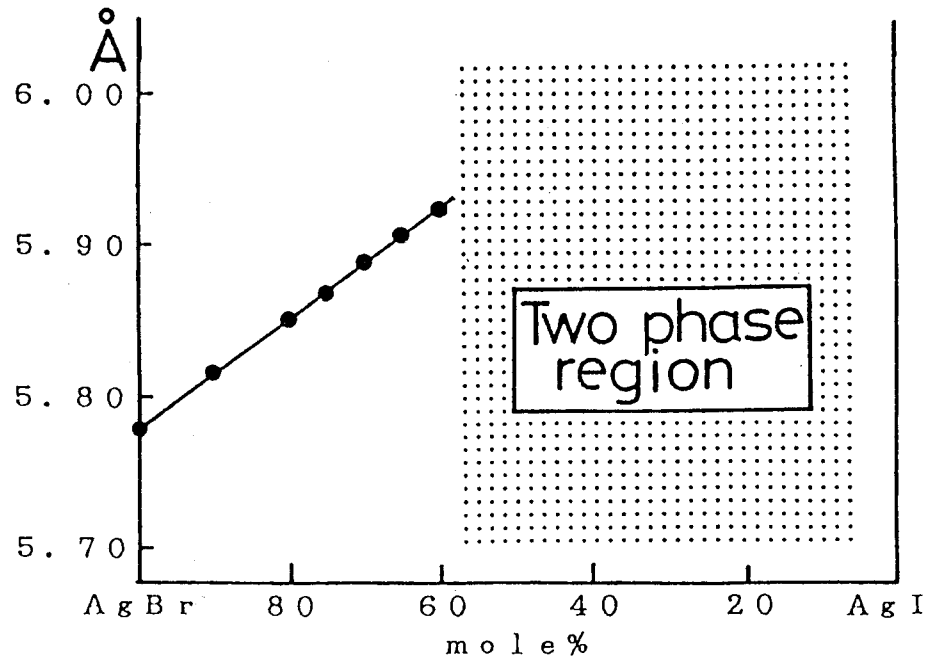

Fig. 1. Cell parameter vs composition in the system $AgBr_{1-x}I_x$ with the rock-salt type structure.

radiation (60 KV, 200 mA) was monochromatized by pyrolytic graphite. Symmetry independent reflections were obtained by averaging the equivalent reflections in an octant in reciprocal space. Absorption and extinction corrections were made for each data set. The structure refinements were carried out with isotropic temperature factors, assuming that both anions occupy the normal octahedral sites statistically in the rock-salt type structure with space group Fm3m. Crystal data and parameters refined are listed in Table 2.

2-3 X-ray absorption measurement

For X-ray absorption measurements, well-ground powder samples were mixed with boron nitride in an agate mortar and pressed into pellets of 0.6 to 0.8 mm in thickness and 10.0 mm in diameter.

The X-ray absorption measurements near the Br K- and Ag K-edges were made with synchrotron radiation by use of the EXAFS facilities installed at the beam line 10B of the 2.5 GeV storage ring of Photon Factory in KEK. Gas mixture in the ion chamber detector was selected for optimum signal to noise ratio. The X-ray absorption spectra were observed from 13.170 to 14.700 KeV in energy for Br K-edge and from 25.230 to 26.600 KeV for Ag K-edge. The survey regions and scanning steps of X-ray energy are shown in Table 3.

2-4 EXAFS data analysis

EXAFS data analyses were carried out using the programs EXAFS and CURFIT (Maeda et al., 1982). In obtaining the EXAFS function $\chi(k)$, the background level was subtracted from the observed absorption spectra by using Viktoreen fit and the

Table 2. X-ray data and parameters refined.

		AgBr	$Ag(Br_{96}I_4)$	$Ag(Br_{91}I_9)$	$Ag(Br_{86}I_{14})$	$Ag(Br_{84}I_{16})$	$Ag(Br_{82}I_{18})$	$Ag(Br_{75}I_{25})$	$Ag(Br_{70}I_{30})$
a (Å)		5.776(2)	5.790(1)	5.811(2)	5.829(2)	5.836(1)	5.843(4)	5.869(1)	5.887(7)
No. of reflec.		41	46	38	40	43	37	36	26
G	Br	1.0	0.95(1)	0.92(2)	0.90(2)	0.88(2)	0.79(4)	0.76(4)	0.70
	I	0.0	0.05	0.08	0.10	0.12	0.21	0.24	0.30
B ($Å^2$)	(Br,I)	1.6(2)	2.02(4)	2.2(1)	2.3(1)	2.2(1)	2.5(2)	2.6(1)	2.9(3)
	Ag	2.3(2)	2.55(3)	3.0(1)	3.0(1)	3.2(1)	3.4(2)	3.7(2)	6.3(10)
wR-factor		0.027	0.012	0.013	0.015	0.015	0.023	0.023	0.052

Table 3. Servey regions and scanning steps of X-ray absorption spectra in Br K-edge (a) and Ag K-edge (b).

(a) Br K-edge

13.170 - 13.440 (KeV)	5.3 (eV)
13.440 - 13.550	1.0
13.550 - 14.050	2.4
14.050 - 14.700	3.1

(b) Ag K-edge

25.230 - 25.480 (KeV)	5.0 (eV)
25.480 - 25.570	0.9
25.570 - 26.120	2.1
26.120 - 26.600	3.1

absorption spectrum for the isolated atom was approximated by the cubic spline technique. Typical $\chi(\underline{k})$ data (multiplied by $\underline{k}^3$) are shown in Fig. 2. The Fourier transform of $\chi(\underline{k})$ to real space yields a radial structure function $\psi(\underline{r})$ (Sayers et al., 1971). The Fourier transform for Ag K-edge is shown in Fig. 3 where no phase shift corrections are made. The peak in each radial structure function indicates the nearest-neighbors around the absorbing atom.

For the purpose of curve-fitting, the distance range of interest for $\psi(\underline{r})$ was filtered with a smooth filtering window, and transformed back to $\underline{k}$-space, $\chi'(\underline{k})$. Carrying out non-linear least-squares program of Marquardt's method (Marquardt,1963), $\chi'(\underline{k})$ was fitted with analytical EXAFS function $\chi(\underline{k})$;

$$\chi(\underline{k})=\Sigma_j N_j/(\underline{k}R_j^2)\ |f_j(\pi,\underline{k})|\ \exp[-2\sigma_j^2\underline{k}^2]\ \exp[-2R_j/\lambda(\underline{k})]$$
$$\sin[2\underline{k}R_j + \Phi_{ij}(\underline{k})].$$

Here N_j is the number of atoms in the j-th shell at distance R_j, $|f_j(\pi,\underline{k})|$ is the back-scattering amplitude, σ_j is a Debye-Waller factor (this Debye-Waller factor differs from the Debye-Waller factor for X-ray diffraction; σ_j is the root-mean-square average of the difference of displacements along the equilibrium bond direction (Teo,1986)), $\exp[-2R_j/\lambda_j(\underline{k})]$ is a damping factor due to inelastic losses in the scattering process with the electron mean free path $\lambda_j(\underline{k})$ and $\Phi_{ij}(\underline{k})$ is the phase shift experienced by the photoelectron. The back-scattering amplitude $|f_j(\pi,\underline{k})|$ and the phase shift $\Phi ij(\underline{k})$ are parameterized as follows (Teo et al., 1977 and Lee et al., 1977),

$$|f_j(\pi,\underline{k})| = A_j/(1 + B_j^2(\underline{k}-C_j)^2)$$

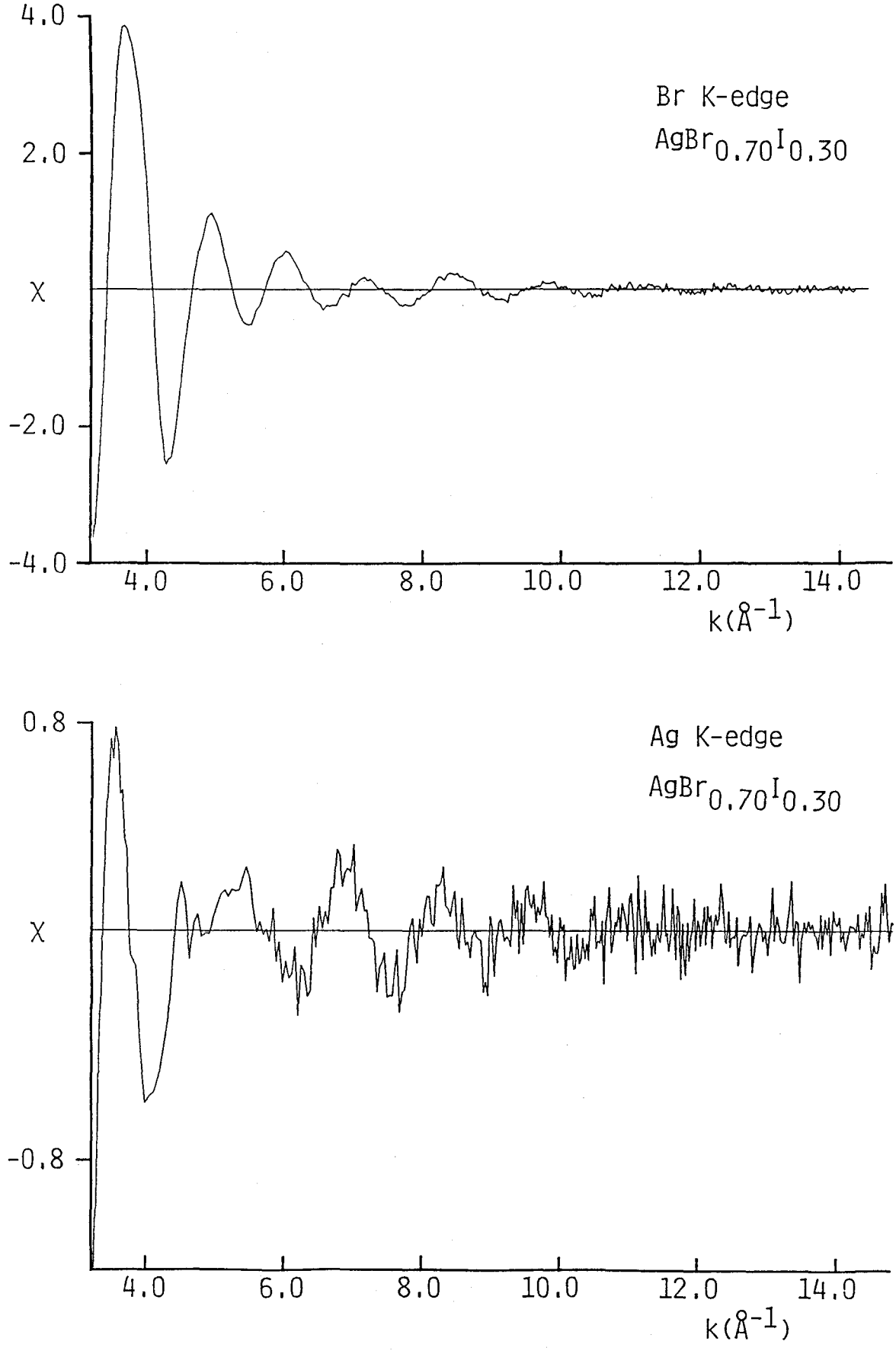

Fig. 2. Br K- and Ag K-edge EXAFS oscillations for $AgBr_{0.7}I_{0.3}$.

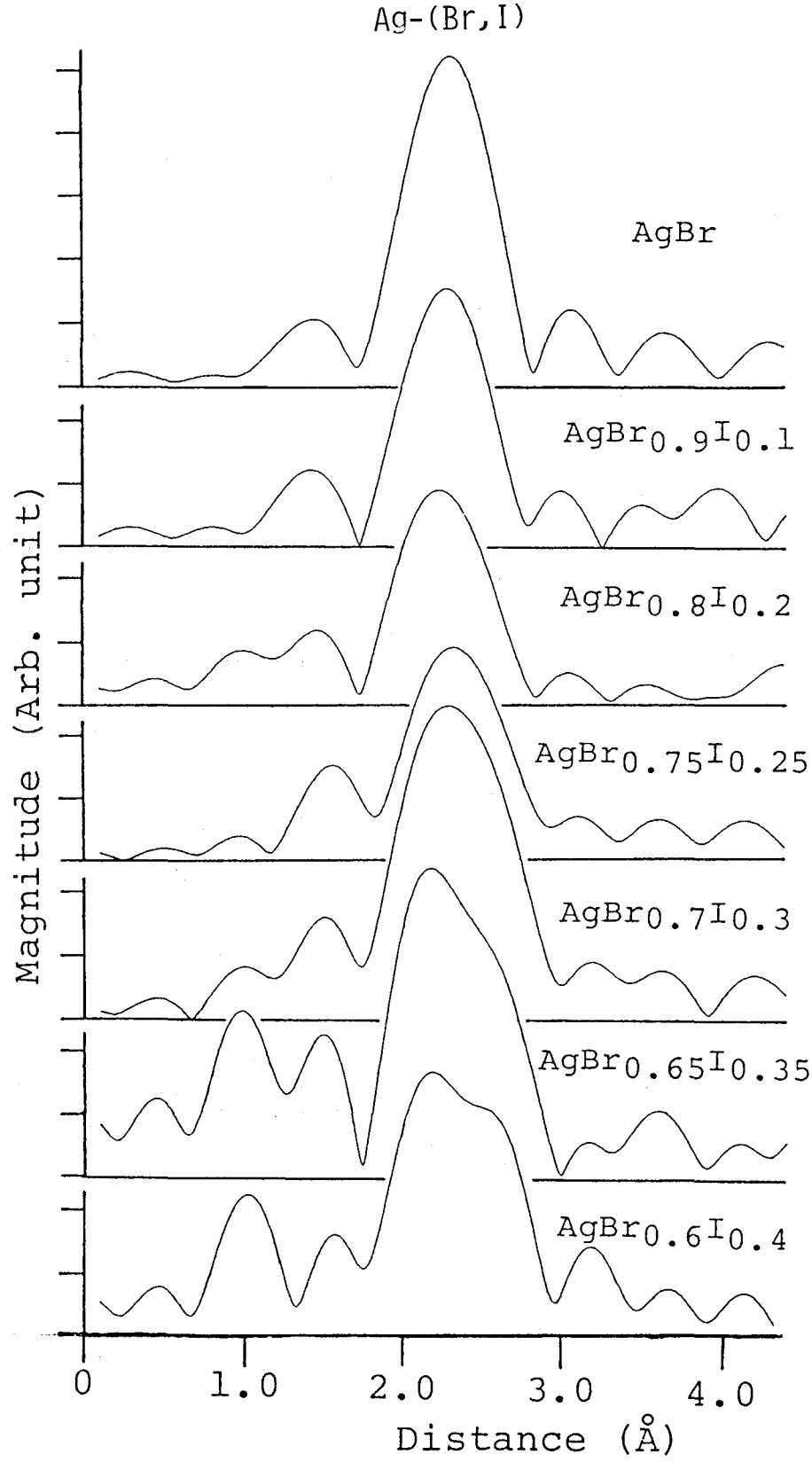

Fig. 3. Fourier transforms for Ag K-edge of $AgBr_{1-x}I_x$ solid-solution (x=0.0, 0.2 and 0.3). No phase shift corrections were made.

$$\Phi_{ij}(\underline{k}) = a_j + b_j\underline{k} + c_j\underline{k}^2 + d_j/\underline{k}^3$$

$$\underline{k} = [\underline{k}'^2 - 0.2625(\Delta E_0)]^{1/2},$$

where k' and ΔE_0 are the experimental wave number of photoelectron and the difference in energy threshold between theory and experiment, respectively. The parameters in the j-th shell [A_j, B_j, C_j], [a_j, b_j, c_j, d_j] determined from the end-members (AgBr and β-AgI) were fixed through the refinement of the solid-solution. The refinement is applied to ΔE_0 and three structure parameters; the coordination number N_j, interatomic distance d_j and Debye-Waller factor σ_j. Varying ΔE_0 can correct for errors in the determination of the energy origin and compensate for the effects of changes in electronic configurations on phase shifts (Teo & Lee, 1979).

The interatomic distances for the end-members (pure AgBr ang β-AgI) at 293 K were determined by the structure analysis with X-ray single crystal data (Yoshiasa et al., 1986 and 1987). The structure parameters obtained by the least-squares parameter fitting are listed in Table 4. The analysis has been made assuming that the peak in each radial structure function for the Ag K-edge of the solid-solution is composed of double shells (i.e. the Ag-Br and Ag-I distances), and that for the Br K-edge is single shell (the Br-Ag distance). The reliability of fit parameter, $R = \Sigma_s|\underline{k}_s^3\chi(\underline{k}_s)_{exp.} - \underline{k}_s^3\chi(\underline{k}_s)_{calc.}| \,/\, |\underline{k}_s^3\chi(\underline{k}_s)_{exp.}|$, between the experimental and calculated EXAFS functions is also listed in Table 4. The quality of the fit on the Ag-(Br,I) peak for $AgBr_{0.7}I_{0.3}$ is shown in Fig. 4.

Table 4. Structure parameters determined by the least-squares parameter fitting; co-ordination numbers [N], interatomic distances [R(Å)] and Debye-Waller factors (σ).

Ag K-edge

	N[Ag-Br]	N[Ag-I]	R[Ag-Br]	R[Ag-I]	σ [Ag-Br]	σ [Ag-I]	R-factor
AgBr	6 *		2.888(2)*		0.10(1)		
$AgBr_{0.90}I_{0.10}$	4(2)	2(17)	2.87(2)	3.0(3)	0.09(2)	0.2(5)	0.1%
$AgBr_{0.80}I_{0.20}$	3(1)	2(9)	2.86(2)	2.9(2)	0.09(1)	0.2(3)	0.1%
$AgBr_{0.75}I_{0.25}$	4(3)	1(1)	2.89(3)	3.0(1)	0.09(2)	0.12(8)	0.2%
$AgBr_{0.70}I_{0.30}$	5(3)	2(1)	2.86(3)	2.9(1)	0.11(3)	0.12(4)	0.4%
$AgBr_{0.65}I_{0.35}$	4(2)	1(2)	2.85(5)	2.9(1)	0.09(3)	0.12(8)	0.1%
$AgBr_{0.60}I_{0.40}$	3(3)	2(2)	2.87(3)	2.9(1)	0.10(4)	0.12(6)	0.1%
β-AgI		4 *		2.813(3)*		0.10(1)	

Br K-edge

	N	R[Br-Ag]	σ	R-factor
AgBr	6 *	2.888(1)*	0.11(2)	
$AgBr_{0.90}I_{0.10}$	6(1)	2.88(1)	0.11(1)	0.01%
$AgBr_{0.80}I_{0.20}$	5(1)	2.88(1)	0.11(1)	0.02%
$AgBr_{0.75}I_{0.25}$	6(1)	2.88(1)	0.12(1)	0.05%
$AgBr_{0.70}I_{0.30}$	5(1)	2.87(1)	0.11(1)	0.07%
$AgBr_{0.65}I_{0.35}$	5(1)	2.88(1)	0.11(1)	0.04%
$AgBr_{0.60}I_{0.40}$	6(1)	2.88(2)	0.12(1)	0.11%

3) Results and discussion

3-1 Local structure of the solid-solution

The cell dimensions of the $AgBr_{1-x}I_x$ solid-solution increase linearly with increasing AgI content because of the substitution of larger ion I^- for Br^- (Fig. 1), i.e., it follows Vegard's law. The average Ag-(Br,I) distances determined by X-ray diffraction, therefore, increase apparently. The cell dimension for the rock-salt type AgI can be estimated to be ca. 3.06 Å by extrapolation. The value of 3.06 Å is compared well with 3.04 Å for the rock-salt type AgI obtained under 4 kbar by Moore & Kasper (1968).

EXAFS and XANES spectra yield information on the local environments around a particular kind of absorbing atom in random solid-solution. Because the nearest neighbors for Ag ion are both Br and I ions in the $AgBr_{1-x}I_x$ solid-solution, the peak in each radial structure function for the Ag K-edge of the solid-solution (Fig. 3) gradually develops a shoulder at longer distance with increasing AgI content and is composed of double shells of the Ag-Br and Ag-I distances as shown in Table 4. The distances from Br to the first nearest neighbor, Ag, and from Ag to that of Br obtained by EXAFS gradually decrease with AgI content (Fig. 5), which exhibits a contrast with the phenomenon observed in the $Ga_{1-x}In_xAs$ solid-solution where short Ga-As distances increase with InAs content (Mikkelsen & Boyce, 1982). It will be expected that Ag^+ is locally attracted to Br^-, which has larger effective anion charge than I^-, by replacing Br^- with I^- (Fig. 6). The similar variation in bonding distance of a particular atom pair is observed in other systems such as α-quartz type $GaPO_4$ and

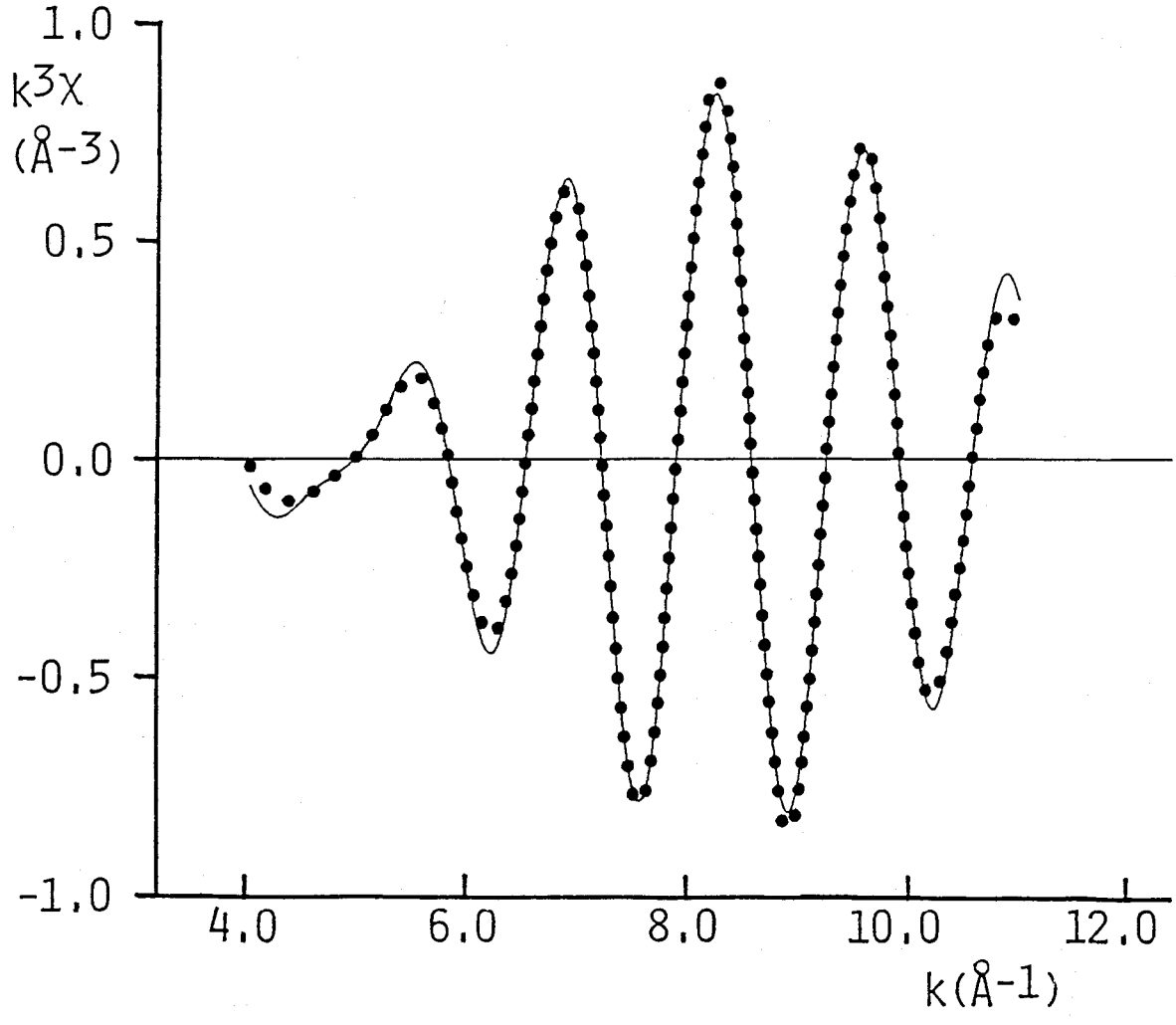

Fig. 4. Fourier-filtered EXAFS spectra (solid curve) and least-squares fit (dotted curve) for Ag K-edge of $AgBr_{0.7}I_{0.3}$.

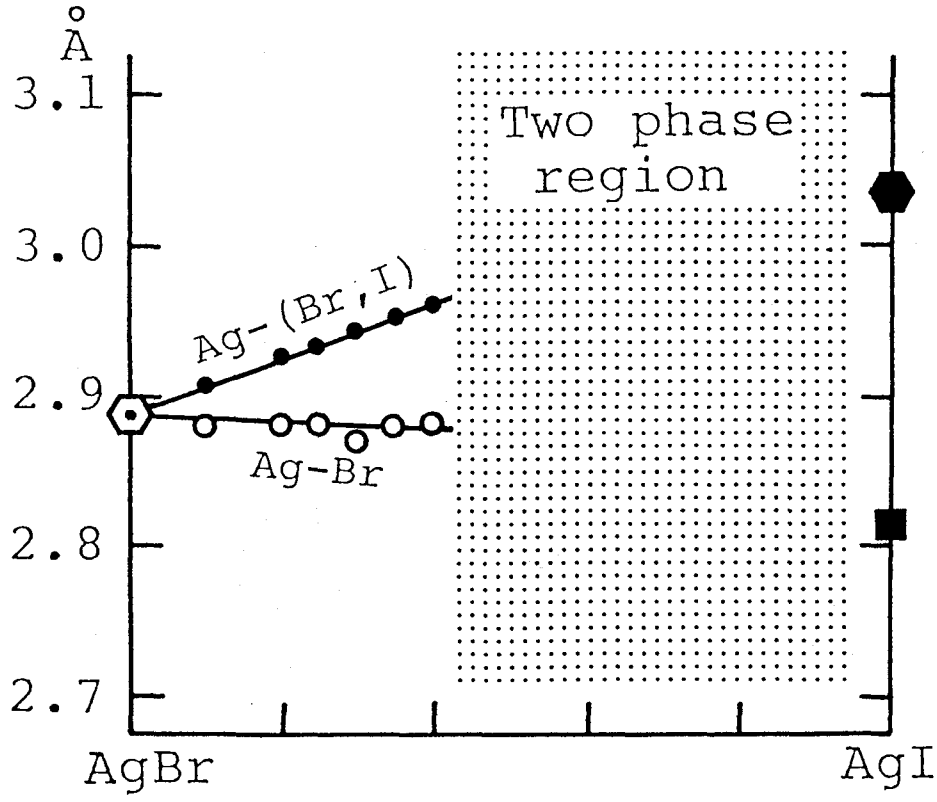

Fig. 5. The Ag-Br nearest neighbor distance measured by EXAFS (open circles) vs composition in the $AgBr_{1-x}I_x$ rock-salt type solid-solution at room temperature. Closed circles denote the mean Ag-(Br,I) distances obtained from diffraction experiments.

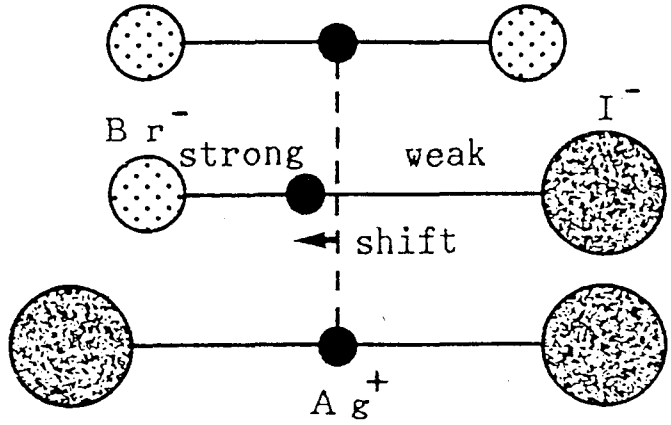

Fig. 6. Schematic representations of the local changes around Ag^+ ion. Ag^+ is attracted to Br^- haveing stronger bond than I^-.

$GaAsO_4$ in which the silicon positionsare regularly occupied by two kinds of atoms. The Ga-O distances (data from Goiffon et al.,1986) are varied with the kind of atom standing on the opposite side (P or As) by the displacement of two-coordinated oxygen atoms (Fig. 7).

In Table 4, it is interesting to note that the Debye-Waller factors σ are almost constant value of 0.11. This Debye-Waller factor σ is different obtained by diffraction experiments; only the component of the relative displacement which lies along the bond direction needs to be considered (Teo, 1986).

The XANES region of the absorption spectrum contains the information on relative orientation and bond angles of atom surrounding the X-ray absorbing atoms (e.g. Fujikawa et al., 1983). The experimental Br K- and Ag K-edge XANES spectra of the solid-solution are shown with the reference samples in Fig. 8 and Fig. 9, respectively. There are systematic changes in both Br K- and Ag K-edge XANES spectra with increasing AgI content (e.g., the third peak becomes gradually indistinguishable from the second peak), which will be correlated to the change in the local structure of the solid-solution.

3-2 Average distribution of atoms in the unit cell

X-ray diffraction experiments allow the determination of the three-dimensional distributions of atoms in the unit cell and provide information about the average distribution of atoms occupying an equivalent position in a solid-solution. In the $AgBr_{1-x}I_x$ solid-solution, the Br and I ions are distributed at random over the 4(a) sites of space group Fm3m. It thus appears

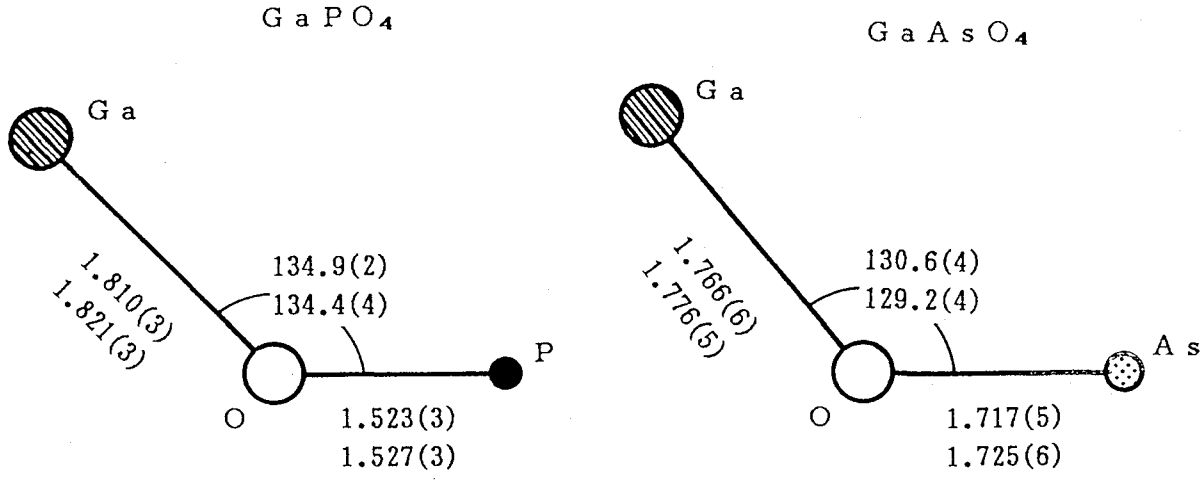

Fig. 7. Schematic diagram showing the variation in the Ga-O distances in α-quartz type $GaPO_4$ and $GaAsO_4$. Bond distances (Å) and angles (°) are given.

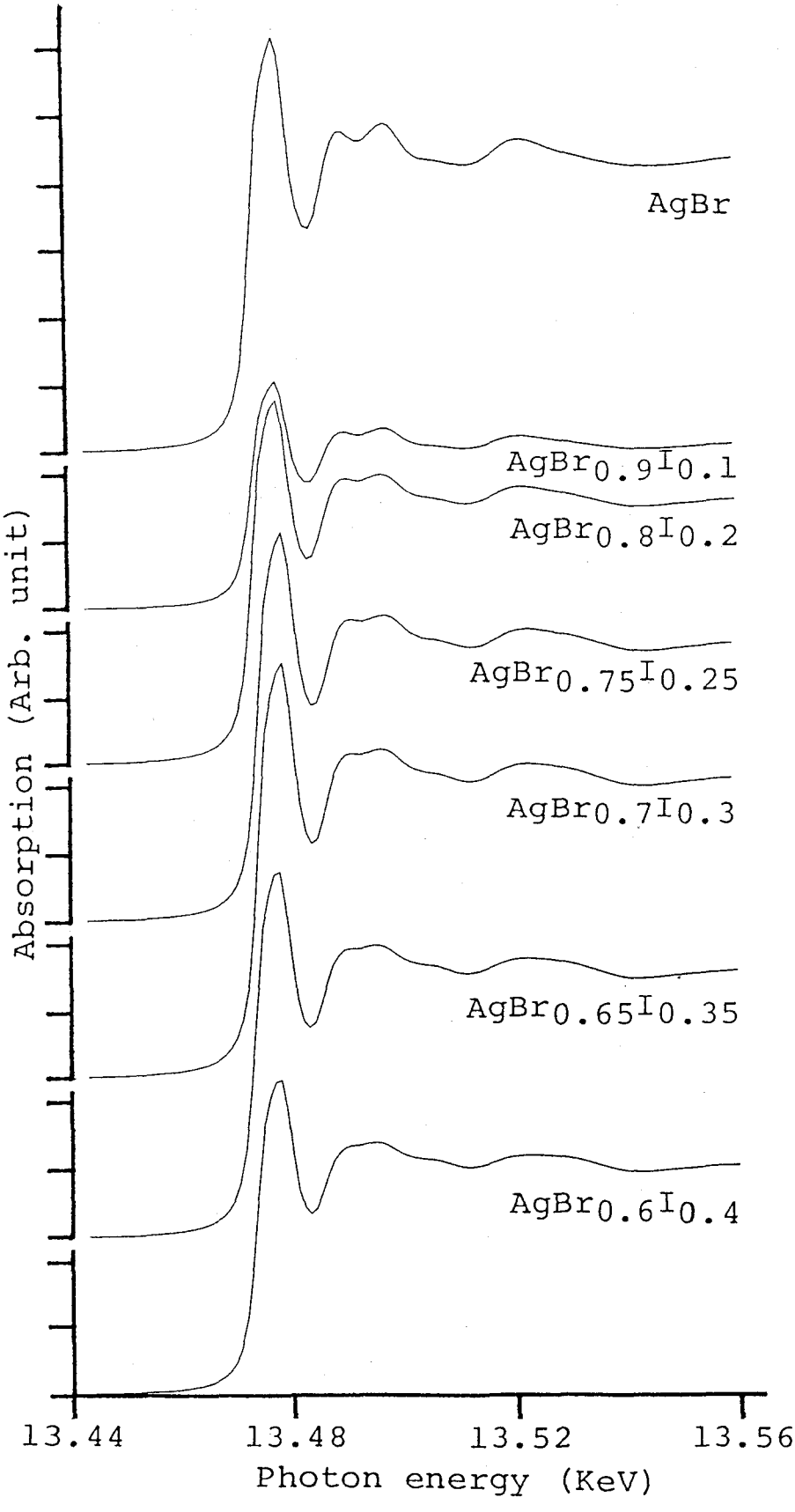

Fig. 8. Experimental XANES spectra of the $AgBr_{1-x}I_x$ solid-solutions for Br K-edge regions.

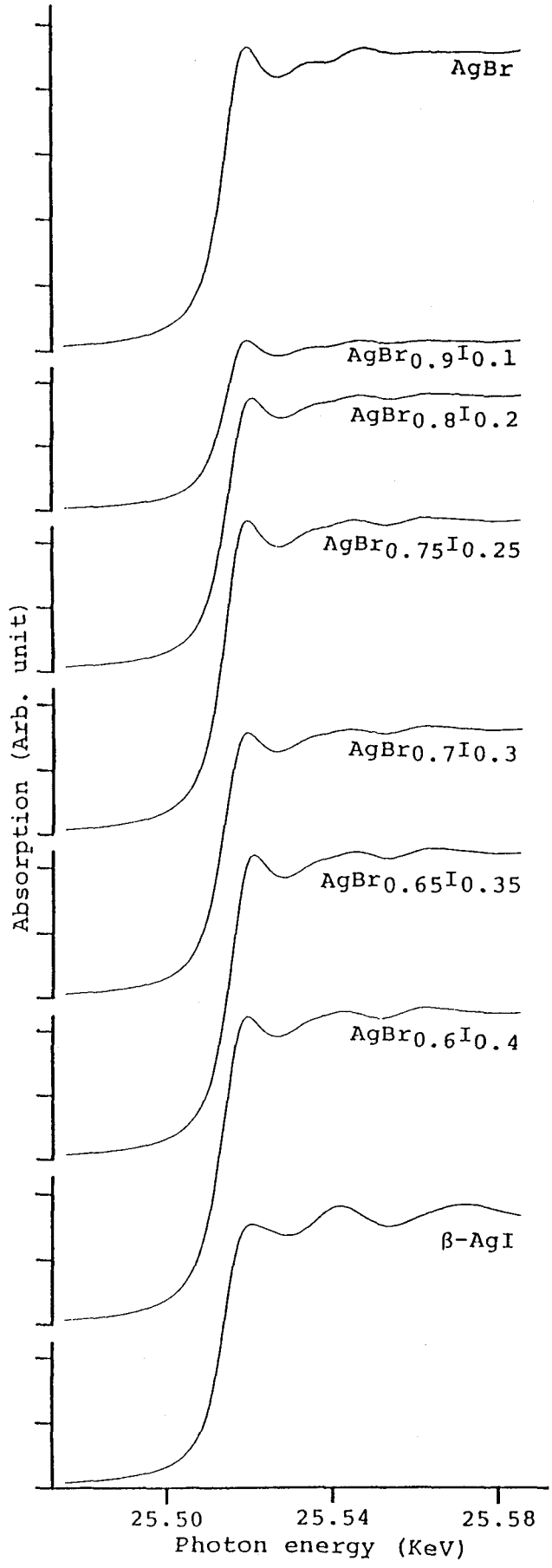

Fig. 9. Experimental XANES spectra of the $AgBr_{1-x}I_x$ solid-solution for Ag K-edge regions. That for β-AgI is also shown for comparison.

that static deviations of both cation and anion from the lattice site occur because the Ag-Br and Ag-I distances in the solid-solution are closer to the respective distances in the pure rock-salt type compounds, AgBr and hypothetical rock-salt type AgI, than to an average distance. The electron density section of the difference-Fourier syntheses in the (100) plane, where both sites for cation and anion just cut through their centers, is shown in Fig. 10. The small residual electron density indicates the preferred displacement of atoms along the <100> direction though the electron density distributions of both caion and anion are almost isotropic. In difference-Fourier maps for various compositions, there is little residual electron density at the tetrahedral site (1/4,1/4,1/4) for Ag.

The temperature factors [B($\mathring{A}^2$)] for both cation and anion determined by X-ray diffraction, which arise from both dynamic disorder due to thermal vibrations and static disorder, increase with AgI content (Fig. 11). In AgBr, the heavier Ag ion has a larger temperature factor than the lighter Br ion in agreement with the results of lattice-dynamical study (Dorner et al., 1976). The root-mean-square (r.m.s.) displacement for (Br,I) and Ag in $AgBr_{0.75}I_{0.25}$ is 0.18(4) and 0.22(5) $\mathring{A}$, respectively, and they have a considerably larger value than that in pure AgBr (0.14(4) $\mathring{A}$ for Br and 0.17(4) $\mathring{A}$ for Ag). The difference in the r.m.s. displacement of each (Br,I) and Ag between pure AgBr and $AgBr_{0.75}I_{0.25}$ (i.e., 0.04 = 0.18 - 0.14 for (Br,I) and 0.05 = 0.22 - 0.17 for Ag) accords well with the average displacement from the lattice sites (i.e., 0.04 = (| 2.93 - 2.88 |X0.75 + |

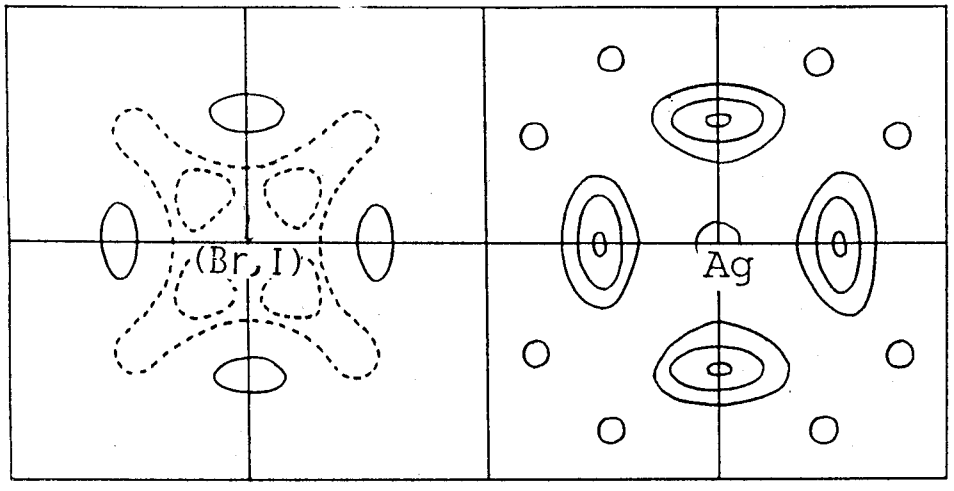

Fig. 10. (100) electron density section of the difference-Fourier syntheses. Contours are drawn at an interval of 0.5 e/Å^3. Positive contours are represented as solid lines and negative contours broken, zero contors being omitted.

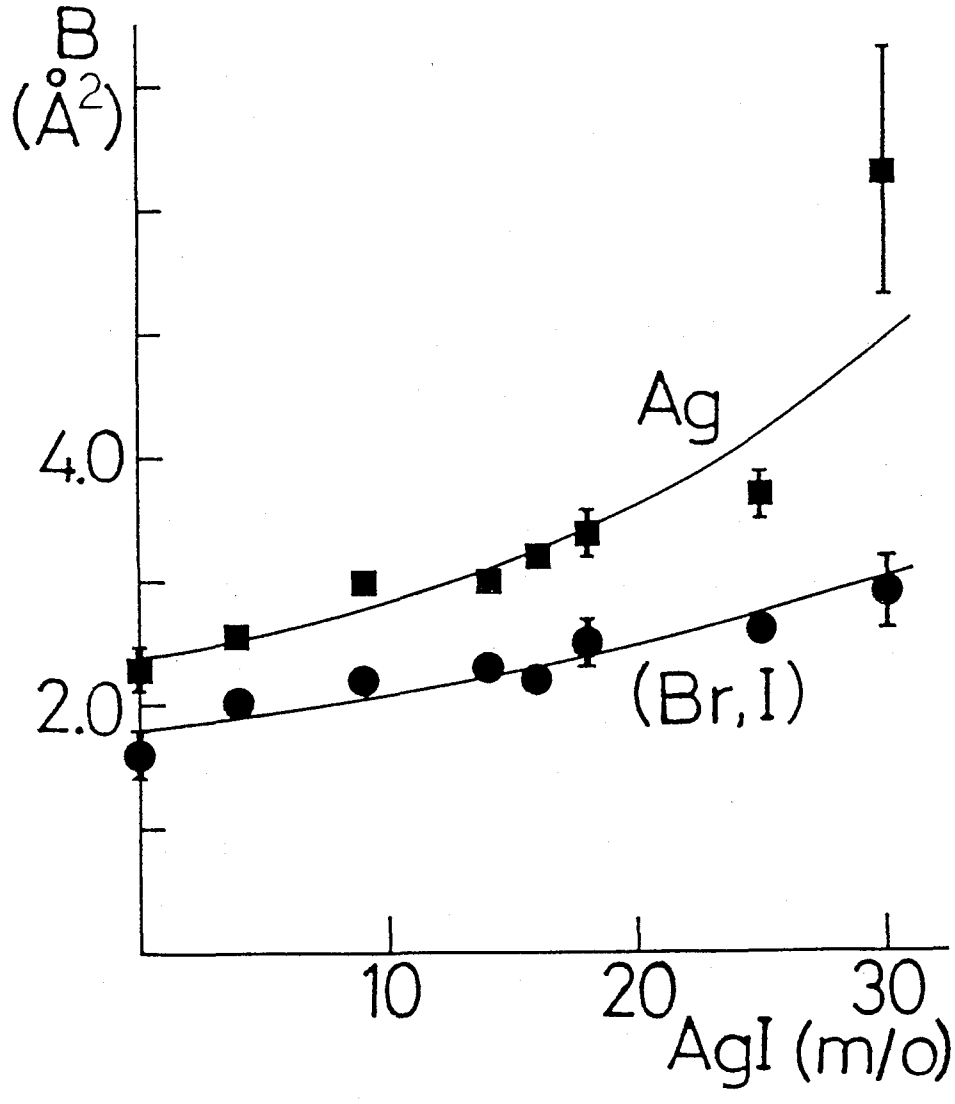

Fig. 11. Relationship between composition and isotropic temperature factors, B(Å^2), for both Ag and (Br,I) in the normal octahedral sites.

2.93 - 3.06 (×0.25)/2) asumming that the Ag-Br, Ag-I and average Ag-(Br,I) distances in the solid-solution are 2.88, 3.06 and 2.93 Å, respectively. The particular increase in temperature factors should result from the displacements of atoms from the normal octahedral site owing to the fact that Br and I randomely occupy the normal sites in the rock-salt type structure and that the Ag-Br and Ag-I distances in the solid-solution are different.

3-3 Local structure and ionic conduction in the solid-solution

The conduction mechanism of AgBr was introduced in detail by Shewmon (1963). The high ionic conductivity of AgBr results from Frenkel defects. The measurements for the diffusion of silver in AgBr single crystals using radioactive tracers (Friauf, 1957) showed that the most probable mechanism for the movement of the interstitial silver ions is the interstitialcy mechanism. The introduction of a large amount of AgI into AgBr leads to a large increase in the ionic conductivity (Cain & Slifkin, 1980 and Shahi & Wagner, 1982). It appears that the conductivity in the intrinsic region increases monotonically with increasing AgI content and that a large enhancement of ionic conductivity in AgI rich region will be ascribed to an increase in the concentration of the Frenkel defect in an equilibrium state caused by changes in local structures, in addition to the weaker I-Ag bond than the Br-Ag bond. The activation energy for the solid-solution in which Br and I ions are distributed at random over octahedral sites without forming clusters is not so much influenced by changes in the local structure.

4) References

W. Bührer, R.M. Nicklow and P. Brüesh (1978) Phys. Rev., B17, 3362-3370

L.S. Cain and L.M. Slifkin (1980) J. Phys. Chem. Solids, 41, 173-178

B. Dorner, W. von der Osten and W. Bührer (1976) J. Phys. C: Solid State Phys., 9, 723-732

R.J. Friauf (1957) Physical Review, 105, 843-848

T. Fujikawa, T. Matsuura and H. Kudoda (1983) Journal of the Physical Society of Japan, 52, 905-912

A. Goiffon, J.C. Jumas, M. Maurin and E. Philippot (1986) J. Solid State Chem., 61, 384-396

P.A. Lee, B.K. Teo and A.L. Simons (1977) J. Am. Chem. Soc., 99, 3856-3859

H. Maeda, H. Terauchi, K. Tanabe, N. Kamijo, M. Hida and H. Kawamura (1982) Jpn. J. Appl. Phys., 21, 1342-1346

D.W. Marquardt, J. Soc. Indust. Appl. Math. 11 (1963) 431

J.C. Mikkelsen Jr. and J.B. Boyce (1982) Phys. Rev. Lett., 49, 1412-1415

M.J. Moore and J.S. Kasper (1968) The Journal of Chemical Physics, 48, 2446-2450

D.E. Sayers, E.A. Stern and F.W. Lytle (1971) Phys. Rev. Lett., 27, 1204-1207

K. Shahi and J.B. Wagner Jr. (1982) J. Phys. Chem. Solids, 43, 713-722

P.G. Shewmon (1963) Diffusion in Solids, McGraw-Hill Book Company, Inc.

O. Stasiw and J. Teltow (1949) Z. Anorg. Allgem. Chem., 259, 143-153

B.K. Teo, P.A. Lee, A.L. Simons, P. Eisenberger and B.M. Kincaid (1977) J. Am. Chem. Soc., 99, 3854-3856

B.K. Teo and P.A. Lee (1979) J. Am. Chem. Soc., 101, 2815-2832

B.K. Teo (1986) EXAFS: Basic Principles and Data Analysis,

A. Yoshiasa, K. Koto, S. Emura and F. Knamaru (1986) J. Phys. Colloq., 47, C-8 803-807

A. Yoshiasa, K. Koto, F. Kanamaru, S. Emura and H. Horiuchi (1987) Acta Cryst. B43, 434-440

Chapter 4

Local structure of the superionic conducting α-AgI type $AgI_{1-x}Br_x$ solid- solution

1) Introduction

The α-phase silver iodide is the classical and typical superionic conductor of Ag ions. The high-conducting state is achieved through a first-order phase transition (T_c = 420 K) and the ionic conductivity increases by four orders of magnitude (e.g. Shahi & Wagner, 1984). In α-AgI, the iodine ions form a regular body-centered cubic lattice with the statistically disordered distribution of the highly mobile Ag ions. A decrease in volume (ca. 7%) occurs at the transition from the low-temperature wurtzite-type structure (β-phase). α-AgI is stable over a wide range of temperature to the melting point of 825 K. A pronounced anomaly in the heat capacity of α-AgI was not observed (Nolting & Rein, 1969). However, a memory effect occurs at temperature below 443 K because the distribution of Ag ion is not completely random near the transition temperature (Burley, 1967).

The crystal structure and dynamical behavior of atoms in α-AgI have been studied extensively through several techniques; e.g., X-ray and neutron diffraction (Hoshino et al.,1977 and Cava et al.,1977), EXAFS (Boyce et al.,1977 and Hayes et al.,1978), far-infrared absorption (Brüesch et al.,1975), Raman (Hanson et al.,1975, Burns et al.,1976 and Delaney & Ushioda,1976). From the crystal chemical considerations and interpretation of the experimentally observed spectra, it has been suggested that only the 12(d) sites (tetrahedral) of space group Im3m are appreciably occupied at equilibrium. Boyce et al. (1977), however, proposed from EXAFS study that the Ag ions in α-AgI

occupy the sites slightly displaced from the center of the distorted iodine tetrahedron.

The phase diagram of the AgI-AgBr system (Fig.1) has been reported by Stasiw & Teltow (1949). α-AgI type $AgI_{1-x}Br_x$ solid-solution with cubic symmetry is stable over a wide range of composition and temperature. The substitution of iodine with bromine in α-AgI lowers the melting temperature. Under ambient conditions AgI is stable in the wurtzite type structure (β-phase) and is metastable in the sphalerite type structure (γ-phase). While AgBr is stable only in the rock-salt type structure up to the melting point and does not exhibit superionic conduction. The tetrahedrally-coordinated β- and γ-phases of AgI transform to the rock-salt type phase under high pressure (Moore & Kasper,1968). Covalent character is increasing from AgBr to AgI. The ionicities (f) of both AgI and AgBr based on the Phillips scale are close to the critical value of 0.785 which separate tetrahedral covalent compounds from octahedral ionic ones; f(AgI) = 0.77 and f(AgBr) = 0.85 (Phillips, 1970).

In the α-$AgI_{1-x}Br_x$ solid-solution with disordered distribution of Ag ions, the chemical composition and basic structure are simple. Nevertheless, it will be presumed that the local environments of the Br ions differ from those of the I ions. EXAFS spectroscopy is a useful probe for investigating the local environment around a particular kind of absorbing atom in the disordered structure and/or in the random solid-solution.

In this work, EXAFS and XANES structural analyses were made for the α-$AgI_{1-x}Br_x$ solid solution ($0 \leq x \leq 0.4$) at 573 K to elucidate the distribution and the thermal behavior of the Ag

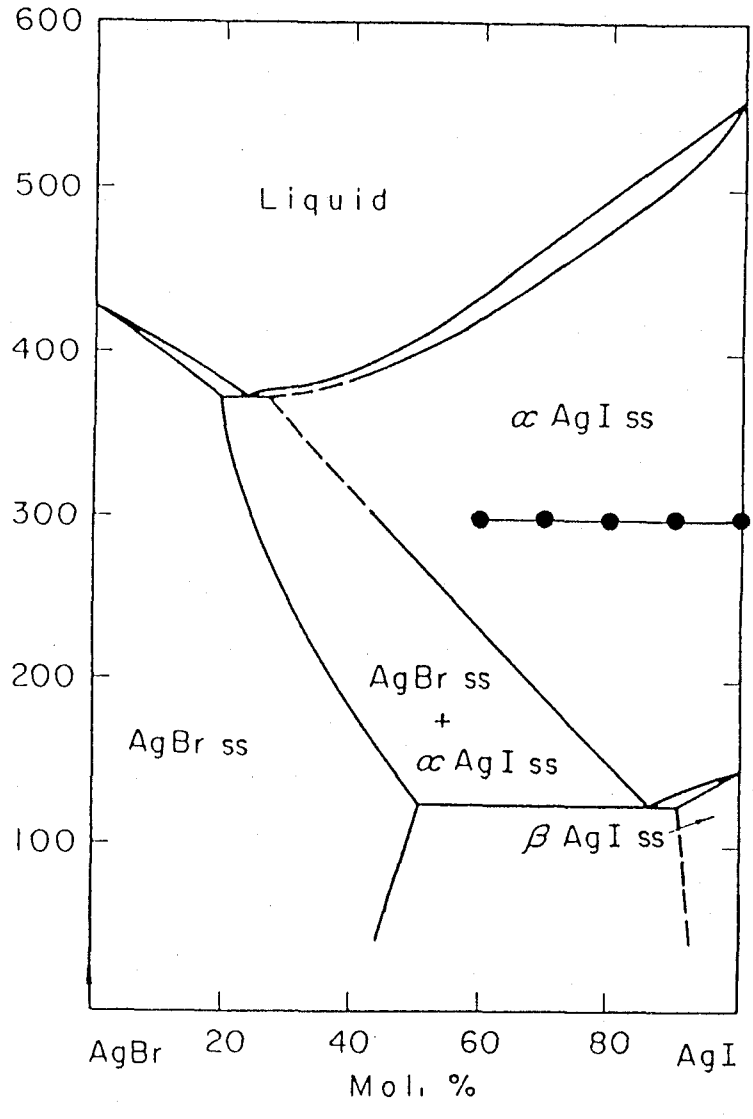

Fig. 1. The phase diagram of the AgI-AgBr system by Stasiw & Teltow (1949). Solid circles stand for the samples studied by EXAFS spectroscopy

ions. The structure investigations are reviewed, and the diffusion mechanism of Ag ions in this famous superionic conductor are discussed from a view point of structural chemistry.

2) Experimental

2-1 Synthesis

AgI and AgBr in powder form (99.99% pure from Koso Chemicals) were mixed together in appropriate proportions. The mixture was melted under the iodine atmosphere of about 100 mmHg at 973 K for 20 hours in silica tube and then quenched into cold water. The sample was taken out from the silica tube and ground to a fine powder. The powder was annealed at 623 K for two hours before measurements. The formation of single phase α-AgI type $AgI_{1-x}Br_x$ solid solution ($0 \leq x \leq 0.4$) was confirmed by X-ray powder diffraction technique at 573 K. Special precaution was paid to prevent from exposure of light. The compositions of the samples were assumed to be the same as those of the starting mixtures. The cell dimensions (Table 1 and Fig. 2) decrease linearly with increasing AgBr content.

For the high temperature X-ray absorption measurements the fine powder samples were mixed with powder of boron nitride and pressed into pellets of 0.6 to 0.8 mm in thickness and 10.0 mm in diameter. The samples had the edge-jumps ($\Delta\mu d$) of $1.8 \sim 0.5$ for the Br K-edge and $1.3 \sim 0.9$ for the Ag K-edge, where μ is the linear absorption coefficient and d, the sample thickness.

2-2 Furnace

Table 1. Cell dimensions (a) and cell volumes (V) in Å for α-AgI type $AgI_{1-x}Br_x$ solid-solution at 573 K.

	a (Å)	V (Å^3)
α-AgI	5.082(4)	131.3(4)
α-$Ag(I_{0.9}Br_{0.1})$	5.031(4)	127.3(4)
α-$Ag(I_{0.8}Br_{0.2})$	5.002(5)	125.2(4)
α-$Ag(I_{0.7}Br_{0.3})$	4.969(6)	122.7(5)
α-$Ag(I_{0.6}Br_{0.4})$	4.934(3)	120.1(2)

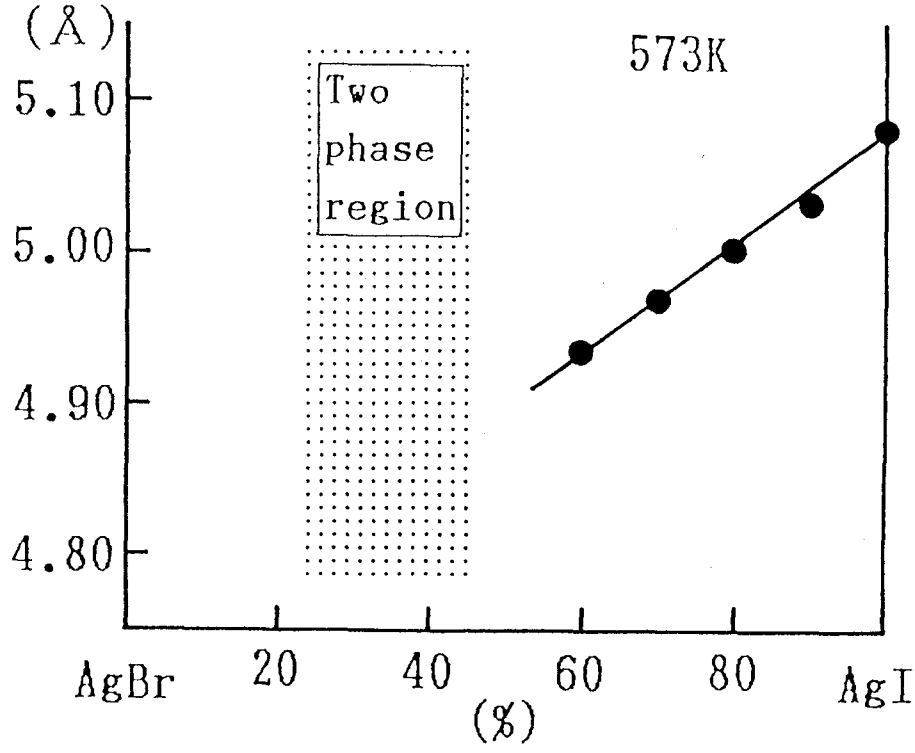

Fig. 2. Relationship between cell paramater and composition of the α-AgI type $AgI_{1-x}Br_x$ solid-solution at 573 K.

A photograph of the fabricated heating furnace for X-ray absorption measurements is shown in Fig. 3. The overall dimensions of the furnace are with approximately 100 mm in diameter, 150 mm in height and approximately 7 kg weight. Two pellets of samples can be supported on the lower heating element. Two thermocouples mounted inside the furnace serve to control the temperature and measure the specimen temperature. It is possible to evacuate or to flow desired gases. The samples can be heated up to 850 K with a stability of $\pm$ 1 K.

2-3 X-ray absorption measurements

The X-ray absorption measurements near the Br K- and Ag K-edges at 573 K were made with synchrotron radiation by use of the EXAFS facilities installed at the beam line 10B of the 2.5 GeV storage ring of Photon Factory in KEK.

A Si(311) channel-cut monochromator was used. The incident and transmitted X-ray intensities were measured with ionization chambers filled with N_2 and Ar gas. Gas mixtures were selected for optimum singnal to noise ratio. The survey regions and scanning steps of X-ray absorption spectra for the Br K- and Ag K-edges are shown in Table 2. During the runs, the storage ring was operated at the energy of 2.5 GeV with an electron current of 210 - 110 mA.

2-4 Structure analysis

Data processing and analysis applied to the absorption spectra are described in detail in chapter 3. We extracted the EXAFS function $\chi(k)$ from the measured absorption spectra and made a Fourier transformation into real space. The same k range, k =

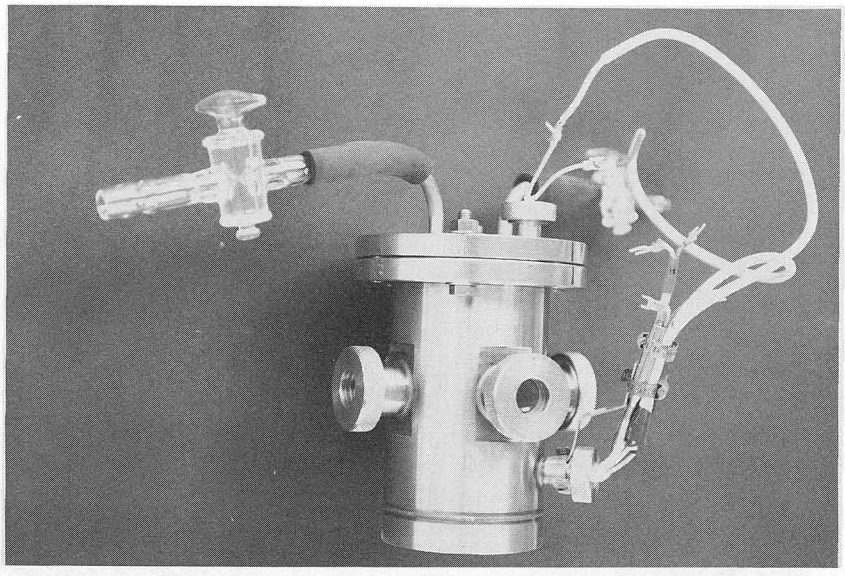

(a)

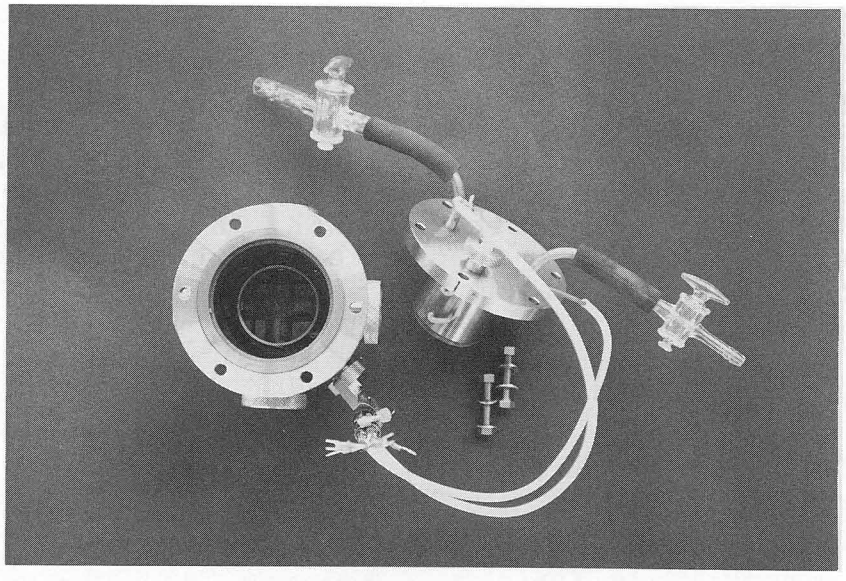

(b)

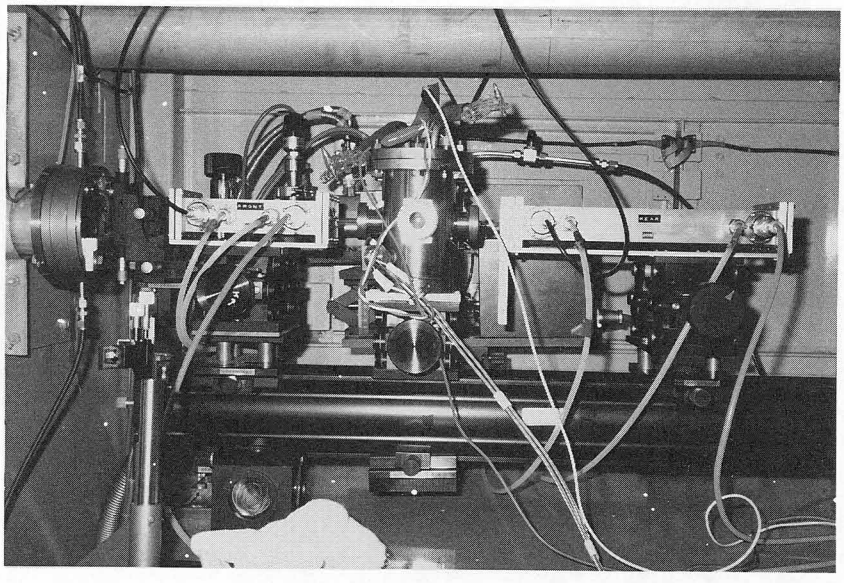

Fig. 3. (a)Photographs of the fabricated heating furnace for high temperature EXAFS measurements. Refer to the text for a detailed description. (b) The furnace mounted on the EXAFS spectrometer at BL10B of Photon Factory in KEK. The synchrotoron source is situated to the left of the ionchamber detector and guide-pass.

Table 2. Survey regions and scanning steps of X-ray absorption spectra in Br K- and Ag K-edge.

Br K-edge	
13.220 – 13.450 (KeV)	5.1 (eV)
13.450 – 13.530	1.0
13.530 – 13.950	2.6
13.950 – 14.170	3.6

Ag K-edge	
25.230 – 25.490 (KeV)	5.1 (eV)
25.490 – 25.570	0.9
25.570 – 25.950	2.4
25.950 – 26.200	3.4

4.5 - 11.0 $\mathring{A}^{-1}$ for the Br K-edge and k = 4.5 - 11.0 $\mathring{A}^{-1}$ for the Ag K-edge, were used in each case. Typical $\chi(\underline{k})$ data and the Fourier transforms for the Br K- and Ag K-edges are shown in Fig. 4, Fig. 5 and Fig. 6, respectively. The highest peak in each radial structure function indicates the nearest-neighbors around the absorbing atom. With increasing temperature from 293 K to 573 K, the peak in radial structure function around the Ag ion of pure AgI shifts to a shorter distance and the peak magnitude decreases. Using a curve-fitting analysis of EXAFS, the structure parameters (the coordination number N, interatomic distance d and Debye-Waller factor σ) of α-$AgI_{1-x}Br_x$ solid solution ($0 \leq x \leq 0.4$) at 573 K are determined by the least-squares parameter fitting as mentioned in chapter 3 (Table 3). The amplitude and phase shift parameters were obtained from the reference samples (pure β-AgI and AgBr at 293 K). The interatomic distances for the reference samples were determined by the single crystal structure analysis with X-rays (Yoshiasa et al., 1986 and 1987). The analysis has been made assuming that the first peak in each radial structure function for the Ag K-edge of the solid-solution is composed of double shells (i.e. the Ag-I and Ag-Br distances), and that for the Br K-edge is single shell (the Br-Ag distance). The reliability of fit parameter, $R = \Sigma_s |\underline{k}_s{}^3\chi(\underline{k}_s)_{exp.} - \underline{k}_s{}^3\chi(\underline{k}_s)_{calc.}| / \Sigma_s |\underline{k}_s{}^3\chi(\underline{k}_s)_{exp.}|$, between the experimental and calculated EXAFS functions is also listed in Table 3. The quality of the fit for the Ag K-edge of the $AgI_{0.7}Br_{0.3}$ is shown in Fig. 7. The curve-fitting analysis satisfactorily reduced the magnitude of R-factor by roughly 1 %.

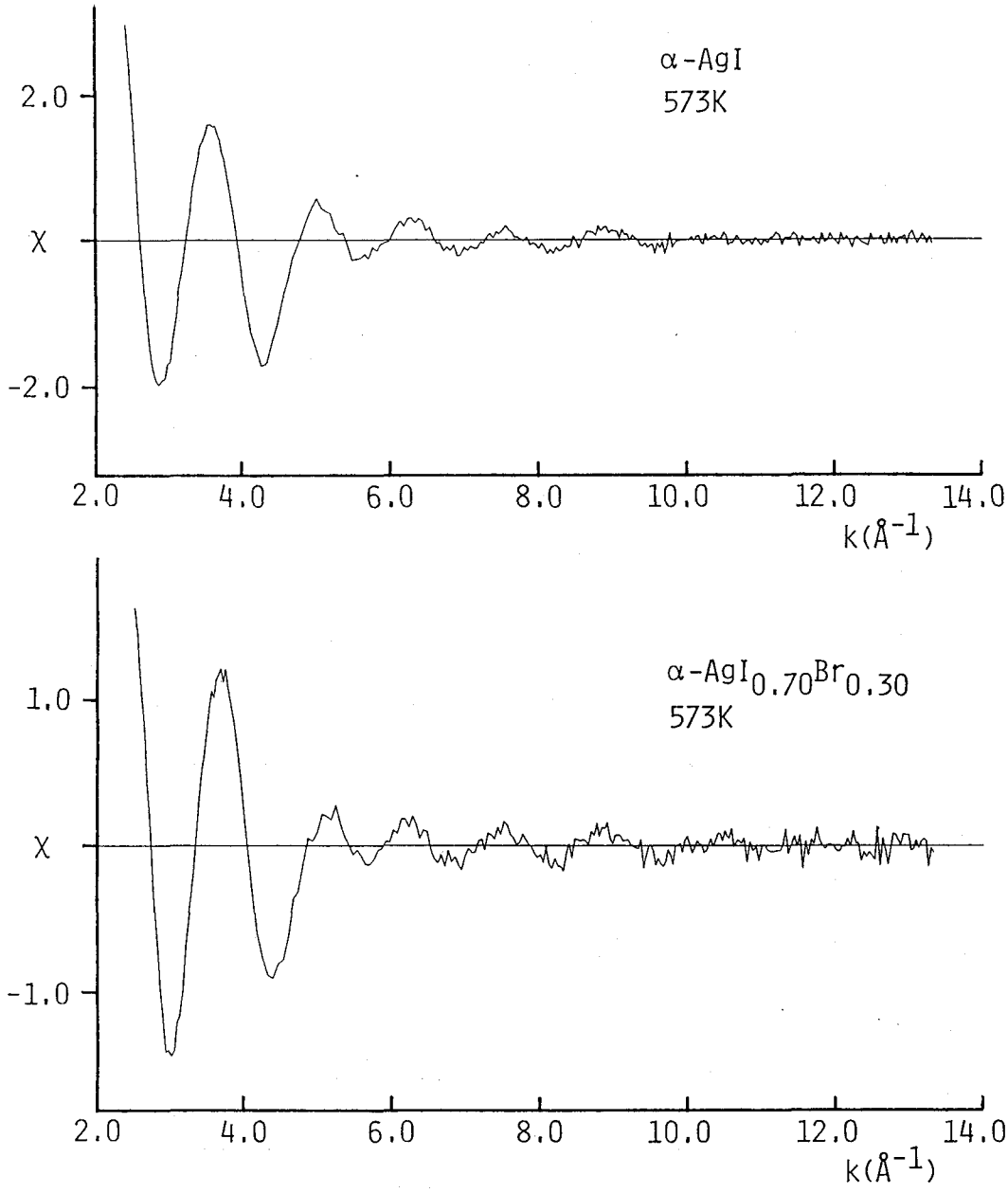

Fig. 4. Ag K-edge EXAFS oscillations for α-AgI and α-$AgI_{0.7}Br_{0.3}$ at 573 K.

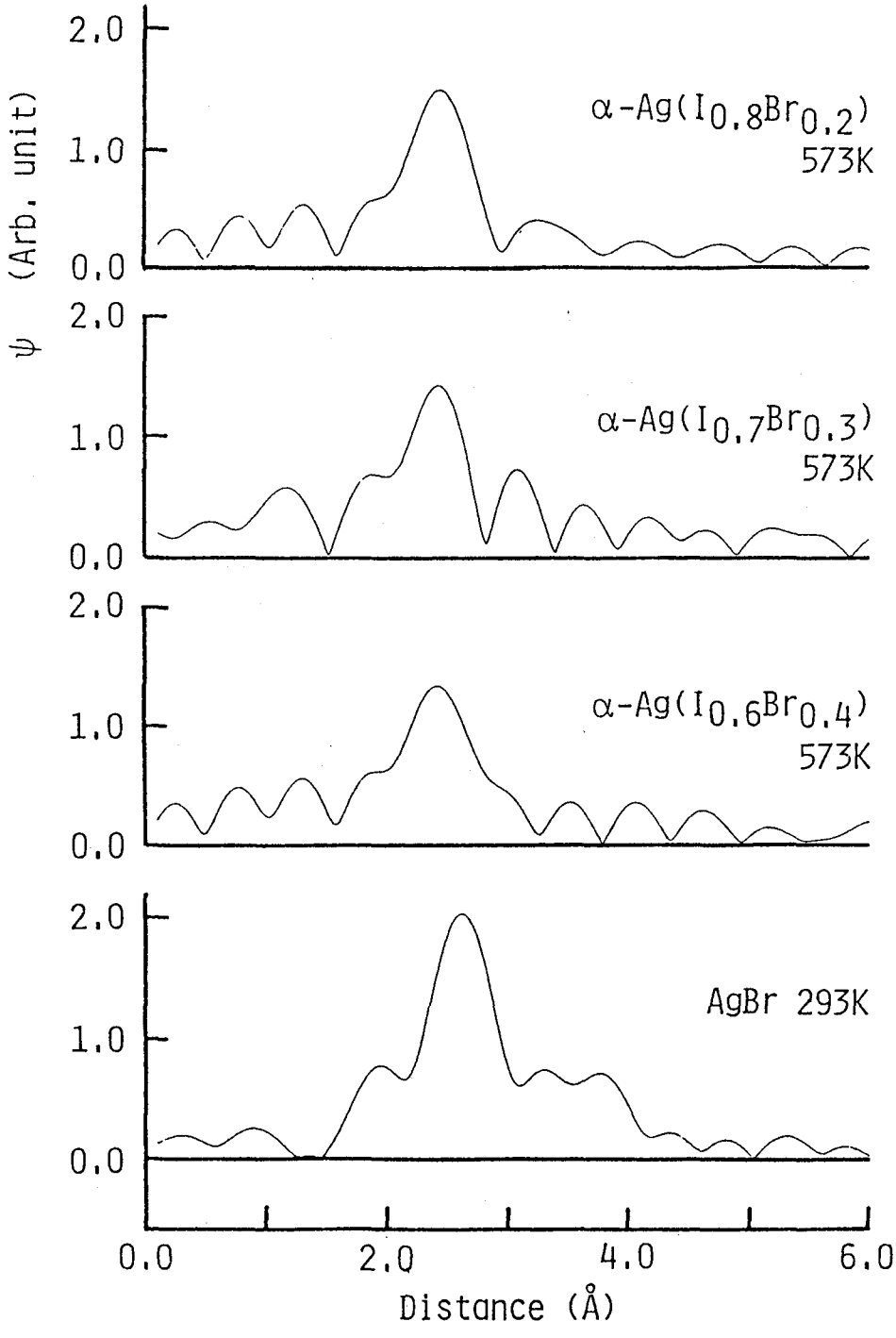

Fig. 5. Fourier transforms for Br K-edge of α-AgI type $AgI_{1-x}Br_x$ solid-solution (x = 0.2, 0.3, 0.4) at 573 K. No phase shift corrections were made.

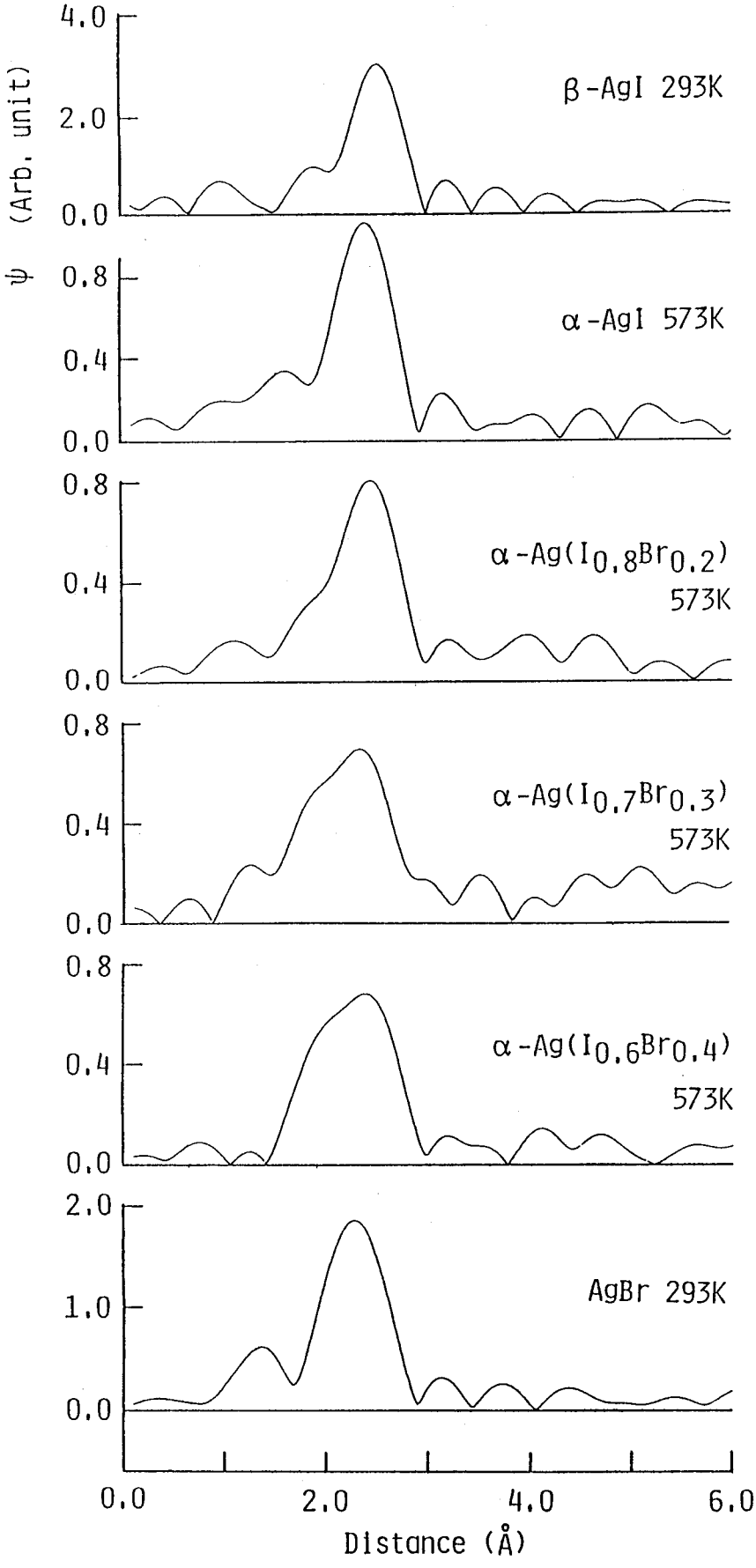

Fig. 6. Fourier transforms for Ag K-edge of α-AgI type $AgI_{1-x}Br_x$ solid-solution (x = 0.0, 0.2, 0.3, 0.4) at 573 K with the reference samples. No phase shift corrections were made.

Table 3. Structure paramaters by the least-squares paramater fitting : coordination numbers [N], interatomic distances [R(Å)] and Debye-Waller factors [σ].

Ag K-edge

	N_{Ag-I}	N_{Ag-Br}	R_{Ag-I}	R_{Ag-Br}	σ_{Ag-I}	σ_{Ag-Br}	R-factor
β-AgI [293K]*	4		2.813		0.08(3)		
α-AgI [573K]	1.7(5)		2.76(2)		0.09(2)		1.53%
α-$Ag(I_{0.8}Br_{0.2})$	1.3(14)	0.3(9)	2.79(6)	2.68(6)	0.09(4)	0.05(22)	0.26%
α-$Ag(I_{0.7}Br_{0.3})$	1.3(12)	0.6(9)	2.73(8)	2.67(3)	0.10(4)	0.06(8)	0.08%
α-$Ag(I_{0.6}Br_{0.4})$	1.0(2)	0.7(2)	2.77(2)	2.68(2)	0.09(2)	0.07(2)	0.04%
AgBr [293K]*		6		2.888		0.09(1)	

Br K-edge

	N_{Br-Ag}	R_{Br-Ag}	σ_{Br-Ag}	R-factor
α-$Ag(I_{0.8}Br_{0.2})$	3.0(7)	2.71(1)	0.09(1)	0.01%
α-$Ag(I_{0.7}Br_{0.3})$	2.1(6)	2.69(1)	0.08(1)	0.04%
α-$Ag(I_{0.6}Br_{0.4})$	3.1(7)	2.70(1)	0.10(1)	0.30%
AgBr [293K]*	6	2.888	0.10(1)	

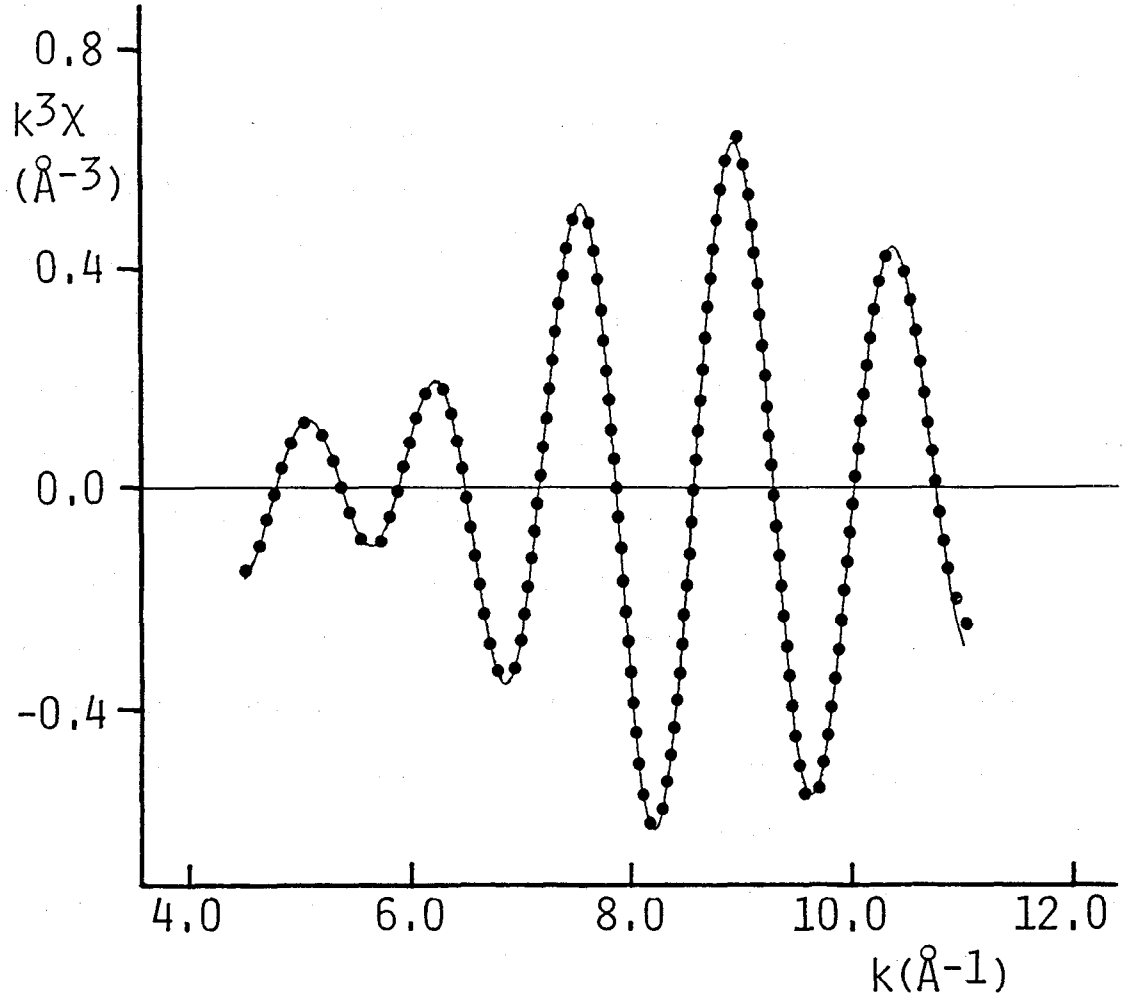

Fig. 7. Fourier-filtered EXAFS spectra (solid curve) and least-squares fit (dotted curve) for Ag K-edge of α-AgI type $AgI_{0.7}Br_{0.3}$.

The quality of the fit on the peaks for solid-solutions is sufficent and should justify the validity of our models.

3) Discussion

3-1 The effective one-particle potentials in the high and low temperature phases of AgI

Here, the crystal structure of α-AgI is reviewed in comparison with that of β-AgI. X-ray or neutron diffraction experiments allow the determination of the three-dimensional distributions of atoms in the unit cell and provide information about the average distribution of atoms around their equilibrium positions. We have studied the behavior of anharmonic thermal vibrations in β-AgI as a function of temperature by X-ray diffraction method (Yoshiasa et al., 1987). The probability-density functions (P.D.F.) were presented and the effective one-particle potentials (O.P.P.) of both Ag and I atoms were derived from the P.D.F.s. The O.P.P. has an absolute energy scale and is almost independent of temperature.

Cava et al. (1977) refined the structure of α-AgI by single-crystal neutron diffraction method and showed that the equilibrium position of Ag is only the tetrahedrally-coordinated site at (1/4 0 1/2) and that the complex silver distribution is completely accounted for by anharmonic thermal vibration. We have calculated the P.D.F. and the O.P.P. for α-AgI with the temperature factors published by Cava et al. (1977). Fig. 8 shows the O.P.P. curves of both atoms in α-AgI (solid curves) and β-AgI (dashed curves) along the Ag-I bond at the individual temperatures. Fig. 9 shows the O.P.P. curve of Ag in α-AgI

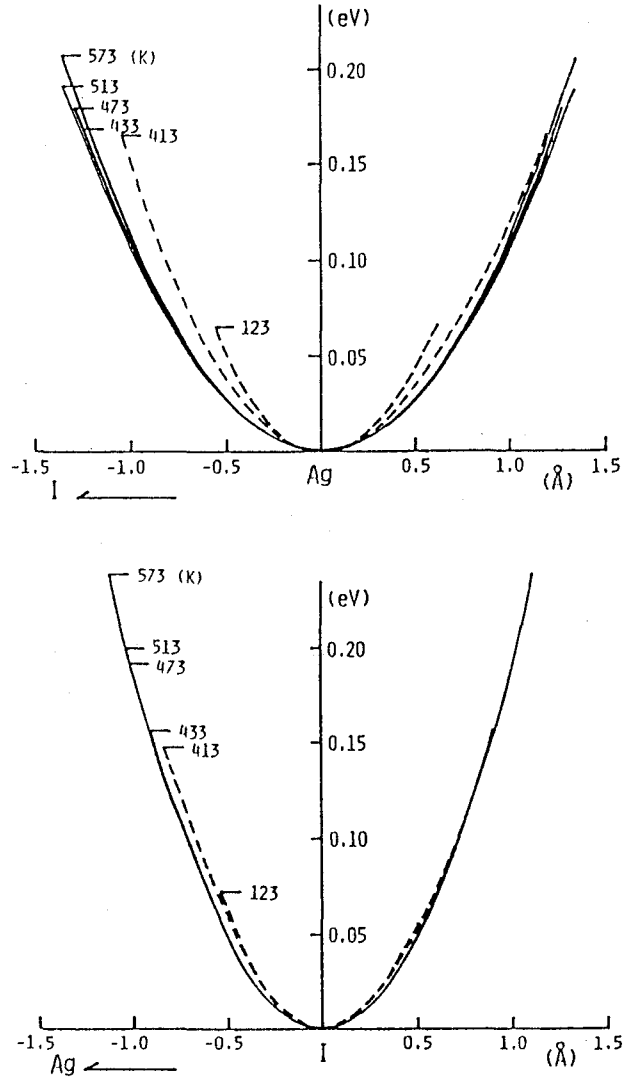

Fig. 8. Effective one-particle potential of Ag and I atoms in α-AgI (solid curves) and β-AgI (dashed curves) along the Ag-I bond at individual temperature.

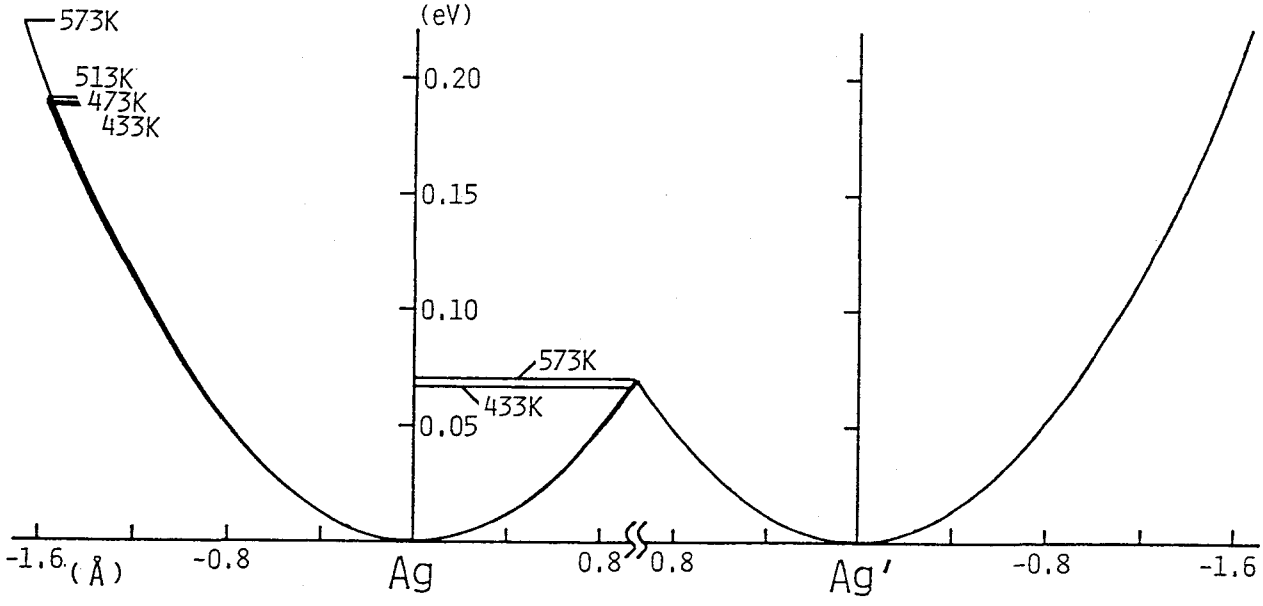

Fig. 9. Effective one-particle potential of Ag atom in α-AgI along the diffusion path between neighboring equivalent tetrahedral sites (dashed curve). The straight lines indicate the heights of col in the potential barrier at 433 K and 573 K, respectively.

perpendicular to the Ag-I bond (parallel <201>). The Ag and I atoms in α-AgI are located in 12(d) sites (noncentrosymmetric site symmetry 42m) and in 2(a) sites (centrosymmetric, m3m) of space group Im3m, respectively, while in β-AgI both Ag and I atoms are located in 2(b) site (noncentrosymmetric, 3m) of space group $P6_3mc$. The O.P.P. curves for the I atoms in α-AgI are symmetric as shown in Fig. 8 because the 2(a) sites have a center of symmetry. The O.P.P. provides some useful information with respect to an isolated atom vibrating in equilibrium position. For the interpretation of this potential, Bachmann & Schulz (1984) have demonstrated that the temperature dependence of potential is different between ordered structures (dynamic disorder due to thermal vibrations only) and disordered structures (in addition to thermal vibrations, static deviations from the crystal symmetry); i.e. for ordered structures the O.P.P. curves are almost independent of temperature and for disordered structures a temperature-dependent pseudo potential is obtained.

Since the Ag atoms in α-AgI are distributed at random over the 12(d) sites and only one sixth of the sites is occupied, it may be considered that static deviations from the lattice sites contribute appreciably to the O.P.P.. Nevertheless, in Fig. 8, the obtained potentials of both atoms in α-AgI are considerably similar to those in β-AgI of which structure is quite different. It is, therefore, suggested that the obtained potentials of both atoms in α-AgI are not far removed from the actual potentials though diffraction experiments provide space averaged information for the disordered structure. The potentials do not change

appreciably through the β-α phase transition. It is also noteworthy that the curves of both atoms in α-AgI toward the bonding direction are characteristically located lower than those in β-AgI. These features suggest that the I ions are localized on the body-centered cubic lattice and do not deviate appreciably from their lattice sites by the statistical distribution of the Ag ions.

The P.D.F. map in the (010) plane is presented in Fig. 10. The P.D.F. is defined as the probability of finding an atom in a volume element (Willis & Pryor, 1975) and provides information about the average distribution of atoms around the equilibrium positions. The widespread distribution obtained for both atoms exhibits that the periodicity is substantially disturbed by the large thermal motion of the atoms. The Ag ions are statistically distributed over the iodine tetrahedra. Each tetrahedron shares faces with four other tetrahedra in the body-centered structure. The P.D.F. for the Ag ion extends to neighboring tetrahedra. Consequently, the Ag ion can jump to the neighboring site with appreciable probability by the thermal motion. It is proposed that the disordered nature of α-AgI is due to the thermal motion coupled with the lattice vibration of the I ions, and diffusive and vibrational motions are not independent. Although the directions of motion having the largest amplitude for the Ag ions are the $\langle 100 \rangle$ directions toward two longer edges of the tetrahedra, the positions having the highest probability density on the boundaries between neighboring tetrahedral sites, i.e., the col in the potential barriers, are indicated by the arrows in

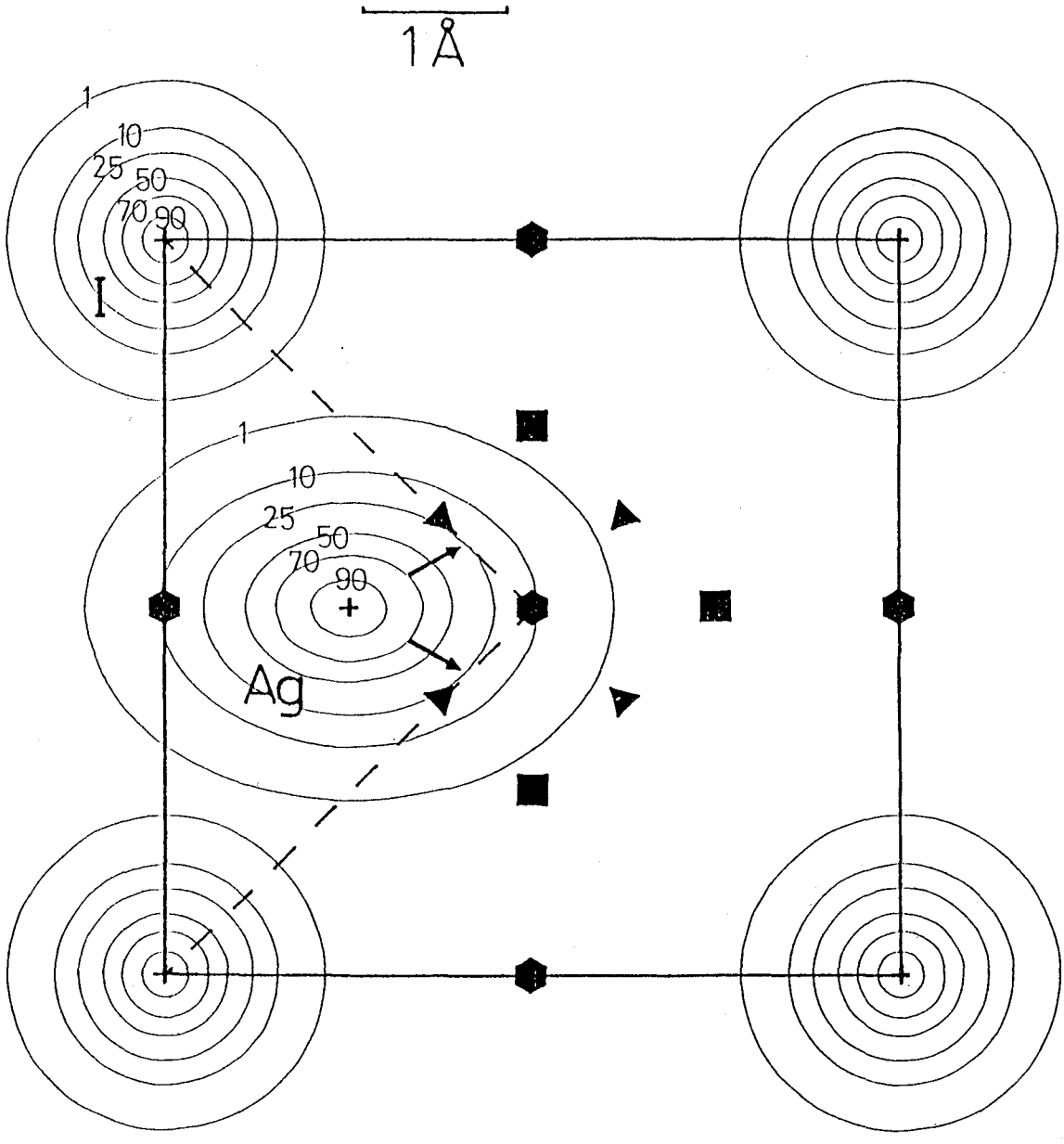

Fig. 10. The probability density function in the (010) plane. The contours are scaled to 100 units at the centers. The arrows show the highest probability density on the boundaries between neighboring tetrahedral sites.

Fig. 10. It is, therefore, suggested that diffusion occurs mainly between four face-shared tetrahedral sites. Based on the Ag density in Fourier maps (Fig. 11), Cava et al. (1977) pointed out that the location of the three-coordinated saddle point (0.39,0,0.39) is significantly different from the geometrically-anticipated 24(h) site (3/8,0,3/8). Our interpretation accounts completely for the discrepancy of the location; the col in the potential barriers corresponds to the saddle point.

3-2 Local environment of the Ag ion in α-AgI

In Table 3, we showed the coordination number and interatomic distance for α-AgI at 573 K by a curve-fitting analysis of EXAFS. Apparent decrease in the coordination number is observed in α-AgI. This results are compatible with the previous EXAFS results. Boyce et al.(1977) reported that in α-AgI only ~75% of the Ag atoms contribute to the sharp EXAFS features at 471 K. And they explained such a loss in intensity by considering a residence time and a flight time; a sharp EXAFS signal does not yield during the flight time because the Ag-I distances are distributed over a large range. Indeed, large static and thermal disorder can lead to a reduction of the EXAFS amplitude, and hence a lowering of the apparent coordination number (Teo, 1986). The residues were detected on the radial structure function because of broadening of EXAFS signal.

EXAFS spectroscopy is sensitive to the local environment around the Ag ions in α-AgI which has a statistical distribution of Ag ions over the 12(d) sites, while spatially averaged information over the 12(d) site (the average of one site occupied

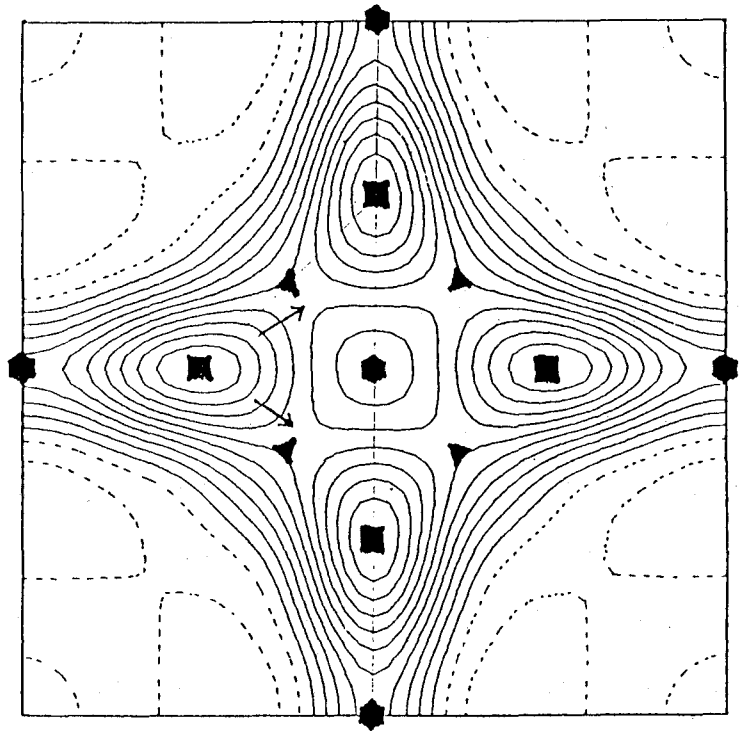

Fig. 11. Distribution of silver scattering density for α-AgI in the (010) plane at 573 K (contribution of I subtracted) from the neutron scattering results of Cava et al, (1977). Tetrahedral sites (■), octahedral sites (⬢) and trigonal sites (▲).

by the Ag ion and five unoccupied sites) are obtained by diffraction experiments. We have obtained the distance from Ag to the first nearest neighbor, Ag-I = 2.76 Å, at 573 K by EXAFS as listed in Table 3. On the other hand, at the center of the iodine tetrahedron the Ag atom has four nearest neighbours at 2.84 Å by diffraction experiments at 573 K. The Ag-I distance obtained by EXAFS in α-AgI is, therefore, significantly shorter than that by diffraction experiments.

Here, let's discuss the local structure of α-AgI on the basis of the comparison with β-AgI. β-AgI has a negative thermal expansion and transforms to α-AgI with higher density at 420 K. In β-AgI, the nearest Ag-I distances are 2.811(1) Å and 2.819(3) Å at 123 K and as the result of increasing thermal vibration of atoms the distance of 2.819 Å becomes short with temperature (Yoshiasa et al., 1987). The O.P.P. curves of both Ag and I atoms in α-AgI are sufficiently similar to those in β-AgI (Fig. 8). In addition, the curves in α-AgI toward the bonding direction are located lower than those in β-AgI. It thus appears that the tetrahedral sites occupied by Ag ions in α-AgI are smaller than those in β-AgI and that the Ag-I distance obtained from EXAFS method represents the nearest-neighbor distance in α-AgI. The average distances between the nearest I ions in α-AgI are 4.38 Å (433 K) and 4.40 Å (573 K) which are compared to 4.59 Å in β-AgI over a wide range of temperature, and the larger thermal expansion in α-AgI results from the dilation of unoccupied I cages. Hokazono et al. (1984) analysed dynamical correlation between anions and cations by a molecular-dynamic technique, and they pointed out that the average volume of tetrahedra which

contain Ag ions are smaller than that of unoccupied tetrahedra.

The Debye-Waller factor for EXAFS experiments differs from that for diffraction experiments. In EXAFS only the component of the relative displacement which lies along the bond direction needs to be considered (Teo, 1986). The much larger root-mean-square deviation from the average lattice position are obtained from diffraction studies. In Table 3, it is interesting to note that the Debye-Waller factor for the nearest neighbor Ag-I atom pair in α-AgI (573K) is not significantly larger than that in β-AgI (293 K) though the motion of the Ag atom in α-AgI is extremely violent.

3-3 Local structure of the α-$AgI_{1-x}Br_x$ solid-solution

The cell dimensions of α-$AgI_{1-x}Br_x$ solid-solutions (Fig. 2) decrease linearly with increasing AgBr content because of the substitution of smaller Br ion for larger I ion and follow Vegard's law. The cell dimension for the α-AgI type structure of AgBr at 573 K is estimated to be ca. 4.72 Å by extrapolation. The values of 4.72 Å for the α-AgI type structure and of 5.77 Å for the rock-salt type structure (293 K) in AgBr are compared well with 5.08 Å for the α-AgI type (573 K) and 6.07 Å for the rock-salt type (at room temp. and 4 kbar, Moore & Kasper, 1968) in AgI. From the cell dimension of 4.72 Å for the α-AgI type AgBr, the Ag-Br distance of the tetrahedral site is 2.64 Å ($\sqrt{5}a/4$), while the average Ag-Br distance of the octahedral site is 3.01 Å ($(2\sqrt{2}a + a)/6$).

EXAFS and XANES spectra yield information on a specific ion's immediate environment. The peak in each radial structure

function for the Ag K-edge of the solid-solution at 573 K (Fig. 6) gradually develops a shoulder at shorter distance with increasing AgBr content and is composed of double shells of the Ag-I and Ag-Br distances as shown in Table 3. On the other hand, the peak for the Br K-edge of the solid-solution (Fig. 5) does not vary with AgBr content and is composed of single shell of the Br-Ag distance. In the solid-solution range, the Ag-I and Ag-Br distances are constant and are 2.76 Å and 2.69 Å, respectively. Though apparent decrease in the coordination number is also observed in the solid-solution, the ratio of the coordination number of I ions around the Ag ion to that of Br ions is reasonably proportional to the chemical composition.

The XANES region of the absorption spectrum contains the information on relative orientation and bond angles of atoms surrounding the X-ray absorbing atoms (e.g. Fujikawa et al., 1983). The experimental Br K- and Ag K-edge XANES spectra of the solid-solution at 573 K are shown in Fig. 12 with the reference samples. There are little changes in the Br K- and Ag K-edge XANES spectra through the solid-solution range. It is, therefore, proved from EXAFS and XANES spectra that only tetrahedral sites are appreciably occupied at equilibrium in the solid-solution though the α-AgI type structure has several kinds of available sites among interstices of the b.c.c. lattice formed by anions, and that the Ag atoms in the solid-solution are restricted by long-range order.

3-4 Superionic conduction of α-AgI

The Ag ions in α-AgI vibrate about the tetrahedral 12(d)

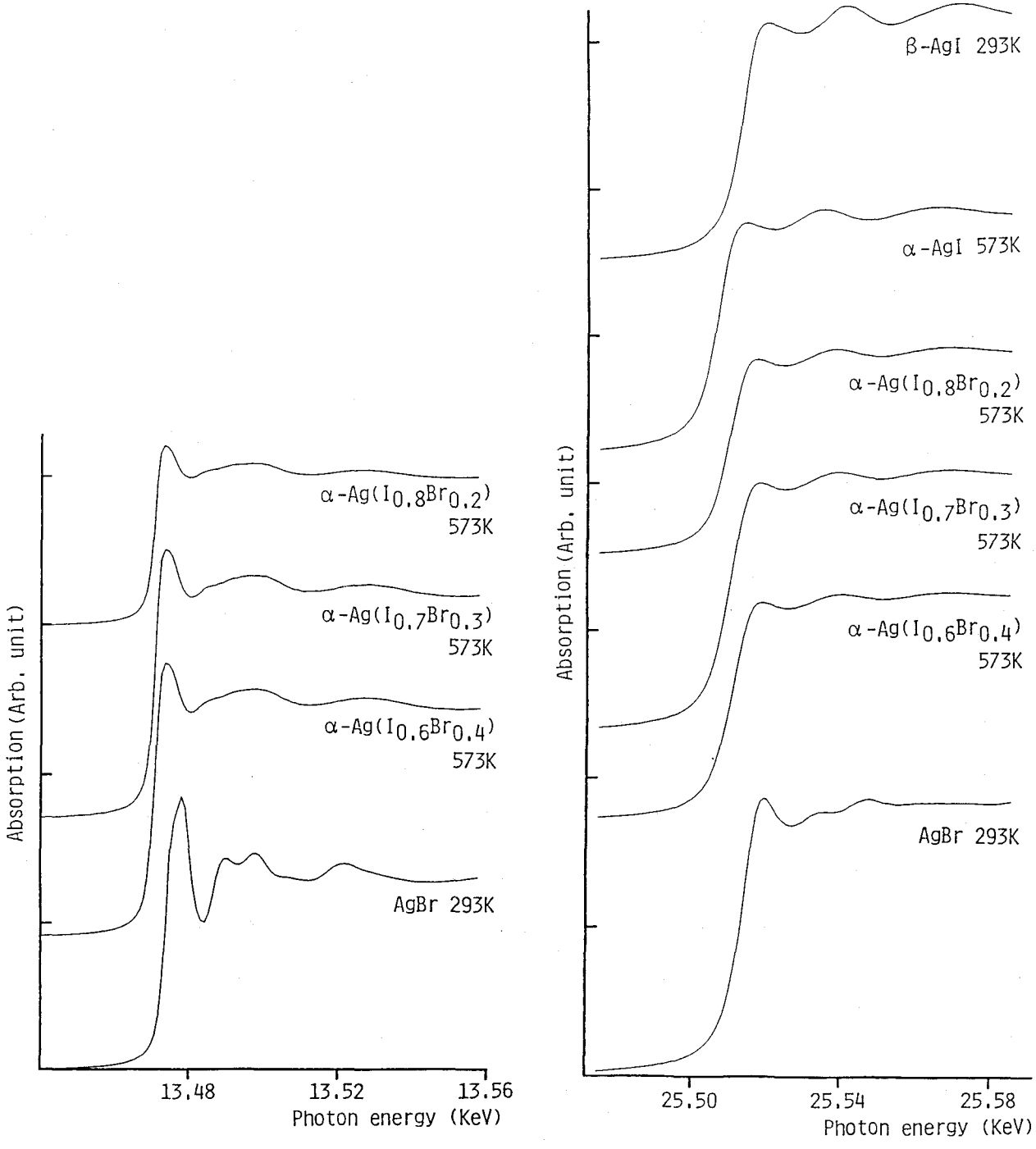

Fig. 12. Experimental Br K-edge and Ag K-edge XANES spectra of α-AgI type $AgI_{1-x}Br_x$ solid-solution at 573 K with the reference samples (pure β-AgI and AgBr at 293 K).

sites with large amplitude and then jump to a nearest neighbor site in a manner coupled with the lattice vibration of the I ions. Cooperative effects will be important for the dynamics of the diffusion (e.g. Alben & Burns,1977 and Hoshino et al.,1977). The ionic conduction is closely related to the phonon spectrum and the knowledge of the lattice vibrations should be of primary importance for understanding of the ionic conduction.

The structural feature proposed in the present study of α-AgI is consistent with the spectroscopic considerations for the Ag ion having a tetrahedral symmetry. The far-infrared (Bruesch et al.,1975) and Raman studies (Burns et al.,1976) showed that the frequency of the To mode in the α-AgI is essentially the same as in β-AgI and that the interatomic forces are nearly the same in both phases. Buhrer et al. (1978) attempted preliminary lattice-dynamical calculations of α-AgI using the force constants of β-AgI, and obtained an agreement for the frequencies of the To modes. Beyeler et al. (1978) calculated the diffuse scattering pattern of β-AgI with the valence shell model parameters of Buhrer et al. (1978) and concluded that in β- and α-AgI a large part of the strong diffuse scattering is of thermal nature originating from the large number of low-frequency lattice excitations whose frequency is determined by weak bending forces. In bond-bending modes, the tetrahedral angles are mainly changed but not the Ag-I distances. The weakness of bond-bending forces appears to be a characteristic for superionic conductors (Phillips, 1976).

Using a molecular-dynamics technique nature of ionic motions

in α-AgI was studied by Vashishta & Rahman (1978), Parrinello et al. (1983), Vashishta (1986), Chiarotti et al. (1986) and Tallon (1986). They showed to some extent that a simple potential function successfully describes the β-α phase transition and that the structural and dynamical properties of α-AgI are in good agreement with experiments. These reports, therefore, suggest that the interparticle potential in AgI does not change appreciably through the β-α phase transition.

At 420 K, the β-AgI transforms into the superionic α-AgI in which Ag ions are mobile with large constant of self-diffusion. β-AgI has low conductivity with appreciable activation energy, while α-AgI has high conductivity with little apparent thermal activation. It should be emphasized that these appreciable difference in the ionic conductivity between these phases is attributed to the difference in the atomic arrangements. A necessary condition for superionic conduction is the availability of many energetically nearly equal sites per ion for the conducting species as conduction paths. In α-AgI, iodine cages share the faces and edges with each other; accordingly there is a continuous path through the crystal. The P.D.F. maps involve valuable information about diffusion paths and the O.P.P. curve, which has an absolute energy scale, allows estimation of the potential barrier along the diffusion path of the mobile ions. It is known that the estimated potential barrier along the path compares well with the activation energy of conductivity (Bachmann & Schulz, 1984). Fig. 9 shows the O.P.P. curve for the Ag atom along the diffusion path between face-shared equivalent tetrahedral sites (the direction of the arrows in Fig. 10).

Thermally excited Ag ions can overcome the barrier height of 0.07 eV to change their positions. The value of 0.07 eV agrees well with the activation energy for ionic diffusion as derived from an Arrhenius plot of conductivities (σ); the activation energy as calculated from the plot of $\log(\sigma T)$ vs $1/T$ (Rice & Roth,1972) or the plot of $\log\sigma$ vs $1/T$ (Shahi & Chandra, 1975) has been found to be 0.10 eV or 0.05 eV for the conduction of Ag ion in α-AgI (both plots yield adequately straight lines from the literature data (Tubandt & Lorenz, 1914 and Kvist & Josefson, 1968)).

4) References

R. Alben and G. Burns (1977) Physical Review, B16, 3746-3752

R. Bachmann and H. Schulz (1984) Act Cryst., A40, 668-675

H.V. Beyeler, P. Brüesch and T. Hibma (1978) Phsical Review, B18, 4570-4575

J.B. Boyce, T.M. Hayes, W. Stutius and J.C. Mikkelsen, Jr. (1977) Physical Review Letters, 38, 1362-1365

P. Brüesch, S. Strässler and H.R. Zeller (1975) Phys. Stat. Sol., 31, 217-226

W. Bührer, R.M. Nicklow and P. Brüesh (1978) Physical Review, B17, 3362-3370

G. Burley (1967) Acta Cryst., 23, 1-5

G. Burns, F.H. Dacol and M.W. Shafer (1976) Solid State Communications, 19, 291-295

R.J. Cava, F. Reidinger and B.J. Wuensch (1977) Solid State Communications, 24, 411-416

G.L. Chiarotti, G. Jacucci and A. Rahman (1986) Physical Review Letters, 57, 2395-2398

M.J. Delaney and S. Ushioda (1976) Solid State Communications, 19, 297-301

T. Fujikawa, T. Matsuura and H. Kuroda (1983) Journal of the Physical Society of Japan, 52, 905-912

R.C. Hanson, T.A. Fjeldly and H.D. Hochheimer (1975) Phys. Stat. Sol., 70, 567-576

T.M. Hayes, J.B. Boyce and J.L. Beeby (1978) J. Phys. C. : Solid State Phys., 11, 2931-2937

S. Hoshino, T. Sakuma and Y. Fujii (1977) Solid State Communications, 22, 763-765

M. Hokazono, A. Ueda and Y. Hiwatari (1984) Solid State Ionics, 13, 151-155

A. Kuist and A.M. Josefson (1968) Z. Naturforsch., 23a, 625-626

M.J. Moore and J.S. Kasper (1968) The Journal of Chemical Physics, 48, 2446-2450

J. Nolting and D. Rein (1969) Zeitschrift fur Physikalische Chemie Neue Folge, 66, 150-160

M. Parrinello, A. Rahman and P. Vashishta (1983) Physical Review Letters, 50, 1073-1076

J.C. Phillips (1970) Rev. Mod. Phys., 42, 317-356

J.C. Phillips (1976) J. Electrochem. Soc., 123, 934-940

M.J. Rice and W.L. Roth (1972) Journal of Solid State Chemistry, 4, 294-310

K. Shahi and S. Chandra (1975) Z. Naturforsch., 30a, 1055-1059

K. Shahi and J.B. Wagner Jr. (1984) Solid State Ionics, 12, 511-516

V.O. Stasiw and J. Teltow (1949) Zeitschrift für Anorganische Chemie, 259, 143-153

J. Tallon (1986) Physical Review Letters, 57, 2427-2430

B.K. Teo (1986) EXAFS : Basic Principles and Data Analysis,

C. Tubandt and E. Lorez (1914) Z. Phys. Chem., 87, 513

P. Vashishta and A. Rahman (1978) Physical Review Letters, 40, 1337-1340

P. Vashishta (1986) Solid State Ionics, 18 & 19, 3-12

B.T.M. Willis and A.W. Pryor (1975) Thermal Vibration in Crystallography, Cambridge University Press

A. Yoshiasa, K. Koto, S. Emura and F. Kanamaru (1986) J. Phys. Colloq., 47, C-8 803-807

A. Yoshiasa, K. Koto, F. Kanamaru, S. Emura and H. Horiuchi (1987) Acta Cryst., B43,434-440

Chapter 5.

General conclusion

1) Anharmonic thermal vibrations in wurtzite-type AgI

The thermal behavior of atoms in wurtzite-type AgI (β-AgI) was investigated by X-ray diffraction at 123, 297, 363 and 413 K. The several reflections which violate the extra conditions of the systematic absences of the wurtzite-type structure were first observed and explained by anharmonic thermal vibrations. It is concluded that the anharmonic character is essential to the β-AgI structure.

The effective one-particle potentials of both Ag and I atoms in β-AgI were evaluated and the anharmonic thermal vibrations of both atoms are demonstrated by the probability density functions. The degree of anisotropic thermal motion of the I atom was getting more prominent than that of the Ag atom at higher temperatures and the thermal motion of the I atom reveals a salient anharmonicity toward the structural change corresponding to the transformation from β- to α-AgI. The c-axis becomes shorter with raising temperature. The structural changes versus temperature can be explained from the anharmonic thermal vibration.

The apical distances of wurtzite-type compounds are longer than the basal ones due to the difference in the contribution to hybridization between three equivalent directions and another symmetrically non-equivalent directions. The apical distance becomes shorter at higher temperature owing to the thermal vibrations which are dependent on the bonding force. It is proved that the anharmonicity causes the structural variations in the wurtzite-type compounds.

The magnitudes of temperature factors are larger for mobile Ag atoms than for I atoms. The appreciable anisotropy of the thermal motion is not directly related to the macroscopic characteristics of ionic conduction.

2) Variations of Ag bonding distances in the $AgBr_{1-x}I_x$ rock-salt type solid-solution by X-ray and EXAFS analyses

The local structure of the $AgBr_{1-x}I_x$ rock-salt type solid-solution ($0 \leq x \leq 0.4$) was investigated by both EXAFS and single crystal X-ray diffraction. The first nearest neighbor distances from Br to Ag, and those from Ag to Br in the solid-solution can determine from EXAFS method. On the other hand, X-ray diffraction methods provide the average Ag-(Br,I) distances because the Br and I ions occupy the crystallographically equivalent positions. Because Ag^+ surrounded by both Br^- and I^-ions is locally attracted to Br^-, which has larger effective negative charge than I^-, the Ag-Br distances gradually decrease with AgI content. There are observed systematic changes in both Br K- and Ag K-edge XANES spectra with increasing AgI content in connection with the change of the local structure in the solid-solution.

In the solid-solution, the Br and I ions are distributed at random over the 4(a) sites of space group Fm3m without forming clusters. Static deviations of both cation and anion from the lattice site occur because the Ag-Br and Ag-I distances in the solid-solution are closer to the respective distances in the pure rock-salt type compounds, AgBr and hypothetical rock-salt type AgI, than to an average distance. The particular increase in temperature factors by X-ray diffraction results from the static displacements of both cations and anions from the normal

octahedral site.

A large enhancement of ionic conductivity in AgI rich region will be ascribed to an increase in the concentration of the Frenkel defect caused by changes in local structures in an equilibrium state. The activation energies in the intrinsic region for the solid-solutions in which both anions are distributed at random over octahedral sites without forming clusters are not so much influenced by changes in the local structure.

3) Local structure of the superionic conducting α-AgI type $AgI_{1-x}Br_x$ solid-solution.

EXAFS and XANES structural analyses were made for the α-AgI type $AgI_{1-x}Br_x$ solid-solution ($0 \leq x \leq 0.4$) at 573 K to elucidate the distribution of Ag ions. The Ag-I and Ag-Br distances in the solid-solution keep constant values over whole range, respectively: 2.76 Å for Ag-I and 2.69 Å for Ag-Br. There are little changes in the Br K- and Ag K-edge XANES spectra through the solid-solution range. It is, therefore, concluded that only tetrahedral sites are appreciably occupied by Ag ions at equilibrium in the solid-solution though α-AgI type structure has several kinds of available sites among interstices of the b.c.c. lattice formed by anions, and that the Ag atoms distribute statistically over the tetrahedral sites with long-range order.

The Ag-I distance obtained by EXAFS is significantly shorter than that by diffraction experiments. The Ag-I distance obtained from EXAFS method represents the nearest-neighbor distance in α-AgI, while space averaged information over the 12(d) site (the average of one site occupied by the Ag ion and five unoccupied

sites) are obtained by diffraction experiments. The larger thermal expansion in α-AgI results from the dilation of unoccupied I cages.

We have calculated the effective one-particle potentials and the probability-density functions of both Ag and I atoms in α-AgI. Judging by comparison with the o.p.p in β-AgI, it is suggested that the calculated potentials of both atoms in α-AgI are not so different from the actual potentials though diffraction experiments provide spatially averaged information for the disordered structure. It is surprised that the potentials along the Ag-I bond do not change appreciably through the β-α phase transition though ion conductivity remarkably change through the transition.

The wide spread distribution of both atoms exhibits that the periodicity of atomic arrangement is substantially disturbed by the large thermal motion of the atoms. The probability-density function for the Ag ion extends to neighboring tetrahedra. Consequently, the Ag ion can jump to the neighboring site with appreciable probability by the thermal motion. The highest probability density is found on the boundaries between four face-shared tetrahedral sites though the directions of motion having the largest amplitude for the Ag ions are the <100> directions toward two longer edges of the tetrahedra. It is proposed that the disordered nature of α-AgI is due to the thermal motion of Ag ions.

The effective one-particle potential allows estimation of the potential barrier along the diffusion path of the mobile

ions. The Ag ions which are thermally excited more than 0.07 eV can overcome the barrier. The appreciable difference in the ionic conductivity between β- and α-phases is attributed to the difference in the atomic arrangements. A necessary condition for superionic conduction is that the structure has many available energetically nearly equal sites per mobile ion and diffusion paths with low energy barrier.

Acknowledgement

The author expresses his greatest gratitude to Professor F. Kanamaru for his kind suggestion and support in coordinating this work. The author also expresses his heartly thanks to Dr. K. Koto for helpful discussion, accurate instruction and encouragement. The author wishes to express his thanks to Drs. K. Kihara, Kanazawa University, K. Tanaka, Tokyo Institute of Technology, and H. Maeda, Okayama University, for providing the computer programs. The author is grateful to Drs. S. Nomura and A. Koyama, the National Laboratory for High Energy Physics (KEK), for their indispencable assiatance on EXAFS measurements, and to Dr. S. Emura of this institute for cooperation of measuring the Raman spectra. Discussion with and useful information from Professor T. Matsumoto, Kanazawa University, and Dr. S. Ohba, Keio University, are much appreciated. Thanks are also due to many members of this institute for helpful assistances and encouragement. The X-ray diffraction measurements were performed at the Materials Analyzing Center of this institute and all computations were carried out at the Crystallographic Research Center, Institute for Protein Research, Osaka University. This work has been performed under the approval of the Photon Factory Program Advisory Committee (Proposal No.86-007).